

Politechnika Lubelska
Wydział Budownictwa i Architektury

BUDOWNICTWO
I ARCHITEKTURA

Vol. 18(4) 2019

Politechnika Lubelska
Lublin, 2019

Politechnika Lubelska
Wydział Budownictwa i Architektury

**BUDOWNICTWO
I ARCHITEKTURA**



Vol. 18(4) 2019

Politechnika Lubelska
Lublin, 2019

Rada Naukowa/Scientific Council

Tomasz Bajda (AGH Kraków)
Ivan Baláž (University of Economics in Bratislava)
Mykola Bevez (National University Lviv Polytechnic)
Eduard-Marius Craciun, Ovidius (University of Constanta)
Grażyna Dąbrowska-Milewska (Politechnika Białostocka)
Wiesława Głodkowska (Politechnika Koszalińska)
Adam Goliger (The Council for Scientific and Industrial Research - CSIR)
Zbyněk Keršner (Brno University of Technology)
Halit Cenani Mertol (Atılım University)
Carlos M. Mozos (University of Castilla - La Mancha)
Adam Nadolny (Politechnika Poznańska)
Sandro Parrinello (Pavia University)
Stanislav Pospíšil (Institute of Theoretical and Applied Mechanics)
Wojciech Radomski (Politechnika Łódzka i Politechnika Warszawska)
Elżbieta Radziszewska-Zielina (Politechnika Krakowska)
Petro Rychkov (National University of Water Management and Nature Resources Use)
Shamsher Bahadur Singh (Birla Institute of Technology and Science)
Anna Sobotka (AGH Kraków)
Bogusław Szmygin, Lublin University of Technology, Poland
Thomas Thiis (Norwegian University of Life Sciences)
Viktor Tur (Technical University of Brest)
Tim K.T. Tse (The Hong Kong University of Science and Technology)

Kolegium Redakcyjne/Editorial Board

Redaktor naczelny/Editor-in-Chief: **Wojciech Franus**
Zastępca redaktora naczelnego/Deputy Editor: **Tomasz Lipecki**
Zastępca redaktora naczelnego/Deputy Editor: **Lukasz Borowski**
Sekretariat/Secretary: **Aleksandra Szczypa**

Adres redakcji/Address:

Politechnika Lubelska, Wydział Budownictwa i Architektury
ul. Nadbystrzycka 40, 20-618 Lublin, e-mail: wb.bia@pollub.pl

Strona czasopisma/Journal website:

ph.pollub.pl

Indeksacja/Indexed in:

Arianta, BASE, BazTech, CEEOL, Dimensions, DOAJ, EBSCO, ERIH Plus, Google Scholar, Index Copernicus, Infona, PBN/POL-Index, TIB, WorldWideScienc

Publikacja wydana za zgodą Rektora Politechniki Lubelskiej.
Published with the consent of the Rector of Lublin University of Technology.

Finansowana w ramach środków Ministra Nauki i Szkolnictwa Wyższego.
Financing by the Polish Ministry of Science and Higher Education.

© Copyright by Politechnika Lubelska 2019

ISSN 1899-0665

Realizacja/Published by: Biblioteka Politechniki Lubelskiej
Ośrodek ds. Wydawnictw i Biblioteki Cyfrowej
ul. Nadbystrzycka 36A, 20-618 Lublin, email: wydawca@pollub.pl

SPIS TREŚCI
CONTENTS

**Myroslav Sanytsky, Tetiana Kropyvnytska, Hanna Ivashchyn,
Oksana Rykhlitska:**

Eco-efficient blended cements with high volume of supplementary cementitious materials 5

Jacek Kudryś:

Spectral analysis of multi-year GNSS code multipath time-series 15

**Abhay Chaubey, Ajay Kumar, Małgorzata Grzegorzczak-Frańczak,
Małgorzata Szafraniec:**

*The impact of moisture and temperature on the laminated rhombic
hyperbolic paraboloid* 23

Andrzej Szewczak:

Impact of epoxy resin modification on its strength parameters 41

Barbara Ksit, Roman Pilch:

*Liquid plastic films as a solution in terms of tightness problems
and roofs aesthetics improvement – review* 51

Mykoha Bevz:

*The wooden architectural complex of the city and royal residence of the John III Sobieski
in Kukizów* 59

Barbara Turoń, Bartosz Miller:

The possibility of DIC system application in numerical models updating 83

Magdalena Sulima:

Houses of the Polish-Belarusian borderland as areas of value 103

Eco-efficient blended cements with high volume of supplementary cementitious materials

Myroslav Sanytsky¹, Tetiana Kropyvnytska², Hanna Ivashchyshyn³, Oksana Rykhlitska⁴

¹ Department of Building Production; Institute of Civil and Environmental Engineering; Lviv Polytechnic National University; Bandera Street 12, 79013 Lviv, Ukraine; msanytsky@ukr.net; ORCID: 0000-0002-8609-6079

² Department of Building Production; Institute of Civil and Environmental Engineering; Lviv Polytechnic National University; Bandera Street 12, 79013 Lviv, Ukraine; tkropyvnytska@ukr.net; ORCID: 0000-0003-0396-852X

³ Department of Building Production; Institute of Civil and Environmental Engineering; Lviv Polytechnic National University; Bandera Street 12, 79013 Lviv, Ukraine; aiwaszczyszyn@gmail.com; ORCID: 0000-0003-4927-6561

⁴ Department of Building Production; Institute of Civil and Environmental Engineering; Lviv Polytechnic National University; Bandera Street 12, 79013 Lviv, Ukraine; o.rykhlitska@knu.ua; ORCID: 0000-0002-6603-9915

Abstract: The ways of reducing CO₂ emissions in the cement industry were analysed for the purposes of implementation of the low carbon development strategy. The optimal solution to this problem is the technologically optimised blended cements with high volume of supplementary cementitious materials of various genesis and fineness. The design of eco-friendly blended cements was achieved by a synergistic combination of the main constituents such as granulated blast furnace slag, superfine zeolite, fly ash and limestone, as well as by optimisation of the their granulometric composition, taking into account their bimodal particle size distribution by volume and surface area. Moreover, the article presents the technical, environmental and economic benefits of using eco-efficient blended cements.

Keywords: eco-efficient blended cements, supplementary cementitious materials, superfine zeolite, particle size distribution, synergistic combination additives

1. Introduction

Integrated solutions for the cement industry to provide low carbon development strategies are aimed at reducing energy consumption, as well as at improvement of technology and better environmental policy. The release of high-tech products in the construction industry, taking into account the reduction of the degree of environmental pollution, is largely realised by the introduction of eco-efficient (low-CO₂) cements. According to the Roadmap “The role of cement in the 2050 low carbon economy” for the Cement Sector of the EU, by 2050, the cement carbon footprint could be reduced by 32% compared with 1990 levels, using mostly conventional means. The use of SCMs in cement production has a positive effect on the economic aspect of production and, what is extremely important, is a significant factor in improving the state of the environment [1-3].

The global average clinker content in 2014 was 0.65. Reducing this indicator is technically feasible, but the availability of suitable supplementary cementitious materials in a given region may be a limiting factor. However, in the process of cement production, an important problem is the creation of suitable combinations of clinker with mineral constituents whose characteristics will increase the effectiveness of cements. Most cement plants use granulated blast furnace slag and fly ash as active mineral additives, and limestone as microfiller [4]. At the same time, blended cements based on them, as a rule, have an increased water demand, bleeding, and are characterised by low early strength. It should also be noted that in the coming years a shortage of high-quality granulated blast furnace slag is expected in the cement industry. Some countries have limited resources of these components, which is why cement plants are making efforts to find new types of blended cements with high volume of SCMs. This determines the need for new combinations of SCMs, including those containing natural and industrial pozzolans.

The high dispersity of low-calcium fly ash and the appropriate chemical composition contribute to its widespread use in the cement industry as SCMs, but fly ash-containing cements are usually characterised by low early strength. The European Region has rich resources of natural pozzolanic material – zeolite tuffs, which can be a good solution to this problem. Using zeolite tuff as a partial replacement for Portland cement clinker leads to economic benefits and an increase of durability [5]. However, zeolite tuffs need more water to obtain a paste of the same consistency as for CEM I. Therefore, such an additive can adversely affect a number of mechanical properties of concrete, since the early strength of blended cements usually decreases. Investigation of mechanical properties of concretes incorporating natural zeolite has shown that the substitution of cement by zeolite results in some reduction of strength until 90 days of hardening, but after 180 days compressive strength of such concrete exceeds the strength of concrete without zeolite [6]. It should be noted that in this study the natural zeolite was characterised by bimodal PSD curve and dominating grain in the range of 90-2000 μm , with the largest share of particles of 300 μm . At the same time, using superfine zeolite is really promising, as it can increase the packing density, improve the workability and cohesion of the cement paste [7].

Rational usage of material and energy resources with a simultaneous decrease in the negative impact on the environment in construction is largely ensured by developing an approach based on the principles of constructing multicomponent cements [8, 9]. The synergistic effect of SCMs which exhibit various types of actions has a positive impact on the properties of blended cements compared to cements containing only one type of SCMs. Insignificant development of production of multicomponent binders with high volume of SCMs is associated with insufficient practical experience in the application of these cements in concrete technology [10]. The result of these efforts, according to the cement standard EN 197-1, is the wider introduction of composite cement CEM V/A and pozzolanic cement CEM IV/B, which are characterised by a significantly reduced amount of Portland clinker. Such eco-efficient blended cements will become an alternative for traditional, commonly used cements. This paper presents the results of research into blended cements containing high volume of supplementary cementitious materials, which confirm the relevance of further development of blended cements with low-CO₂ footprint.

2. Materials and methods of research

2.1. Materials

Commercially available Ordinary Portland cement (OPC) CEM I 42.5R, composed of C₃S: 62.42, C₂S: 13.62, C₃A: 7.06, C₄AF: 12.32, wt.%, was used as the reference cement in the

investigation. Ground granulated blast furnace slag (GGBFS) Kryvyi Rih, (glassy phase – 80%), consisting of 92-96 wt.% CaO + SiO₂ + Al₂O₃ + Fe₂O₃, fine (FZ) and superfine (SFZ) zeolites with 70.5 wt.% SiO₂ provided from Sokyrnytsky quarry were utilised as SCMs. Clinoptilolite [(Na₄K₄)(Al₈Si₄₀O₉₆)·24H₂O] content in natural zeolite tuff was 60%. Siliceous fly ash (FA) from Burshtyn TPP with SiO₂ and CaO content of 55.18% and 2.23% respectively was used. Limestone powder with 95 wt.% CaCO₃, 40.14 wt.% LOI was used as microfiller. Limestone powder belongs to the LL type according to the EN 197-1 in terms of total content of organic carbon. The chemical composition of the main components of the cement is presented in Tab. 1.

Table 1. The chemical composition of main constituents of cement. Source: own study

Components	Oxide content, wt.%							
	CaO	SiO ₂	Al ₂ O ₃	Fe ₂ O ₃	MgO	K ₂ O	Na ₂ O	SO ₃
CEM I 42.5 R	66.83	20.93	5.13	4.28	0.80	1.14	0.05	0.84
GGBFS	48.10	39.26	6.55	0.82	3.45	0.31	0.33	1.18
Zeolite tuff	1.63	76.92	12.95	3.95	0.18	3.68	0.53	0.16
Fly ash	2.23	55.18	24.21	12.17	2.01	2.57	0.61	1.02
Limestone powder	49.86	6.71	2.14	0.31	0.38	0.32	0.00	0.14

The Blaine specific surface area of OPC, GGBFS, FZ, SFZ, FA and LL is 3460; 4000, 6000, 12000, 4300 and 9600 cm²/g respectively. The particle size distributions of OPC and SMCs are presented in Tab. 2. It can be seen that volume average diameter D[4;3] for OPC is 24.8 μm and for SCMs – 19.3...48.7 μm. The maximum of average diameter D[3;2] by the specific surface distribution for SFZ is 4.24 μm, for OPC – 5.21 μm and for other SCMs – 5.42...11.0 μm. It should be noted that superfine zeolite and limestone powder are characterised by a bimodal particle size distribution by volume.

Table 2. The granulometric composition of OPC and SCMs. Source: own study

Components	Ø <5 μm, %	Ø <10 μm, %	Ø <20 μm %	Ø <60 μm, %	D[3;2] μm	D[4;3] μm	Dv (10) μm	Dv (50) μm	Dv (90) μm
OPC	21.86	37.46	60.41	97.52	5.21	24.8	2.76	18.1	56.5
GGBFS	27.04	47.21	66.01	93.45	5.42	19.3	2.24	10.9	50.2
FZ	14.21	23.87	37.49	69.85	11.0	47.3	3.68	32.7	115.0
SFZ	34.58	48.86	68.79	90.67	4.24	21.2	1.53	11.2	55.6
FA	16.98	33.74	52.88	85.28	7.21	21.8	3.10	15.6	50.0
LL	25.71	35.72	45.15	65.79	7.08	48.7	2.29	28.7	128.0

Blends of OPC with GGBFS-SFZ-LL and OPC with SFZ-FA were prepared by mixing in a laboratory ball mill to produce CEM V/A and CEM IV/B cement types with high volume of SCMs according to EN 197-1.

2.2. Methods

The study of fractional composition and grinding fineness of the cements was carried out by sieve analysis and by determination of the specific surface areas with the Blaine method. The Mastersizer 3000 uses the technique of laser diffraction to measure the particles size distribution by volume. At the same time, using the specially developed methodology [11], differential coefficient of particle size distribution by surface area, K_{isa} , was calculated. It is

determined by the product A/V (the ratio of the surface area of the particles to their volume) for the content of each material fraction. This coefficient makes it possible to determine the degree of particles' additional active interphase surface. The phase composition of the resulting products was determined by X-ray powder diffraction. Scanning electron microscope Philips XL30 ESEM-FEG was used for studying morphology of the cement paste.

Determination of the workability of fresh cement mortars (consistence by flow table) was carried out according to EN 1015-3. Two samples of fresh mortar were investigated and the average value was determined, since the difference between them did not exceed 10%. The compressive strength data of the blended cements was determined on 40x40x160 mm mortar prisms after 2; 7; 28 and 90 days with water/cement ratio of 0.50 according to EN 196-1. Specimens were cured in moulds for 24 h in controlled temperature and humidity conditions. After extraction from moulds and labelling, the samples were placed in water for storage before testing.

The bleeding of cements was measured by the cylinder method and was determined according to the Ukrainian national standard DSTU B V. 2.7-186:2009. The evaluation of the pozzolanic activity of the SCMs was carried out by testing the ability of the mineral additive to absorb $\text{Ca}(\text{OH})_2$ from its saturated solution. In this case, the criterion was the amount of absorbed $\text{Ca}(\text{OH})_2$ (in mg) with 1 g of mineral additive.

3. Research results

For the development of blended cements, a complex assessment of the dispersion of mineral components and water demand was carried out. Ultrafine SCMs are characterised by a highly developed specific surface area that causes an increase of water demand. Water demand is particularly high for mineral additives of sedimentary origin (zeolite). For GGBFS and FA, water demand is 22 and 27% respectively; SFZ is characterised by the highest water demand – 55%. For limestone powder, water demand is 24%. As can be seen from Fig. 1, combinations of SCMs of various genesis and fineness, namely those that exhibit hydraulic action (blast furnace granulated slag), pozzolanic action (fly ash, superfine zeolite), and micro-filler (limestone powder), can ensure an acceptable level of water demand ($\text{WD} \leq 30\%$). At the same time, superfine zeolite, due to the features of the crystalline structure of clinoptilolite and high surface area to volume ratio, can noticeably decrease liquidity and cause difficulties in achieving a desired blend of workability.

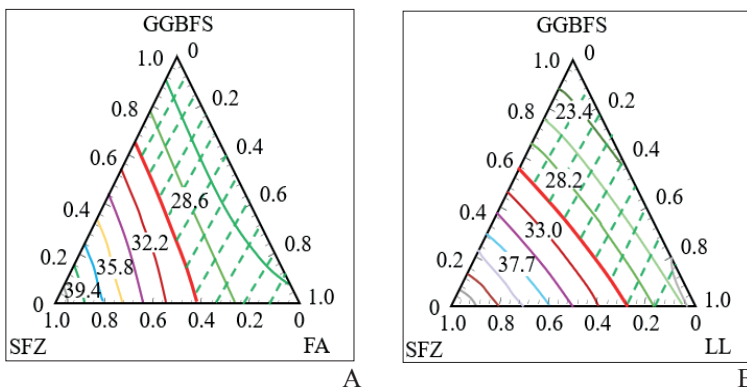


Fig. 1. The impact of additives on the water demand of SCMs blends in the GGBFS-SFZ-FA (a) and GGBFS-SFZ-LL (b) systems. Source: own study

The GGBFS and FA are characterised by high bleeding – after 120 minutes, bleeding coefficients (K_{vol}) are 27.1 and 39.7% respectively (Fig. 2). At the same time, FZ and SFZ are characterised by the lowest bleeding coefficient ($K_{vol} = 2.0-3.3\%$). For limestone powder, bleeding coefficient is 24.1% after 120 min. The suspension with the addition of SFZ is the most stable – after 2 h, the level of bleeding does not change. The combined use of SCMs such as GGBFS, SFZ, FA and LL with different genesis and properties reduces bleeding of the blends (acceptable level of less than 18%).

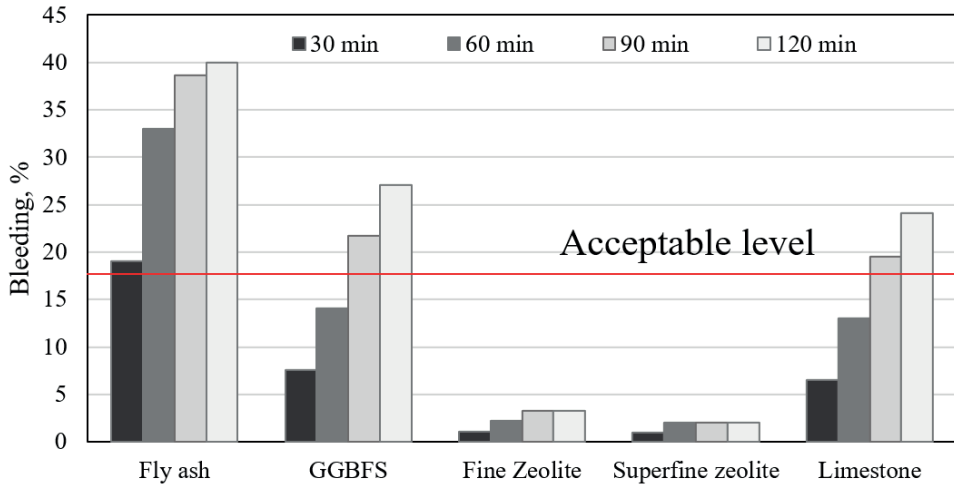


Fig. 2. The bleeding of SCMs. Source: own study

The reactivity of SCMs was determined by the method of lime absorption by the additive from a lime solution (Fig. 3). As demonstrated, SFZ is characterised by the highest pozzolanic activity (after 30 and 38 days – 192 and 230 mg CaO/g respectively). At the same time, pozzolanic activity for fly ash is the lowest and amounts to 30 and 42 mg CaO/g respectively after 30 and 38 days. GGBFS after 30 days has such reactivity as SFZ after 10 days, that is 3 times lower.

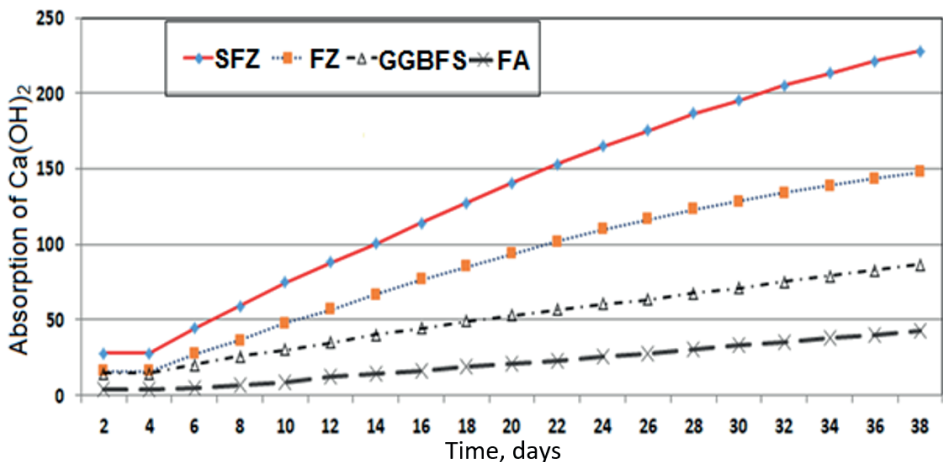


Fig. 3. The absorption kinetics of Ca(OH)_2 by SCMs. Source: own study

The impact of high volume of GGBFS, SFZ and LL additives on the physical and mechanical properties of blended cements was investigated. Results of the study into the consistency of fresh mortars determined by the flow table according to EN 1015-3 demonstrate (Fig. 4a) that an addition of SFZ significantly reduces the workability of blended cements, but limestone powder contributes to an increase in their workability. Compressive strength test results have shown (Fig. 4b) that the use of high volume of SCMs leads to a significant decrease in the strength of blended cements, especially at an early age.

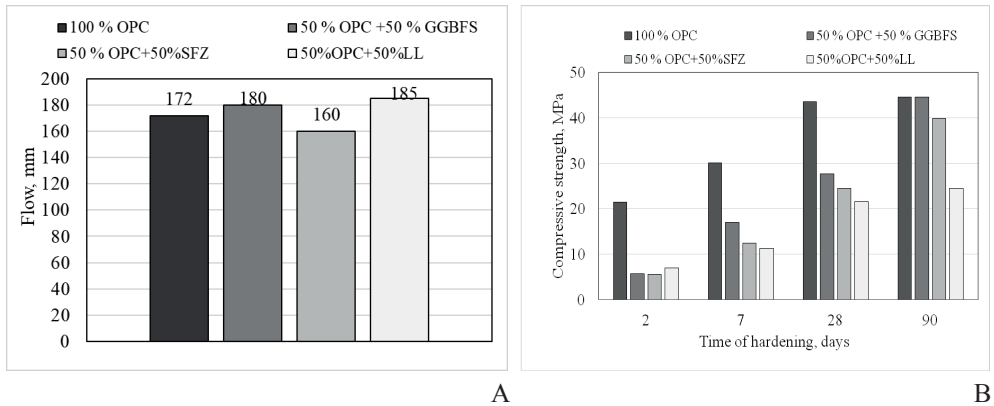


Fig. 4. The consistency of fresh mortars (a) and the compressive strength (b) of blended cements. Source: own study

The study of the influence of the ratio of the main components (GGBFS, SFZ and LL) on the properties of blended cements obtained by mixing 50 wt.% SCMs and 50 wt.% CEM I was carried out by the method of mathematical planning in accordance with the plan of a two-factor three-level experiment. Based on the isoparametric lines of SCMs' influence on the strength of multi-composite CEM V/A-type cements at 2 and 28 days, it was established that the optimal balance between non-clinker constituents is 25 wt.% GGBFS, 18 wt.% SFZ and 7 wt.% LL, with the compressive strength at 2 and 28 days amounting to 11.4 MPa and 38.5 MPa respectively. According to EN 197-1, this composition complies with CEM V/A 32.5.

In order to increase the effectiveness of quaternary composite cements CEM V/A, mechanical activation was performed in a vibration mill. According to the particle size distribution by volume of such mechanically activated composite cement ($SSA=7210 \text{ cm}^2/\text{g}$) fractions $\emptyset 1$; $\emptyset 5$; $\emptyset 10$ and $\emptyset 20 \text{ }\mu\text{m}$ constitute respectively 8.05; 29.77; 43.73 and 63.24%, and the grain size d_{10} ; d_{50} and d_{90} corresponds to 2.05; 18.2 and 61.7 μm (Fig. 5a). To assess the contribution of individual particles to total specific surface area, particle size distributions by surface area were calculated and an incremental coefficient of surface area (K_{isa}) was suggested. The maximum value of K_{isa} (8.72 $\mu\text{m}^{-1}\cdot\text{vol.}\%$) for composite cement was achieved for the fraction of 0.35 μm , and for the fraction of 5.0 μm this coefficient decreases by 2.9 times; with a further increase in particle size, it is significantly reduced (Fig. 5b).

It is demonstrated that the superfine fraction of up to $\emptyset=1.0 \text{ }\mu\text{m}$, despite its small content ($V = 8.05\%$), makes a significant contribution (up to 50%) to the specific surface area of mechanically activated composite cement. Such quaternary composite cement is characterised by a significant reserve of excess surface energy, primarily due to ultrafine particles of superfine

zeolite and limestone powder. The high level of excess surface energy of CEM V/A cement leads to an increase of its hydration rate at an early age of hardening.

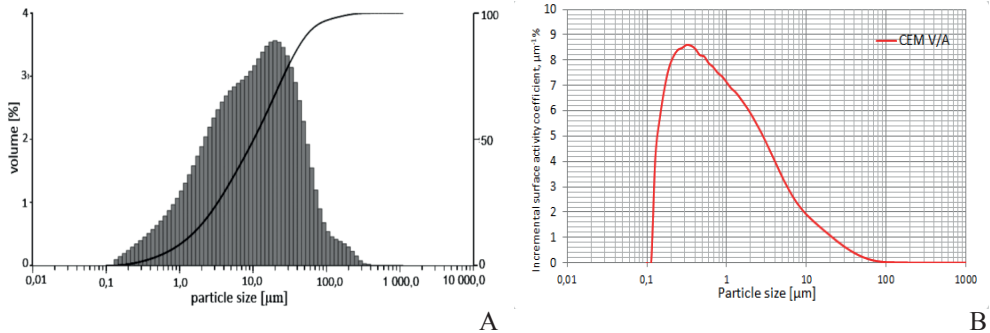


Fig. 5. The particle size distribution by volume (a) and surface area (b) of mechanically activated composite cement CEM V/A. Source: own study

As can be seen from Fig. 6, the flow of fresh mortar based on mechanically activated CEM V/A is 183 mm and the compressive strength of tested mortars after 2, 28 and 90 days of hardening is 17.5, 46.2 and 57.4 MPa respectively. Such composite cement corresponds to the class 42.5 of CEM V/A according to EN 197-1. Polycarboxylate ether superplasticizer PCE (1.0%) was added to obtain composite cements CEM V/A with improved properties. In this case, due to the addition of PCE, the flow of fresh mortar increased by 68% (technological effect). On the other hand, due to the reduction of water-cement ratio ($\Delta W/C = 38\%$), the strength after 2, 7, 28 and 90 days increased by 53, 76, 46 and 36%, respectively (technical effect). Thus, such a composite cement CEM V/A is characterised by high early strength and a significant increase in strength (over 70 MPa) after 28 days of hardening.

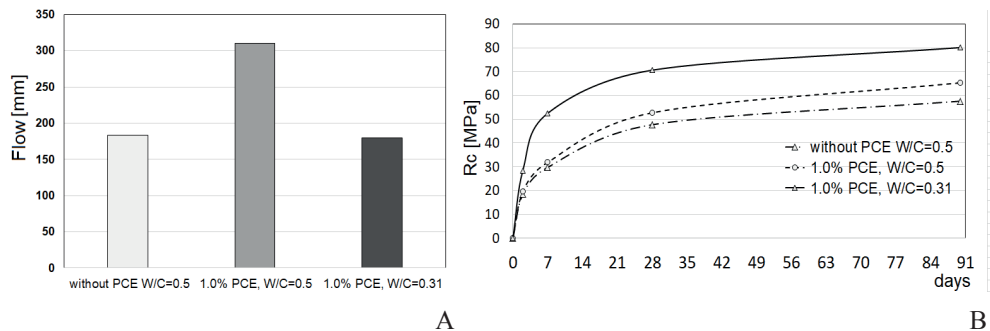


Fig. 6. The influence of PCE on workability (a) and compressive strength (b) of CEM V/A. Source: own study

The phase composition of hydration products of the CEM V/A paste ($W/C = 0.50$) after 28 days of hardening is represented by ettringite (4.39 wt.%) and a small amount of portlandite (3.64 wt.%). Amorphous C-S-H phase content is 53.9 wt.%. According to the SEM data, the crystalline structures of ettringite, calcium hydroaluminates, portlandite and calcium hydrosilicates form a dense structure of cement paste (Fig. 7). The use of pozzolanic additives with high pozzolanic activity promotes fuller binding of calcium hydroxide in calcium hydrosili-

cates and significantly affects the ultimate compressive strength, permeability and chemical durability of composite cements. Using superfine zeolite is needed to enhance the hydrolysing ability of the zeolite mineral – clinoptilolite. The increased pH value and the transition to the liquid phase of Na^+ ions create the necessary conditions for the alkaline activation of blast furnace granulated slag as part of modified composite cement, which allows for achieving the required early and standard strength.

A synergetic combination of superfine zeolite as a highly reactive natural pozzolan and limestone powder as a microfiller in composite cement CEM V/A 42.5 ensures the formation of dense microstructure of paste and increases its strength. In addition to the environmental benefits generated by the use of high content of SCMs as a substitute for cement, the obtained results reveal a significant long-term improvement in strength properties and durability performance of composite cements. Superfine zeolite, which is characterised by high surface area, contributes to the intensification of the processes of structure formation in the early period of hydration.

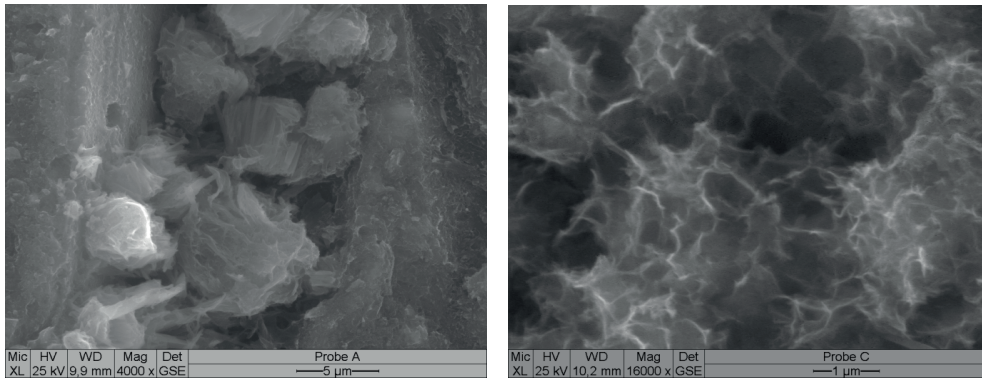


Fig. 7. SEM images of paste based on composite cement CEM V/A 42.5 after 28 days of hardening. Source: own study

High value of SFZ pozzolanic activity in the form of absorption of CaO and CaSO_4 results in the intensive binding of $\text{Ca}(\text{OH})_2$ into calcium hydrosilicates and hydrosulfoaluminates. The surface of limestone particles provides excellent conditions for the nucleation and growth of nanodispersed C-S-H(I) gel, which causes a higher total volume of hydrates and lower porosity whereby higher compressive strength is reached. The clinker factor decreased to 0.50 in CEM V/A reduces the CO_2 emission in the cement production process by 50% per 1 tonne of cement.

Note that for regions deficient in GGBFS, an effective solution to reducing the clinker factor of blended cement is the production of pozzolanic cement CEM IV/B, containing blends of different types of pozzolans such as superfine zeolite and siliceous fly ash. In this case, SFZ has the decisive influence on bleeding and reactivity, while FA decreases water demand due to its spherical particles, as this increases the mobility of the mixture (“roller bearing effect”). On the other hand, a combination of natural (SFZ) and industrial (FA) pozzolans with opposite properties regarding water demand and bleeding makes it possible to improve the workability of the mixtures based on pozzolanic cement CEM IV/B [12, 13].

It is noteworthy that the compressive strength of the ternary pozzolanic cement CEM IV/B (50 wt.% CEM I 42.5 R; 27 wt.% SZ, 23 wt.% FA) exceeded the strength of slag cement

CEM III/A. At the age of hardening, the difference in strength between CEM IV/B and ordinary Portland cement CEM I decreased and the strength activity index of CEM IV/B became higher after 90 days. Power consumption for grinding CEM IV/B is reduced to 31 kWh. The carbon footprint of the products of CEM IV/B is 458 kg of CO₂ per 1 tonne of cement, which is 47% less than in the case of ordinary Portland cement CEM I 42.5 [3, 14].

4. Conclusions

Eco-efficient blended cements with high volume of SCMs are an optimal solution to the problem of improving the energy saving of cement production. The strategy of such development involves combining highly reactive SCMs of different fineness and genesis and with hydraulic and pozzolanic properties with micro-fillers. This helps to reduce the clinker factor. This approach also involves technological optimisation of cement properties (workability, standard and early strength, durability, cost, environmental impact).

Innovative binders (clinker factor – 0.50) which have a combination of the above-mentioned properties are quaternary composite cements CEM V/A, containing granulated blast furnace slag, superfine zeolite and limestone powder, and ternary pozzolanic cement CEM IV/B, containing superfine zeolite and fly ash. The production of eco-efficient blended cements with high volume of SCMs of different genesis and fineness meets the principles of the strategy of sustainable development and is a practical solution to the problem of reducing costs, power consumption and CO₂ emissions in the construction industry.

References

- [1] CEMBUREAU. *The role of cement in the 2050 low carbon economy*, (2013), p. 64.
- [2] Schneider M., “The cement industry on the way to a low-carbon future”, *Cement and Concrete Research*, vol. 124, (2019), pp. 1-19. <https://doi.org/10.1016/j.cemconres.2019.105792>
- [3] Scrivener K. L. et al., *Eco-efficient cements: Potential economically viable solutions for a low-CO₂ cement-based materials industry*. Paris: UN Environment Economy Division, 2017, p. 49. <https://doi.org/10.25561/51016>
- [4] Giergiczny Z., “Fly ash and slag”, *Cement and Concrete Research*, vol. 124, (2019), pp. 1-18. <https://doi.org/10.1016/j.cemconres.2019.105826>
- [5] Janotka I., Krajci L., Dzivak M. “Properties and utilization of zeolite-blended Portland cements”, *Clay and Clay Minerals*, vol. 51, no. 6, (2003), pp. 616-624. <http://dx.doi.org/10.1346/CCMN.2003.0510606>
- [6] Markiv T. et al., “Mechanical and durability properties of concretes incorporating natural zeolite”, *Archives of Civil and Mechanical Engineering*, vol. 16, no. 4, (2016), pp. 554-562. <https://doi.org/10.1016/j.acme.2016.03.013>
- [7] Chen J. J. et al., “Effects of superfine zeolite on strength, flowability and cohesiveness of cementitious paste”, *Cement and Concrete Composites*, vol. 83, (2017), pp. 101–110. <https://doi.org/10.1016/j.cemconcomp.2017.06.010>
- [8] Schöler A. et al., “Hydration of quaternary Portland cement blends containing blast-furnace slag, siliceous fly ash and limestone powder”, *Cement and Concrete Composites*, vol. 55, (2014), pp. 374-382. <https://doi.org/10.1016/j.cemconcomp.2014.10.001>
- [9] Sanytsky M. et al., “Design of rapid hardening quaternary zeolite-containing Portland-composite cement”, *Key Engineering Materials*, vol. 761, (2018), pp. 193-196. <https://doi.org/10.4028/www.scientific.net/KEM.761.193>

- [10] Gerd B. et al, “Development of composite cements characterized by low environmental footprint”, *Journal of Cleaner Production*, vol. 226, (2019), pp. 503–514. <https://doi.org/10.1016/j.jclepro.2019.04.050>
- [11] Sanytsky M. et al., “Effect of the Particle Surface Distribution on the Reactivity of Supplementary Cementitious Materials in Blended Cements”, in Book of abstracts ICCI, 2019, p. 188.
- [12] Ivashchyshyn H. et al., “Study of low-emission multi-component cements with a high content of supplementary cementitious materials”, *Eastern-European Journal of Enterprise Technologies*, vol. 4 no. 6, (2019), pp. 39-47. <https://doi.org/10.15587/1729-4061.2019.175472>
- [13] Kropyvnytska T., Sanytsky M., Rucinska T., Rykhlitska O. “Development of nanomodified rapid hardening clinker-efficient concretes based on Portland composite cements”, *Eastern-European Journal of Enterprise Technologies*, vol. 6 no. 6, (2019), pp. 38-48. <https://doi.org/10.15587/1729-4061.2019.185111>
- [14] Kline J. and Kline Ch. H. “Cement and CO₂: what’s happening” in IEEE-IAS/PCA Cement Industry Technical Conference 2014, 2014, pp. 1-9. <https://www.doi.org/10.1109/CITCon.2014.6820105>

Spectral analysis of multi-year GNSS code multipath time-series

Jacek Kudrys

*Faculty of Mining Surveying and Environmental Engineering;
AGH University of Science and Technology
jkudrys@agh.edu.pl; ORCID: 0000-0002-4986-7436*

Abstract: In the presented study multi-year time series of changes in the L1 pseudo-range multipath are analysed. Data from 8 stations of the EUREF Permanent Network (EPN) were used in the study. Periodic components present in the signal and their stability over time were analysed. Also, the type of background noise was determined, based on the spectral index. In some cases, the presence of weak components with a 1/2 and 1/3 of the Chandler period has also been found. Time-frequency analysis shows that periodic signals are not stationary in most of the examined cases, and particular signal components occur only temporarily. The analysed signals were characterised by pink noise in the lower frequency range and by white noise for higher frequencies, which is also characteristic for time series of coordinates obtained from GNSS measurements.

Keywords: GNSS, code multipath, spectral analysis, spectral index

Introduction

GNSS multipath is studied mainly as a source of errors affecting code and phase observations in positioning. The impact of multipath on GNSS data is widely analysed in both time and frequency domain [1][2][3]. The magnitude of the pseudo-range measurement error caused by multipath can be determined based on linear combinations of code and phase observations [4]. The impact of multipath on phase observations is estimated based on changes in signal power reaching the GNSS receiver (signal to noise ratio) [5][6][7].

The analysis of the multipath phenomenon applies, among others in GNSS reflectometry, where it is often used to study the change in the environment of the GNSS antenna. Periodic oscillations in the multipath are the basis for determining the change in the position of the surface reflecting the satellite signal about the phase centre of the antenna. Multipath oscillations analyses allow assessing changes in snow cover thickness [8], ocean surface [9][10], and soil moisture [11].

At EPN/IGS reference stations, indices of the multipath are routinely monitored [12] [13], with basic statistical parameters characterising the variability of the multipath for daily observations on individual carrier frequencies being mainly calculated. For this purpose, software such as G-Nut/Anubis [14] or teqc [15] is used.

Apart from short-term changes, the multipath is also characterised by seasonal variability, resulting from annual changes in vegetation, soil moisture, and snow or ice layer thickness. Therefore, when analysing the long time series of multipath, one should expect components with a period close to one year. Since the value of the error caused by multipath is also affected by the position of the antenna relative to reflecting obstacles, even small changes in the position of the antenna can also cause changes in indices describing the multipath.

In this work, multi-year time-series of indices characterising GNSS multipath for 8 European permanent stations belonging to the EPN/IGS network (Fig. 1) were analysed in terms of the occurrence of periodic components. The analysed time-series of L1 code multipath were obtained using freely available teqc software.

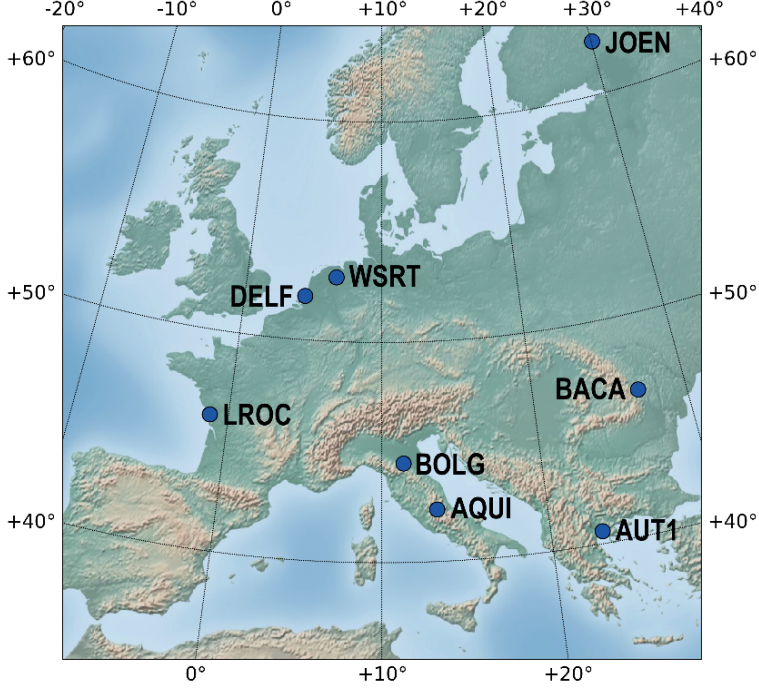


Fig. 1. Analysed EPN/IGS stations

Methodology

The multipath in code pseudoranges at L1 frequency is described by the value of the m_{p1} index, calculated as a linear combination of phase and code observations for a single epoch in accordance to the equation [15]:

$$m_{p1} = p_1 - \left(1 - \frac{2}{1-\beta}\right)\Phi_1 - \frac{2}{1-\beta}\Phi_2 \quad (1)$$

where:

m_{p1} – multiparty error,

p_1 – L1 pseudorange,

Φ_1 – L1 phase,

Φ_2 – L2 phase,

$\beta = (L1/L2)^2$.

The multi-year time series were created on the base of the root mean square of m_{p1} index from daily observations. The calculated value of m_{p1} depends on many factors. In addition to the phenomenon of interference of signals arriving in different ways, the m_{p1} is affected by changes caused by the replacement of the antenna, receiver or firmware upgrade. A change in the configuration of the measuring equipment can cause a jump in the value of m_{p1} as well as a change in the noise level or amplitude of the examined signal. There may also be data gaps in the time series due to the temporary inactivity of the reference station [12][13].

For research purposes, 8 permanent stations were selected from Europe (Fig. 1) with the longest continuous observation possible and the smallest number of changes in equipment in the analysed period. Data in RINEX format comes from the EUREF Permanent Network data centres, and daily RMS m_{p1} values have been calculated using teqc software.

The main goal of the research was to verify the occurrence of the characteristic periodic components in the m_{p1} times series. Before the spectral analysis, data preprocessing had to be carried out. For this purpose, the jumps in value, the linear trend and outliers ($> 5\sigma$) were removed from the obtained m_{p1} time series, which caused additional data gaps in the time series. Due to discontinuity in the observational data, the method of Lomb-Scargle periodogram was used. This method is effective for spectrum analysis in the case of non-evenly data sampling [16] [17]. The existence of predetermined periodic components in the signal has not been assumed in the paper. Based on the spectrum obtained, the presence of components with the tropical year period (356.25 days) and the Chandler wobble period (433 days) and their three subsequent harmonics were verified.

For GNSS observations, the time series of coordinates are most often analysed [18]. Based on the power-law $P \propto f^k$, where P is power spectral density, f is the frequency and k spectral index, it can be shown that in this type of observation, background noise is a combination of pink noise and white noise [19][20].

In this work, for the background noise determination, the spectral index k was estimated based on fitting a straight line to the power spectral density expressed on a logarithmic scale. The verification of stationarity in the frequency domain was performed with wavelet transform, a widely used tool for the characterisation of frequency variations in the signal [21] that preserves information on both the time and frequency of the signal. Individual harmonics in the examined time series were analysed using the continuous wavelet time-frequency spectrum with a complex Morlet wavelet.

Table 1. m_{p1} time-series statistics

station	m_{p1} time series statistics					amplitude of harmonics of annular period				spectral indices	
	time span [y]	epochs	mp1 min [m]	mp1 max [m]	percent of original observ.	1 [mm]	1/2 [mm]	1/3 [mm]	1/4 [mm]	k1	k2
AQUI	14.6	4826	-0.037	0.057	77%	8	4	-	-	-0.53	-0.75
AUT1	14.5	2879	-0.238	0.269	93%	20	23	9	-	-0.69	-0.25
BACA	13.7	4650	-0.178	0.234	97%	9	11	-	-	-0.81	-0.02
BOLG	13.5	4554	-0.095	0.155	85%	17	4	5	-	-1.02	-0.30
DELf	15.4	5363	-0.081	0.124	95%	27	4	5	-	-1.38	-0.33
JOEN	20.6	7011	-0.017	0.136	96%	13	13	5	6	-0.84	-0.66
LROC	13.2	4236	-0.074	0.126	74%	8	3	-	-	-0.96	-0.30
WSRT	19.7	7041	-0.082	0.106	97%	13	4	4	-	-1.33	-0.62

Results

The studied RMS m_{p1} time series covered a period from 13.2 to 20.6 years. At the preprocessing stage, some outliers were removed from the time series obtained directly as a result of the calculations (eq. 1). Depending on the permanent station, between 3% and 26% of the original data was deleted. Based on spectral analysis, the occurrence of annual components was determined at the significance level of 95%. In the case of the BACA, BOLG, DELF and WSRT stations, in addition to the annual component and its higher harmonics, weak signals of 1/2 or 1/3 of the Chandler period are visible (Fig. 3). These weak signals of small amplitude, which appeared in the m_{p1} spectrum require further research. The summary of data regarding the time series for each permanent station tested are presented in Table 1.

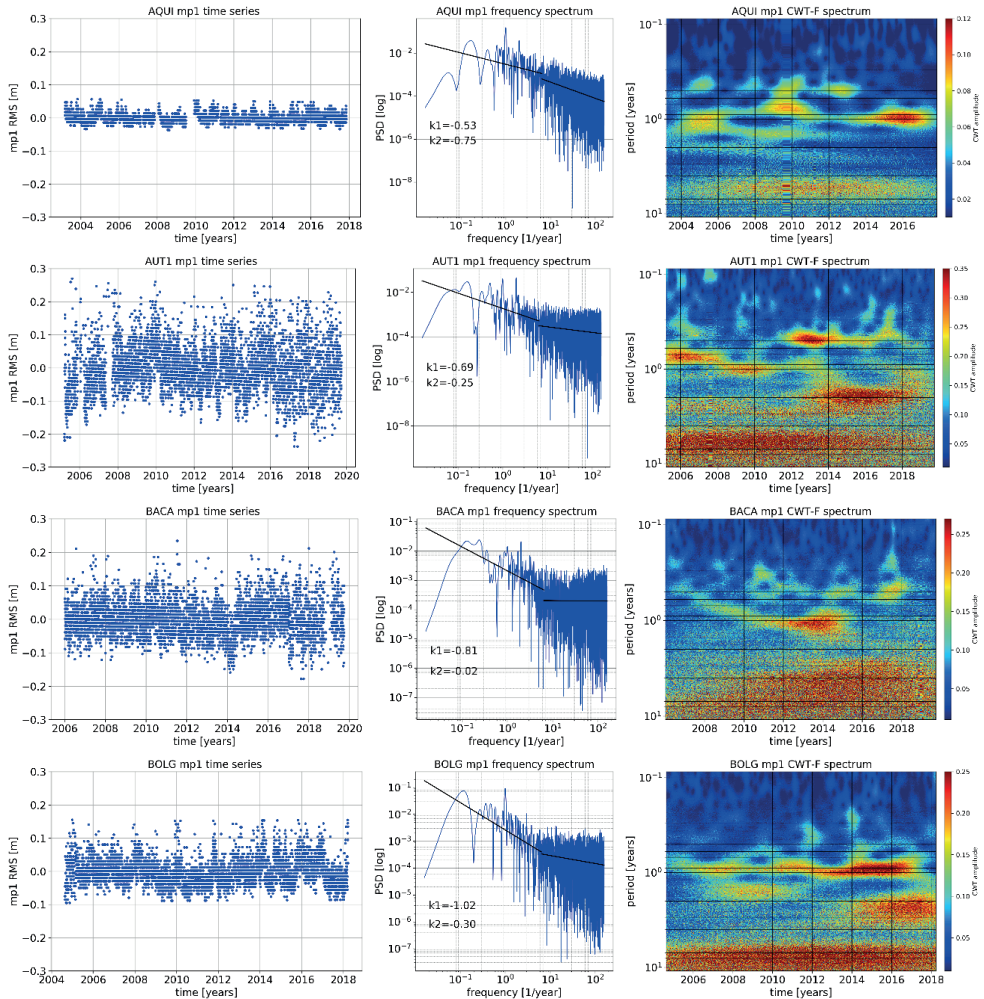


Fig. 2a. Time series of RMS of m_{p1} parameter (left column), frequency spectrum with spectrum indices (middle column) and continuous wavelet time-frequency spectrum (right column) for 4 GNSS stations AQU1, AUT1, BACA and BOLG

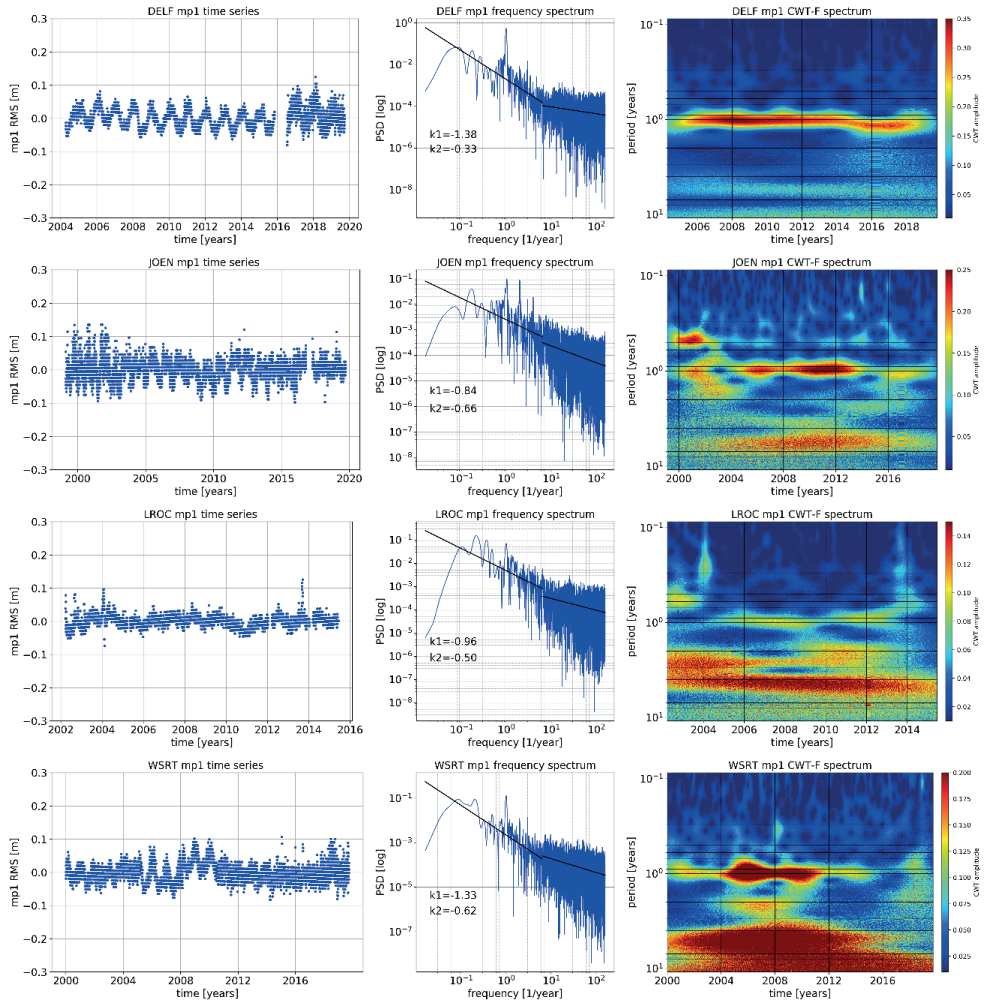


Fig. 2b. Time series of RMS of m_{p1} parameter (left column), frequency spectrum with spectrum indices (middle column) and continuous wavelet time-frequency spectrum (right column) for 4 GNSS stations DELF, JOEN, LROC and WSRT

All the analysed stations show power-law behaviour in the entire spectrum. It was estimated a corner frequency equals 6 cycles per year (cpy) between the low-frequency part where pink noise appears and the higher frequency with dominating uncorrelated white noise. Spectral indices $k1$ and $k2$ were calculated, by dividing the frequency range into two parts, relative to the corner frequency: $k1$ – below 6 cpy and $k2$ – above 6 cpy (middle column in Figures 2a and 2b). In most cases, the background noise in the low-frequency part of the spectrum is close to pink noise, and as the frequency increases, the noise character becomes white noise ($-1.5 < k1 < -0.5 < k2$). For the AQU1 and JOEN stations, pink noise is dominant in the entire frequency range. Table 1 summarises the values of spectral indices $k1$ and $k2$ for the permanent stations analysed.

Time-frequency analysis clearly shows the non-stationarity of long-term multipath changes. In most of the analysed cases, components with an annual period and its higher harmonics appear only in a part of the examined time interval (Fig. 2a and 2b – right column). It may be the result of changes in the station's equipment configuration or changes in the close vicinity of the antenna. Determining precisely the cause of the change in the multipath effect is difficult because not all events that may affect this factor are recorded in the station's logs. For example, for the AQUI stations, the dominant annual component is visible in 2004-2006, 2009-2011 and 2014-2019. In the case of the WSRT station, a strong annual signal appears in the years 2004-2012. Only for the DELF stations, where the antenna and the receiver remain unchanged for the majority of the analysed time interval (2004-2015), can a constant, clear annual component be seen. After changing the antenna at the DELF station in 2015, the correlated change in the time-frequency spectrum is visible.

Conclusions

The time series of the m_{p1} parameter describing the signal's multipath in the observed L1 code was analysed. For the analysis 8 GNSS permanent stations from Europe were chosen. The frequency spectrum obtained with the Lomb-Scargle periodogram indicates the presence of 1 cpy frequency components and some higher harmonics. In the signal spectrum from several reference stations, the second and third harmonic of the Chandler frequency are also visible. The annual component has been expected because it reflects seasonal changes in the vicinity of the GNSS antenna. The occurrence of the Chandler wobble period in the m_{p1} time series requires detailed research. Background noise in the obtained spectrum can be described as pink noise for lower frequencies and white noise for frequencies above 6 cpy. A similar distribution of noise in the spectrum is also characteristic for GNSS coordinate time series. Time-frequency analysis allows confirming non-stationarity and high variability of signal parameters over time. It is caused mainly by the equipment replacement in the reference stations and modification of the operating parameters of the receivers.

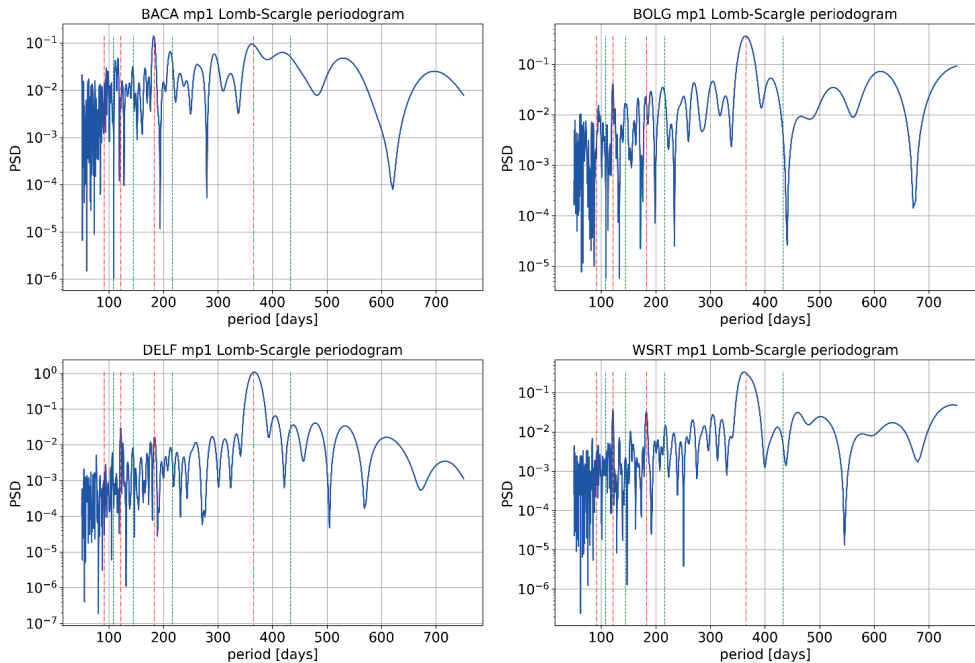


Fig. 3. Periodograms of RMS of daily m_{p1} parameter for the BACA, BOLG, DELF and WSRT stations. Orange (dash-dot) vertical lines correspond to the yearly period and its first three harmonics. Green (dash) vertical lines correspond to the Chandler wobble period and its first three harmonics

Acknowledgements

This work has been supported by AGH-UST statutory research no 16.16.150.545. Calculations were made with NumPy [22], Pandas [23] and PyWavelets [24] Python packages. The Figures were prepared with Python Matplotlib Library [25].

References

- [1] Yang, C., & Porter, A., “Frequency-domain characterization of GPS multipath for estimation and mitigation”, in *Proceedings of the 18th International Technical Meeting of the Satellite Division of The Institute of Navigation*, ION GNSS 2005, 2005, pp. 2104–2118.
- [2] Kong, X., “GPS modeling in frequency domain”, in *The 2nd International Conference on Wireless Broadband and Ultra Wideband Communications*, AusWireless 2007. <https://doi.org/10.1109/AUSWIRELESS.2007.36>
- [3] Zuo, X., Bu, J., Li, X., Chang, J., & Li, X., “The quality analysis of GNSS satellite positioning data”, *Cluster Computing*, 22, 2019, pp. 6693–6708. <https://doi.org/10.1007/s10586-018-2524-1>
- [4] Breivik, K., Forssell, B., Kee, C., Enge, P., & Walter, T., “Estimation of multipath error in GPS pseudorange measurements”. *Navigation, Journal of the Institute of Navigation*, vol. 44(1), 2019, pp.43–52. <https://doi.org/10.1002/j.2161-4296.1997.tb01938.x>
- [5] Rost, C., & Wanninger, L. “Carrier phase multipath mitigation based on GNSS signal quality measurements”, *Journal of Applied Geodesy*, 3(2), 2009. <https://doi.org/10.1515/jag.2009.009>
- [6] Axelrad, P., Comp, C., & MacDoran, P., “Use of signal-to-noise ratio for multipath error correction in GPS differential phase measurements: methodology and experimental results”, in *Proceedings of ION GPS*, 1, 1994, pp. 655–666.

-
- [7] Bilich, A., & Larson, K. M., “Mapping the GPS multipath environment using the signal-to-noise ratio (SNR)”. *Radio Science*, 42(6), 2007. <https://doi.org/10.1029/2007RS003652>
- [8] Yu, K., Ban, W., Zhang, X., & Yu, X., “Snow depth estimation based on multipath phase combination of GPS triple-frequency signals”. *IEEE Transactions on Geoscience and Remote Sensing*, vol. 53(9), 2015, pp. 5100–5109. <https://doi.org/10.1109/TGRS.2015.2417214>
- [9] Komjathy, A., Armatys, M., Masters, D., Axelrad, P., Zavorotny, V., & Katzberg, S., “Retrieval of ocean surface wind speed and wind direction using reflected GPS signals”, *Journal of Atmospheric and Oceanic Technology*, vol. 21(3), 2004, pp. 515–526. [https://doi.org/10.1175/1520-0426\(2004\)021<0515:ROOSWS>2.0.CO;2](https://doi.org/10.1175/1520-0426(2004)021<0515:ROOSWS>2.0.CO;2)
- [10] Kim, S. K., & Park, J., “Monitoring sea level change in arctic using GNSS-reflectometry”, in *ION 2019 International Technical Meeting Proceedings*, 2019, pp. 665–675. <https://doi.org/10.33012/2019.16717>
- [11] Chang, X., Jin, T., Yu, K., Li, Y., Li, J., & Zhang, Q., “Soil moisture estimation by GNSS multipath signal”. *Remote Sensing*, vol. 11, 1st November 2019. <https://doi.org/10.3390/rs11212559>
- [12] “EUREF Permanent GNSS Network”. Available: <http://epncb.eu/> [Accessed: 05 Jan 2020]
- [13] “International GNSS Service”. Available: <http://www.igs.org/> [Accessed: 05 Jan 2020]
- [14] Vaclavovic, P., & Dousa, J., “G-Nut/Anubis – open-source tool for multi-GNSS data monitoring”, in: *IAG Symposia Series*, Springer, vol. 143, 2016, pp. 775–782. https://doi.org/10.1007/1345_2015_157
- [15] Estey, L. H., & Meertens, C. M., “TEQC: The Multi-Purpose Toolkit for GPS/GLONASS Data”, *GPS Solutions*, 3(1), 1999, pp. 42–49. <https://doi.org/10.1007/PL00012778>
- [16] Lomb, N. R., “Least-squares frequency analysis of unequally spaced data”. *Astrophysics and Space Science*, 39(2), 1976, pp. 447–462. <https://doi.org/10.1007/BF00648343>
- [17] Scargle, J. D., “Studies in astronomical time series analysis. II – Statistical aspects of spectral analysis of unevenly spaced data”, *The Astrophysical Journal*, 263, 1982, p. 835. <https://doi.org/10.1086/160554>
- [18] Klos, A., Bogusz, J., Bos, M. S., & Gruszczynska, M., “Different Approaches to Extract Seasonal Signals” in *Modelling the GNSS Time Series*. Springer International Publishing, 2020. https://doi.org/10.1007/978-3-030-21718-1_7
- [19] Bogusz, J., & Klos, A., “On the significance of periodic signals in noise analysis of GPS station coordinates time series”. *GPS Solutions*, 20(4), 2016, pp. 655–664. <https://doi.org/10.1007/s10291-015-0478-9>
- [20] Ray, J. D., Vijayan, M. S. M., Godah, W., & Kumar, A., “Investigation of background noise in the GNSS position time series using spectral analysis – A case study of Nepal Himalaya”. *Geodesy and Cartography*, 68(2), 2019, pp. 375–388. <https://doi.org/10.24425/gac.2019.128468>
- [21] Torrence Christopher, & P. Compo Gilbert., “A Practical Guide to Wavelet Analysis”. *Bulletin of the American Meteorological Society*, 137(2), 1998, pp. 87–92. [https://doi.org/10.1175/1520-0477\(1998\)079<0061:APGTWA>2.0.CO;2](https://doi.org/10.1175/1520-0477(1998)079<0061:APGTWA>2.0.CO;2)
- [22] Stéfan van der Walt, S. Chris Colbert and Gaël Varoquaux, “The NumPy Array: A Structure for Efficient Numerical Computation”, *Computing in Science & Engineering*, 13, 2011, pp. 22–30, <https://doi.org/10.1109/MCSE.2011.37>
- [23] Wes McKinney, “Data Structures for Statistical Computing in Python”, in *Proceedings of the 9th Python in Science Conference*, 2010, pp. 51–56
- [24] Lee et al., “PyWavelets: A Python package for wavelet analysis”. *Journal of Open Source Software*, 4(36), 2019, p. 1237. <https://doi.org/10.21105/joss.01237>
- [25] John D. Hunter, “Matplotlib: A 2D Graphics Environment”, *Computing in Science & Engineering*, vol. 9, 2007, pp. 90–95. <https://doi.org/10.1109/MCSE.2007.55>

The impact of moisture and temperature on the laminated rhombic hyperbolic paraboloid

Abhay Chaubey¹, Ajay Kumar²,
Malgorzata Grzegorzczak-Frańczak³, Malgorzata Szafraniec⁴

¹Department of Civil Engineering; Koneru Lakshmaiah Education Foundation; Vaddeswaram 522502, India; abhaychaubey26@gmail.com; ORCID: 0000-0003-4607-9765

²Department of Civil Engineering; National Institute of Technology Patna; Patna-800005, India; sajaydce@gmail.com; ORCID: 0000-0003-0083-9052

³Faculty of Civil Engineering and Architecture; Lublin University of Technology; Nadbystrzycka 40, 20-618 Lublin, Poland; m.grzegorzczak@pollub.pl; ORCID: 0000-0002-6119-2902

⁴Faculty of Civil Engineering and Architecture; Lublin University of Technology; Nadbystrzycka 40, 20-618 Lublin, Poland; m.szafraniec@pollub.pl; ORCID: 0000-0002-5862-9456

Abstract: The current work presents a hygrothermal analysis of laminated composite rhombic hyperbolic paraboloids. The cubic variation in displacement field together with cross curvature effects of the shell were used to solve the hygrothermal problem. Because of the parabolic variation of the transverse shear deformation, the shear correction factor was not necessary in this paper. In the mathematical model, the zero conditions of the transverse shear stress at the bottom and top of the shell were applied. The nine-noded curved isoparametric element with seven unknowns in each node was used to implement the present realistic mathematical model. The implementation of the finite element C^0 (FE) of the present mathematical model was coded and performed in FORTRAN. The skew hyperbolic paraboloid on which the hygrothermal analysis was conducted had various temperatures, ply orientation, curvatures, moisture concentration, boundary conditions and thickness ratio. The paper shows that with the increase of the skew angle, the non-dimensional deflection decreases, and with the increase of moisture concentration, hygrothermal load and curvature ratio, the deflection increases. The results of the model presented in the paper were compared with other results published in the literature and were found to be consistent with them.

Keywords: temperature; moisture concentration; laminated; skew angle; ply orientation

1. Introduction

Laminated composite structures are gaining more and more attention today due to their improved properties, such as high strength-to-weight ratio, resistance to oxidation corrosion, high strength-to-rigidity ratio and improved toughness. Due to their advantages such as structural lightness and rigidity, laminated composite hyperbolic paraboloids are used in various industries. However, laminated structures are often exposed to moisture

loads and unfavourable temperatures during their service lifespan. Due to their porosity, building materials often contain water in their structure, which contributes to the reduction of their load capacity and thermal properties [1-3]. Temperature and moisture cause stress and deformation of laminated composite structures, which leads to their destruction. This is why it is so important to study laminated composite hyperbolic paraboloids subjected to hygrothermal load.

Pipes et al. [4] examined the hygrothermal response of the laminated composite plate. The classical diffusion equation was used in their study to describe the diffusion of moisture. Their results, though, were limited to thin geometry. The paper [5] presents the results of thermal stress and deformation tests on antisymmetric cross-ply and angle-ply laminates. The effect of moisture and temperature on the cylindrical composite shell was studied by Lee and Yen [6] using the FE method. The paper [7] develops and presents equations for the laminated composite plates which take into account the influence of expansive stress caused by moisture and temperature. To conduct the hygrothermal analysis of plate or shell, researchers have used various methods. In his work, Pell [8] examined the problem of thermal bending of thin anisotropic plates. The FE method with quadratic isoparametric element was used by Ram and Sinha [9] to determine the hygrothermal influence on the bending properties of laminates. Researchers in [10] developed a FE formula for an anisotropic composite panel subjected to thermal and mechanical loads. This study presents an exact closed-form solution for laminated composite plates subjected to sinusoidal loading. In [11], Lawrence and Doxsee applied the higher order theory to study the hygrothermal behaviour of shells. They used various shapes of shells as well as arbitrary temperature and moisture distributions. CLPT and the von Karman large deflection theory were used by Lee et al. [12] to investigate the effect of hygrothermal energy on the cylindrical bending of symmetric angle-ply laminates subjected to uniform transverse loading. Zenkour and Alghanmi [13] applied the sinusoidal shear deformation theory to investigate sinusoidal hygrothermal load of multilayer plates. The paper [14] presents experimental and numerical tests based on FSDT and applied in a dynamic analysis of laminated shallow shells in hygrothermal conditions. A single-layer model designed for thermal bending analysis of laminated cylindrical shells using FSDT was developed by Zenkour and Fares [15]. Singh and Chakrabarti [16] used an efficient HSDT to perform a hygrothermal analysis of laminates. Zenkour [17] applied a unified shear deformation plate theory to study thermo-elastic behaviour of symmetric and anti-symmetric cross-ply laminates. As part of a unified formula, Brischetto [18] proposed an improved 2D model for the bending analysis of multilayer composite and sandwich plates subjected to mechanical and hygrothermal loading. Upadhyaya et al. [19] conducted a non-linear bending analysis of laminates exposed to hygrothermal and mechanical loads. In [20], a hygrothermal analysis of cylindrical shells was carried out using HSDT. Patela et al. [21] applied HSDT to present the dynamic and static behaviour of thick composite laminates in hygrothermal conditions. Ali et al. [22] On the basis of the new higher order displacement theory, Ali et al. [22] developed an accurate model for mechanical and thermal analysis of thick laminates. Bending analysis of multilayer plates subjected to thermomechanical loading was presented by Brischetto and Carrera [23]. In [24], closed-form thermomechanical solutions for the analysis of double curved laminated shells with the use of 2D HSDT theory were described. Tauchert [25] presented the test of reaction to thermal load. The paper discusses large post-bending deformation, buckling, vibration analysis and thermally induced bending. Khdeir et al. [26] demonstrated thermal analysis of cross-ply shallow shells with the use of a precise analytical solution. In their

work [27], Jin and Yao showed an effective, improved C^0 -type global/local model (IGLM) for a bending analysis of thick cross-ply laminates in hygrothermal load conditions. In [28], a direct, iterative C^0 non-linear FE method is presented for a spherical shell panel and plate exposed to hygro-thermo-mechanical loading.

The literature study showed that there are no hygrothermal analysis results concerning laminated composite rhombic hyperbolic paraboloids. Therefore, this paper aims to investigate their hygrothermal behaviour. For this study, the authors have developed a C^0 FE model based on a nine-noded continuous curved isoparametric element.

2. Mathematical formulas

2.1. Strains and displacement fields

Fig. 1 shows a laminated composite shell with the reference plane at $z = 0$ and the curvature R_x and R_y longitudinally to the x and y axes.

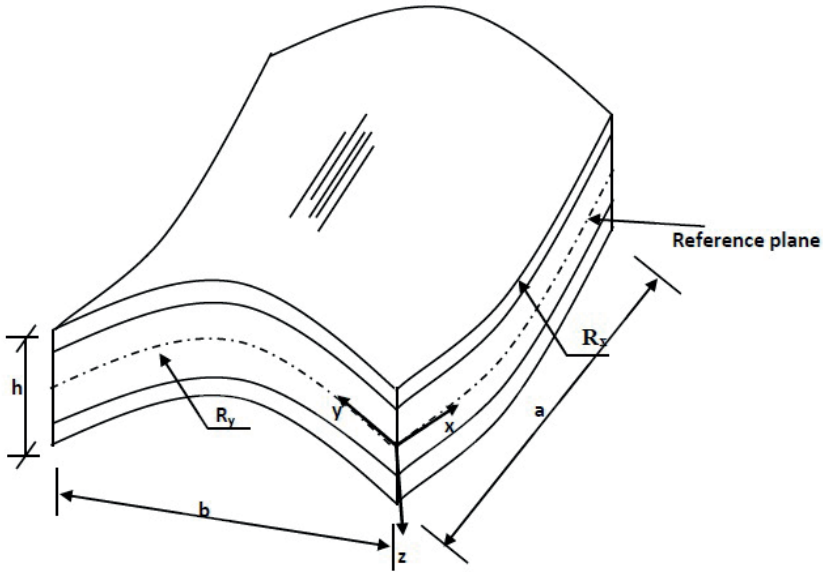


Fig. 1. Laminated composite hyperbolic paraboloid shell, where a and b represent the sides of a hyperbolic paraboloid with a total thickness of h . Source: own study

Based on Reddy [29], the displacement fields are established and indicated as:

$$\{C\} = \{C_0\} + z\{\theta\} + z^2\{\xi\} + z^3\{\zeta\} \tag{1}$$

$$\{C\} = \{u, v, w\}^T, \{C_0\} = \{u_0, v_0, w_0\}^T, \theta = \{\theta_x, \theta_y, 0\}^T, \{\xi\} = \{\xi_x, \xi_y, 0\}^T \text{ and } \{\zeta\} = \{\zeta_x, \zeta_y, 0\}^T$$

where: ξ_x, ξ_y, ζ_x and ζ_y are higher-order terms of Taylor series expansion, v is displacement, v_0 – displacement of midpoints, $\theta_x(x, y)$ is the rotation of the normal along the y axis, u is displacement, u_0 displacement of midpoints, and $\theta_y(x, y)$ is the rotation of the normal along x axis.

The developed displacement field shall be obtained by eliminating the transverse shear stress resultants at $\pm h/2$ of the shell as follows:

$$\{C\} = \{C_0\} + z \left(1 - \frac{4z^2}{3h^2} \right) \{\theta\} - \frac{4z^3}{3h^2} \{\psi^*\} \quad \{C\} = \{C_0\} + z \left(1 - \frac{4z^2}{3h^2} \right) \{\theta\} - \frac{4z^3}{3h^2} \{\psi^*\}, \text{ where} \quad (2)$$

$$\{\psi^*\} = \{\psi_x^*, \psi_y^*, 0\},$$

$$\psi_x^* = \frac{\partial w}{\partial x}, \psi_y^* = \frac{\partial w}{\partial y}$$

$\{R\}$ (the nodal degree of freedom) can be defined as:

$$\{R\} = \{u_0, v_0, w_0, \theta_x, \theta_y, \psi_x^*, \psi_y^*\} \quad (3)$$

Equation (4) shows a linear strain-displacement relationship, which is based on Sanders' approximation.

$$\varepsilon_{xx} = \frac{\partial u}{\partial x} + \frac{w}{R_x}, \quad \varepsilon_{yy} = \frac{\partial v}{\partial y} + \frac{w}{R_y}, \quad \gamma_{xy} = \frac{\partial v}{\partial x} + \frac{\partial u}{\partial y} + \frac{2w}{R_{xy}} \quad (4)$$

$$\gamma_{xz} = \frac{\partial u}{\partial z} + \frac{\partial w}{\partial x} - A_1 \frac{u}{R_x} - A_1 \frac{v}{R_{xy}}, \quad \gamma_{yz} = \frac{\partial v}{\partial z} + \frac{\partial w}{\partial y} - A_1 \frac{v}{R_y} - A_1 \frac{u}{R_{xy}}$$

Substituting Equation (2) in Equation (5):

$$\begin{Bmatrix} \varepsilon_{xx} \\ \varepsilon_{yy} \\ \gamma_{xy} \end{Bmatrix} = \begin{Bmatrix} \varepsilon_{x0} \\ \varepsilon_{y0} \\ \varepsilon_{xy0} \end{Bmatrix} + z \begin{Bmatrix} K_x \\ K_y \\ K_{xy} \end{Bmatrix} - \frac{4z^3}{3h^2} \begin{Bmatrix} (K_x + K_x^*) \\ (K_y + K_y^*) \\ (K_{xy} + K_{xy}^*) \end{Bmatrix} \quad (5)$$

$$\begin{Bmatrix} \gamma_{xz} \\ \gamma_{yz} \end{Bmatrix} = \begin{Bmatrix} \phi_x \\ \phi_y \end{Bmatrix} + z \begin{Bmatrix} K_{xz} \\ K_{yz} \end{Bmatrix} - \frac{4z^2}{h^2} \begin{Bmatrix} K_{xz}^* \\ K_{yz}^* \end{Bmatrix} + \frac{4z^3}{3h^2} \begin{Bmatrix} K_{xz}^* \\ K_{yz}^* \end{Bmatrix}, \text{ where}$$

$$\{\varepsilon_{x0}, \varepsilon_{y0}, \varepsilon_{xy0}\} = \left\{ u_{0,x} + \frac{w}{R_x}, v_{0,y} + \frac{w}{R_y}, u_{0,y} + v_{0,x} + \frac{2w}{R_{xy}} \right\}$$

$$\{\phi_x, \phi_y\} = \left\{ w_{0,x} + \theta_x - A_1 \frac{u_0}{R_x} - A_1 \frac{v_0}{R_{xy}}, w_{0,y} + \theta_y - A_1 \frac{v_0}{R_y} - A_1 \frac{u_0}{R_{xy}} \right\}$$

$$\{K_x, K_y, K_{xy}, K_x^*, K_y^*, K_{xy}^*\} = \{\theta_{x,x}, \theta_{y,y}, \theta_{x,y} + \theta_{y,x}, \psi_{x,x}^*, \psi_{y,y}^*, \psi_{x,y}^* + \psi_{y,x}^*\}$$

$$\{K_{xz}, K_{yz}, K_{xz}^*, K_{yz}^*\} = \left\{ -A_1 \frac{\theta_x}{R_x} - A_1 \frac{\theta_y}{R_{xy}}, -A_1 \frac{\theta_y}{R_y} - A_1 \frac{\theta_x}{R_{xy}}, A_1 \frac{\theta_x}{R_x} + A_1 \frac{\theta_y}{R_{xy}}, A_1 \frac{\theta_y}{R_y} + A_1 \frac{\theta_x}{R_{xy}} \right\}$$

$$\{K_{xz}^*, K_{yz}^*\} = \{\theta_x + \psi_x^*, \theta_y + \psi_y^*\}$$

To shorten the analysis to Love's first approximation, the tracer coefficient (A1) is used.

2.2. Consecutive Equation

$$\begin{Bmatrix} \sigma_x \\ \sigma_y \\ \tau_{xy} \\ \tau_{yz} \\ \tau_{xz} \end{Bmatrix}_k = \begin{bmatrix} \bar{Q}_{11} & \bar{Q}_{12} & \bar{Q}_{16} & 0 & 0 \\ \bar{Q}_{12} & \bar{Q}_{22} & \bar{Q}_{26} & 0 & 0 \\ \bar{Q}_{16} & \bar{Q}_{26} & \bar{Q}_{66} & 0 & 0 \\ 0 & 0 & 0 & \bar{Q}_{44} & \bar{Q}_{45} \\ 0 & 0 & 0 & \bar{Q}_{45} & \bar{Q}_{55} \end{bmatrix}_k \begin{Bmatrix} \varepsilon_x - \alpha_x \Delta T - \beta_x \Delta C \\ \varepsilon_y - \alpha_y \Delta T - \beta_y \Delta C \\ \gamma_{xy} - \alpha_{xy} \Delta T - \beta_{xy} \Delta C \\ \gamma_{yz} \\ \gamma_{xz} \end{Bmatrix}_k \quad (6)$$

where: $[\bar{Q}_{ij}]$ is transformed reduced stiffness matrix, $\beta_x; \beta_y; \beta_{xy}$ – transformed contraction or swelling coefficients (moisture), $\alpha_x; \alpha_y; \alpha_{xy}$ – transformed thermal contraction or expansion coefficients (temperature), ΔC – moisture concentration change, ΔT – temperature change.

3. The formulation of finite elements

Fig. 2 shows a nine-noded isoparametric element used for the analysis in (7).

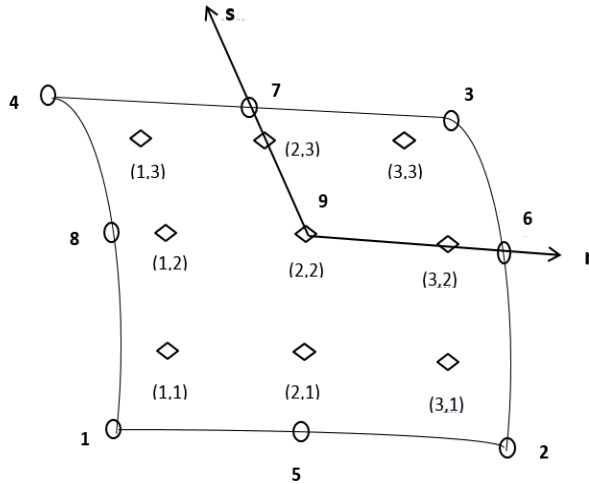


Fig. 2. The curved isoparametric element with nine nodes (Gauss points and typical node numbering).
Source: own study

$$\{w\} = [N] \{\delta\} \quad (7)$$

The equations (8) shown below can be used to find stress at any point.

$$\{\bar{\sigma}\} = [\bar{Q}] \{\bar{\varepsilon}_n\} \quad (8)$$

where: $\{\bar{\varepsilon}_n\} = \{\bar{\varepsilon} - \bar{\varepsilon}_{th} - \bar{\varepsilon}_m\}$.

The total strain ε_n is shown in the equation (9):

$$\{\bar{\varepsilon}\} = [H] \{\varepsilon\}, \quad (9)$$

where: \mathcal{E} is strain from mechanical loads, \mathcal{E}_m – strain from moisture, \mathcal{E}_{th} – strain from thermal loads.

$$\{\varepsilon\} = [B]\{d\}, \tag{10}$$

where: $\{d\}$ – the vector of nodal displacement.

The FE formula consists in interpolating the displacements and moistures/temperatures in the element area by using the same interpolation functions. By equating the work performed by internal forces and by using the virtual work method, the equation (11) is obtained.

$$[K]\{\delta\} = \{P\} \tag{11}$$

where: $[K]$ – element stiffness matrix, $\{P\}$ – nodal load vector.

$$\{P\} = \iiint [N]^T q dx dy \tag{12}$$

Equations (13-16) are used to determine the thermal load.

$$\{Pe^N\} = \iiint [B]^T [H]^T \{F^N\} dx dy \tag{13}$$

$$\{F^N\}^T = [N_x^N, N_y^N, N_{xy}^N, M_x^N, M_y^N, M_{xy}^N, 0, 0, \dots] \tag{14}$$

$$\{N_x^N, N_y^N, N_{xy}^N\}^T = \sum_k^n \int_{z_{k-1}}^{z_k} \{\bar{Q}_{ij}\}_k \{\varepsilon\}_k dz \tag{15}$$

$$\{M_x^N, M_y^N, M_{xy}^N\}^T = \sum_k^n \int_{z_{k-1}}^{z_k} \{\bar{Q}_{ij}\}_k \{\varepsilon\}_k dz \tag{16}$$

where: $i, j = 1, 2, 6$, $\{\varepsilon_k\}^T = [\varepsilon_x, \varepsilon_y, \varepsilon_{xy}]$.

Without losing generality of the form, an arbitrary temperature distribution can be found as shown by equation (17).

$$T(x, y, z) = T_0 + \left(\frac{z}{h}\right) T_1(x, y), \tag{17}$$

where: T_0 – initial constant temperature.

Case No.1. Uniform temperature over the entire depth:

$$\begin{aligned} \begin{Bmatrix} \varepsilon_x \\ \varepsilon_y \\ \varepsilon_{xy} \end{Bmatrix} &= \begin{Bmatrix} \alpha_x \\ \alpha_y \\ \alpha_{xy} \end{Bmatrix} \Delta T \\ \begin{Bmatrix} \alpha_x \\ \alpha_y \\ \alpha_{xy} \end{Bmatrix} &= \begin{bmatrix} c^2 & s^2 & -2cs \\ s^2 & c^2 & 2cs \\ cs & -cs & c^2 - s^2 \end{bmatrix} [Q]_k \begin{Bmatrix} \alpha_1 \\ \alpha_2 \\ \alpha_{12} \end{Bmatrix}, \end{aligned} \quad (18)$$

where: $\alpha_1, \alpha_2, \alpha_{12}$ – coefficients of thermal expansion referred to the main material axes of the laminate; $\alpha_x, \alpha_y, \alpha_{xy}$ – transformed coefficients of thermal expansion referred to the x-y coordinate system.

$$\{F\} = \iiint [B]^T [H]^T \begin{Bmatrix} \alpha_x \\ \alpha_y \\ \alpha_{xy} \end{Bmatrix} T dv. \quad (19)$$

Case No. 2. Temperature varying over the entire depth:

$$\{F\} = \iiint [B]^T [H]^T \begin{Bmatrix} \alpha_x \\ \alpha_y \\ \alpha_{xy} \end{Bmatrix} \left[\frac{1}{2} (T_U + T_L + z/h (T_U - T)) \right] T dv, \quad (20)$$

where: T_U – temperature on the upper surface; T_L – temperature on the lower surface.

3.1. Skew transformations

Due to the fact that the edges of boundary elements of skew shells are not parallel to the global axis, it is not possible to determine the boundary conditions in terms of global displacements u_0, w_0, v_0 etc. (Fig. 3).

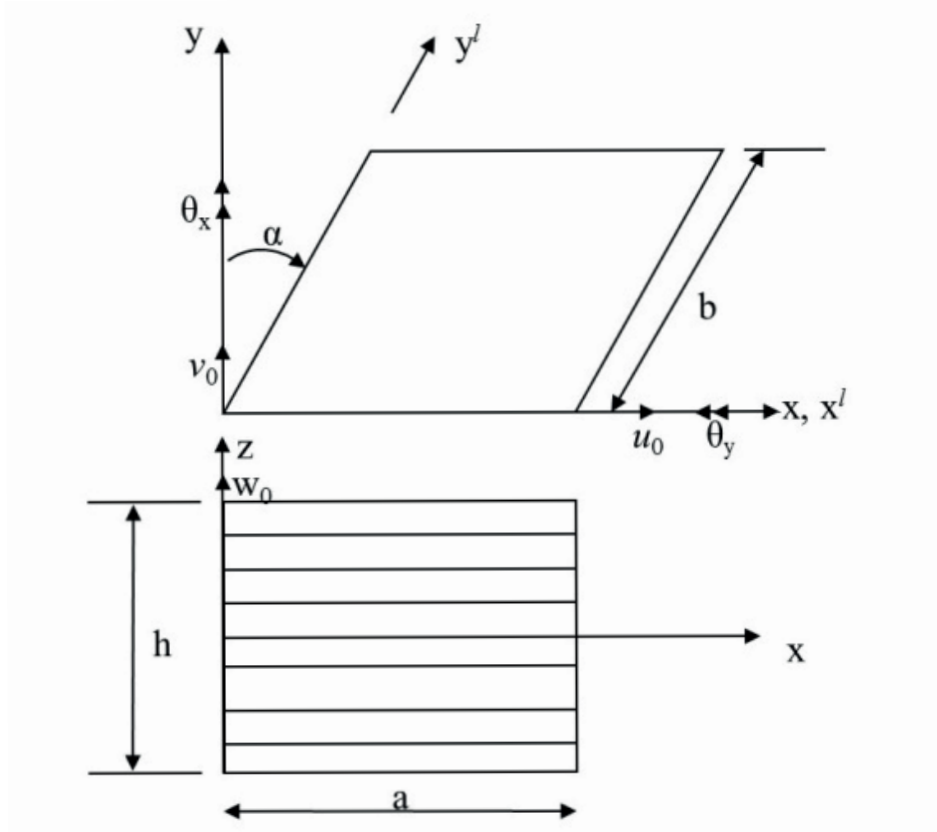


Fig. 3. The geometry of skew laminated hyperbolic paraboloids. Source: own study

Therefore, in order to determine the necessary boundary conditions at the skew edge, edge displacements x', y', z' in the local coordinates u'_0, v'_0, w'_0 should be used. For this purpose, the matrix of elements corresponding to the global axis shall be transformed into a local one [30] (21).

$$d_i = [T]d'_i, \tag{21}$$

where: d'_i, d_i – generalised displacement vectors in the local and global coordinate systems (22)(23).

$$\{d_i\} = \{u_0, v_0, w_0, \theta_x, \theta_y, \psi_x, \psi_y\}^T \tag{22}$$

$$\{d'_i\} = \{u'_0, v'_0, w'_0, \theta'_x, \theta'_y, \psi'_x, \psi'_y\}^T. \tag{23}$$

A nodal transformation matrix on the skew boundary is shown below.

$$\text{Transformation matrix [T]} = \begin{pmatrix} \cos \alpha & -\sin \alpha & 0 & 0 & 0 & 0 & 0 \\ \sin \alpha & \cos \alpha & 0 & 0 & 0 & 0 & 0 \\ 0 & 0 & 1 & 0 & 0 & 0 & 0 \\ 0 & 0 & 0 & \cos \alpha & -\sin \alpha & 0 & 0 \\ 0 & 0 & 0 & \sin \alpha & \cos \alpha & 0 & 0 \\ 0 & 0 & 0 & 0 & 0 & \cos \alpha & -\sin \alpha \\ 0 & 0 & 0 & 0 & 0 & \sin \alpha & \cos \alpha \end{pmatrix}, \quad (24)$$

4. Numerical problems

The following boundary conditions were used in the presented analysis:

a) Simply supported (SS):

$$\text{At } x = 0, a; v = w = \theta_y = \psi_y = 0 \quad (25)$$

$$\text{At } y = 0, b; u = w = \theta_x = \psi_x = 0 \quad (26)$$

b) Clamped (CC):

$$\text{At } x = 0, a \text{ and } y = 0, b; u = v = w = \theta_x = \theta_y = \psi_x = \psi_y = 0 \quad (27)$$

c) Clamped-simply supported (CS):

$$\text{At } x = 0 \text{ and } y = 0; u = v = w = \theta_x = \theta_y = \psi_x = \psi_y = 0 \quad (28)$$

$$\text{At } x = a; v = w = \theta_y = \psi_y = 0 \text{ and at } y = b; u = w = \theta_x = \psi_x = 0 \quad (29)$$

The non-dimensional formulae used in this paper are:

$$\bar{w} = \frac{10wh}{\alpha_0 T_0 a^2}, \quad \bar{\sigma}_x = \left(\frac{a}{2}, \frac{b}{2}, -\frac{h}{2} \right) \frac{\sigma_x}{\alpha_0 T_0 E_T}, \quad \bar{\sigma}_y = \left(\frac{a}{2}, \frac{b}{2}, z \right) \frac{\sigma_y}{\alpha_0 T_0 E_T}, \quad \text{and} \quad \bar{\tau}_{xy} = \left(0, 0, -\frac{h}{2} \right) \frac{\tau_{xy}}{\alpha_0 T_0 E_T}. \quad (30)$$

The following material properties are used in this paper (unless otherwise stated): $\alpha_1/\alpha_2 = 3$, $\rho = 1$, $\mu_{12} = 0.25$, $E_1/E_2 = 25$, $G_{12} = G_{13} = 0.5E_2$ and $G_{23} = 0.2E_2$.

5. Results and discussion

5.1. Validation of the formula – a convergence study

As shown in Tab. 1, the convergence test was carried out by varying the mesh size from 12×12 to 20×20 (N_x and N_y – numbers of elements in x and y-direction).

Table 1. The convergence study of laminated ($0^\circ/90^\circ$) skew hyperbolic paraboloid ($R_x/R_y = -0.5$, skew angle = 15°) subjected to hygrothermal loading ($\Delta T = 1$ and $\Delta C = 0.01\%$). Source: own study

Mesh Size	Non-dimensional deflection
12×12	2.4565
14×14	2.4505
16×16	2.4450
18×18	2.4449
20×20	2.4449

As shown in Tab. 1, the value of non-dimensional deflection converged for $N_x \times N_y = 16 \times 16$. Therefore, all subsequent analyses were carried out with the above-mentioned mesh size.

5.2. Validation of the formula – comparison of results

Tab. 2 shows the middle deflection (mm) of a two-ply ($0^\circ/90^\circ$) perpendicularly supported square laminate with different thickness ratios. The results are similar to those in [23]. The values of the middle deflection for rectangular SS laminated plates exposed to sinusoidal temperature gradient for $(h/r) = 0.01$ are shown in Tab. 3.

Table 2. In-plane and transverse displacements of double-layered ($0^\circ/90^\circ$) square laminate. Source: [23], own study

Thickness Ratio	Brischetto and Carrera [23]	Present
100	5.9448	5.9424
50	1.4857	1.4857
10	0.0587	0.0590
5	0.0141	0.0144

Table 3. Influence of the shape factor on the deflection in SS composite plates. Source: [16], [10], own study

Reference	0/90/0			0		0/90	
	a/b=1	a/b=1.5	a/b=2	a/b=1	a/b=1	a/b=1	a/b=1
Present	1.0174	0.8585	0.6319	1.0226	1.1080		
Singh and Chakrabarti [16]	1.0429	0.8802	0.6566	1.0332	1.1520		
Reddy and Hsu [10]	1.0949	0.9847	0.7643	1.0313	1.6765		

In order to validate the central transverse deflection of laminated shells subjected to sinusoidal temperature load of different curvature, these results were compared with the results of Khare et al. [24] and Brischetto [18] in Tab. 4. It can be seen in Tab. 4 that the current figures are similar to HSDT. Tab. 5 shows non-dimensional middle deflections of three-layer laminated rectangular plates ($0^\circ/90^\circ/0^\circ$) subjected to sinusoidal hygrothermal distribution ($\Delta T = 300^\circ\text{C}$

and $\Delta C = 0.01\%$). Importantly, the current numerical result is in accordance with the results presented by Zenkour et al. [13].

Table 4. Non-dimensional middle deflections of three-layer shells. Source: [24], [26], [18], own study

R/a	Present	Khare et al. [24] [HOST12]	Khare et al. [24] [FOST]	Khdeir et al. [26] [HSDT]	Brischetto [18]
Cylindrical shell (0/90) with $a/b = 1$, $h/a = 0.1$, $R_1 = \infty$, $R_2 = R$					
5	1.1249	1.1261	1.1272	1.1235	--
10	1.1423	1.1434	1.1444	1.1421	--
50	1.1481	1.1493	1.1501	1.1482	--
Spherical shell (0/90) with $a/b = 1$, $h/a = 0.1$, $R_1 = R_2 = R$					
5	1.0574	1.0588	1.0578	1.0545	--
10	1.1243	1.1256	1.1258	1.1235	--
50	1.1474	1.1487	1.1493	1.1475	--
Ten-layered cylindrical shell (0/90/...) with $a/b = 1$, $h/a = 0.1$, $R_1 = \infty$, $R_2 = R$					
5	1.0234	1.0224	1.0234	1.0216	1.0207
10	1.0308	1.0299	1.0307	1.0303	1.0283
50	1.0331	1.0325	1.0330	1.0332	1.0306

Table 5. Non-dimensional middle deflections of three-layer (0°/90°/0°) laminates subjected to sinusoidal hygrothermal distribution. Source: [13], own study

a/b	a/h = 10		a/h = 20		a/h = 50	
	Present	Zenkour and Alghanmi [13]	Present	Zenkour and Alghanmi [13]	Present	Zenkour and Alghanmi [13]
1	2.7360	2.7749	2.1691	2.3654	1.9906	2.2355
1.5	3.2156	3.2273	2.9160	2.8521	2.8168	2.7148
2	3.0517	2.8496	2.9415	2.6631	2.8971	2.5849

5.3. Parametric study

Tab. 6 shows the dimensionless middle deflection of a three-layer hyperbolic paraboloid exposed to sinusoidal hygrothermal loading. The coefficient of curvature (R_x/R_y) was differentiated from -0.50 to -1.50. The value of dimensionless deflection increases as the curvature coefficient increases, and as the skew angle increases, the value of dimensionless deflection decreases.

Table 6. Non-dimensional middle deflections of three-layer ($0^\circ/90^\circ/0^\circ$) skew hyperbolic paraboloid subjected to sinusoidal hygrothermal distribution ($\Delta T = 300^\circ\text{C}$, $\Delta C = 0.01\%$). Source: own study

Curvature	Skew angle	Boundary conditions		
		SS	CC	CS
-0.50	0°	2.669	0.852	1.673
	15°	2.445	0.809	1.480
	30°	1.866	0.673	1.252
	45°	1.137	0.444	1.016
	60°	0.487	0.193	0.686
-0.10	0°	2.741	1.243	1.768
	15°	2.528	1.154	1.576
	30°	1.953	0.904	1.260
	45°	1.194	0.549	0.862
	60°	0.509	0.219	0.450
-1.50	0°	2.763	1.371	1.795
	15°	2.553	1.267	1.604
	30°	1.977	0.978	1.258
	45°	1.210	0.582	0.806
	60°	0.516	0.227	0.369

The dimensionless maximum deflection of skew hyperbolic paraboloids (with different lamination schemes) subjected to sinusoidal temperature and hygrothermal load are shown in Tab. 7. For a shell subjected to hygrothermal load, the value of maximum dimensionless deflection is greater than in a shell subjected to thermal load only. An angle-ply shell has less maximum dimensionless deflection than a cross-ply shell. As the skew angle increases, the dimensionless deflection decreases for the entire lamination scheme under consideration.

Table 7. The non-dimensional central deflections of skew hyperbolic paraboloid under sinusoidal hygrothermal distribution ($\Delta T = 300^\circ\text{C}$, $\Delta C = 0.01\%$). Source: own study

Skew angle	$0^\circ/90^\circ$	$45^\circ/-45^\circ$	$0^\circ/90^\circ/0^\circ$	$45^\circ/-45^\circ/45^\circ$	$0^\circ/90^\circ/90^\circ/0^\circ$
Temperature loading					
0°	1.151	0.698	1.055	0.813	1.044
15°	0.994	0.626	0.939	0.735	0.868
30°	0.642	0.522	0.652	0.586	0.497
45°	0.307	0.272	0.336	0.318	0.194
60°	0.093	0.049	0.110	0.083	0.047
Hygrothermal loading					
0°	6.805	2.728	2.741	2.313	2.559
15°	5.914	3.113	2.528	2.315	2.118
30°	3.893	3.017	1.953	1.950	1.173
45°	1.924	1.857	1.194	1.179	0.426
60°	0.633	0.578	0.509	0.385	0.089

Tab. 8 shows dimensionless middle deflections of laminated hyperbolic paraboloids of varying thickness. The maximum dimensionless deflection is noticeable for the shell for which $a/h = 5$, and when thickness decreases, the dimensionless deflection increases to $a/h = 50$. Tabs 9-10 show the change of material properties with the change in temperature and moisture content. The maximum deflection of laminated hyperbolic paraboloids subjected to

different thermal loads is shown in Tab. 11. The deflection of the shell was found to increase as the temperature rises. Tab. 12 shows the maximum deflection of hyperbolic paraboloids with different moisture concentrations in the laminate layer. The value of dimensionless deflection increases as moisture concentration increases. Tabs 13-15 show non-dimensional stresses ($\bar{\sigma}_x, \bar{\sigma}_y$ and $\bar{\tau}_{xy}$) of a laminated rhombic hyperbolic paraboloid subjected to hygrothermal loading (in the same location as above). The maximum stresses are observed to depend on the skew angle and boundary conditions.

Table 8. The non-dimensional central deflections of a laminated skew hyperbolic paraboloid under sinusoidal hygrothermal loading. Source: own study

Skew angle	a/h = 5	a/h = 10	a/h = 20	a/h = 50	a/h = 100
SS					
0°	6.650	6.805	6.852	6.870	6.860
15°	5.831	5.914	5.896	5.814	5.496
30°	3.883	3.893	3.832	3.673	3.164
45°	1.880	1.924	1.906	1.805	1.494
60°	0.577	0.633	0.648	0.619	0.528
CC					
0°	1.921	1.956	1.887	1.336	0.696
15°	1.692	1.757	1.720	1.256	0.671
30°	1.127	1.233	1.262	1.013	0.592
45°	0.529	0.618	0.674	0.625	0.438
60°	0.153	0.188	0.219	0.230	0.207

Table 9. Material properties at moisture concentrations $G_{13} = G_{12}, G_{23} = 0.5 G_{12}, \nu_{12}=0.3, \beta_1 = 0,$ and $\beta_2 = 0.44$. Source: own study

Elastic moduli	Moisture concentration (C %)						
	0	0.25	0.5	0.75	1.0	1.25	1.5
E_1	130	130	130	130	130	130	130
E_2	9.5	9.25	9.0	8.75	8.5	8.5	8.5
G_{12}	6.0	6.0	6.0	6.0	6.0	6.0	6.0

Table 10. Material properties at various temperatures ($G_{13} = G_{12}, G_{23} = 0.5 G_{12}, \nu_{12} = 0.3, \alpha_1 = -0.3 \times 10^{-6},$ and $\alpha_2 = 28.1 \times 10^{-6}$). Source: own study

Elastic moduli	Temperature T(K)					
	300	325	350	375	400	425
E_1	130	130	130	130	130	130
E_2	9.5	8.5	8.0	7.5	7.0	6.75
G_{12}	6.0	6.0	5.5	5.0	4.75	4.5

Table 11. Maximum deflection of laminated skew hyperbolic paraboloids under various temperature loading. Source: own study

Skew angle	$\Delta T = 300$	$\Delta T = 325$	$\Delta T = 350$	$\Delta T = 375$	$\Delta T = 400$	$\Delta T = 425$
SS						
0°	1.582	1.592	1.685	1.770	1.823	1.912
15°	1.382	1.391	1.470	1.543	1.588	1.665
30°	0.925	0.932	0.983	1.028	1.057	1.107
45°	0.470	0.475	0.499	0.520	0.533	0.557
60°	0.161	0.163	0.170	0.176	0.181	0.188
CC						
0°	0.510	0.517	0.541	0.561	0.575	0.600
15°	0.458	0.464	0.486	0.504	0.517	0.539
30°	0.323	0.327	0.342	0.355	0.364	0.379
45°	0.164	0.167	0.174	0.180	0.184	0.191
60°	0.051	0.052	0.053	0.055	0.056	0.058

Table 12. Maximum deflection of laminated skew hyperbolic paraboloids with different moisture concentrations. Source: own study

Skew angle	Moisture Concentration (C %)					
	0.25	0.5	0.75	1.0	1.25	1.5
0°	0.312	0.613	0.903	1.181	1.560	1.872
15°	0.303	0.596	0.878	1.149	1.516	1.819
30°	0.268	0.527	0.776	1.017	1.339	1.607
45°	0.194	0.382	0.564	0.739	0.971	1.166
60°	0.099	0.196	0.289	0.379	0.496	0.596

Table 13. Non-dimensional stress ($\bar{\epsilon}_{xy}$) of laminated skew hyperbolic paraboloids with different boundary conditions. Source: own study

Skew angle	SS	CC	CS
0°	0.393	0.000	0.000
15°	0.730	0.000	0.000
30°	0.720	0.000	0.000
45°	0.327	0.000	0.000
60°	-0.165	0.000	0.000

Table 14. Non-dimensional in-plane stress ($\bar{\sigma}_x$) of laminated skew hyperbolic paraboloids with different boundary conditions. Source: own study

Skew angle	SS	CC	CS
0°	-10.683	-3.982	2.098
15°	-15.822	-11.624	-5.501
30°	-15.410	-18.386	-12.456
45°	-8.098	-23.419	-13.686
60°	2.064	-25.237	-7.833

Table 15. Non-dimensional in-plane stress ($\bar{\sigma}_y$) of laminated skew hyperbolic paraboloids with different boundary conditions. Source: own study

Skew angle	SS	CC	CS
0°	0.480	0.019	0.250
15°	0.300	-0.151	0.201
30°	0.036	-0.416	0.005
45°	0.637	0.791	0.781
60°	4.664	8.041	4.906

6. Conclusions

A C^0 finite element (FE) formulation was developed using Sanders' approximations and was applied to study the static reaction of a composite skew hyperbolic paraboloid exposed to hygrothermal loading. Many new results were obtained concerning the hygrothermal reaction of laminated hyperbolic paraboloids with different moisture concentration, thickness ratio, skew angle, boundary conditions, radius of curvature, temperature and layer orientation, which should be beneficial for future studies.

General conclusions are as follows:

- As the curvature coefficient increases, the value of dimensionless deflection increases.
- As the skew angle increases, the dimensionless deflection decreases.
- The dimensionless deflection increases as the moisture concentration increases.
- An angle-ply shell shows less maximum non-dimensional deflection than a cross-ply shell.
- The deflection of the shell increases as the temperature changes.
- In a shell subjected to hygrothermal load, the maximum value of non-dimensional deflection is greater than in a shell subjected to thermal load only.

References

- [1] Suchorab, Z., Sobczuk, H., Łagód, G., "Estimation of building material moisture using non-invasive TDR sensors", in Thermophysics 2016: 21st International Meeting. AIP Conference Proceedings, vol. 1752, 2016, pp. 1–7. <https://doi.org/10.1063/1.4955231>
- [2] Suchorab, Z. et al., "A Noninvasive TDR Sensor to Measure the Moisture Content of Rigid Porous Materials", *Sensors (Basel)*, vol. 11(18): 3935, (2018), pp. 1-20. <https://doi.org/10.3390/s18113935>
- [3] Barnat-Hunek, D., Siddique, R., Łagód, G., "Properties of hydrophobised lightweight mortars with expanded cork", *Construction and Building Materials*, vol. 155, (2017) pp. 15–25. <https://doi.org/10.1016/j.conbuildmat.2017.08.052>
- [4] Pipes, R.B., Vinson, J.R., Chou, T.W., "On the Hygrothermal Response of Laminated Composite Systems", *Journal of Composite Materials*, vol. 10 (1976), pp. 129–148. <https://doi.org/10.1177/002199837601000203>
- [5] Wu, C.H. and Tauchert, T.R., "Thermoelastic analysts of laminated plates. 2: Antisymmetric cross-ply and angle-ply laminates", *Journal of Thermal Stresses*, vol. 3, (1980), pp. 365–378. <https://doi.org/10.1080/01495738008926975>
- [6] Lee, S.Y. and Yen, W.J., "Hygrothermal effects on the stability of a cylindrical composite shell panel", *Computers & Structures*, vol. 33, (1989), pp. 551–559. [https://doi.org/10.1016/0045-7949\(89\)90029-1](https://doi.org/10.1016/0045-7949(89)90029-1)

- [7] Whitney, J.M. and Ashton, J.E., “Effect of environment on the elastic response of layered composite plates”, *American Institute of Aeronautics and Astronautics Journal*, vol. 9(9), (1971), pp. 1708–1713. <https://doi.org/10.2514/3.49976>
- [8] Pell, W.H., “Thermal deflections of anisotropic thin plates”, *Quarterly Applied Mathematics*, vol. 4, (1940), pp. 27–44. <https://doi.org/10.1090/qam/16032>
- [9] Sai Ram, K.S. and Sinha, P.K., “Hygrothermal effects on the bending characteristics of laminated composite plates”, *Computers & Structures*, vol. 40, (1991), pp. 1009–1015. [https://doi.org/10.1016/0045-7949\(91\)90332-G](https://doi.org/10.1016/0045-7949(91)90332-G)
- [10] Reddy, J.N. and Hsu, Y.S., “Effects of shear deformation and anisotropy on the thermal bending of layered composite plates”, *Journal of Thermal Stresses*, vol. 3, (1980), pp. 475–493. <https://doi.org/10.1080/01495738008926984>
- [11] Doxsee, L.E., “A higher-order theory of hygrothermal behavior of laminated composite shells”, *International Journal of Solids and Structures*, vol. 25, (1989), pp. 339–355. [https://doi.org/10.1016/0020-7683\(89\)90052-8](https://doi.org/10.1016/0020-7683(89)90052-8)
- [12] Lee, S.Y. et al., “Hygrothermal effects on the linear and nonlinear analysis of symmetric angle-ply laminated plates”, *Composite Structures*, vol. 21, (1992), pp. 41–48. [https://doi.org/10.1016/0263-8223\(92\)90078-Q](https://doi.org/10.1016/0263-8223(92)90078-Q)
- [13] Zenkour, A.M. and Alghanmi, R.A., “Bending of symmetric cross-ply multilayered plates in hygrothermal environments”, *Journal of Mathematical Models in Engineering*, vol. 2, (2016), pp. 94–107. <https://doi.org/10.21595/mme.2016.17405>
- [14] Biswal, M., Sahu, S.K., Asha, A. V., “Experimental and numerical studies on free vibration of laminated composite shallow shells in hygrothermal environment”, *Composite Structures*, vol. 127, (2015), pp. 165–174. <https://doi.org/10.1016/j.compstruct.2015.03.007>
- [15] Zenkour, A.M. and Fares, M.E., “Thermal bending analysis of composite laminated cylindrical shells using a refined first-order theory”, *Journal of Thermal Stresses*, vol. 23, (2000), pp. 505–526. <https://doi.org/10.1080/0149573000403969>
- [16] Singh, S.K. and Chakrabarti, A., “Hygrothermal analysis of laminated composite plates by using efficient higher order shear deformation theory”, *Journal of Solid Mechanics*, vol. 3, (2011), pp. 85–95.
- [17] Zenkour, A.M., “Analytical solution for bending of cross-ply laminated plates under thermo-mechanical loading”, *Composite Structures*, vol. 65, (2004), pp. 367–379. <https://doi.org/10.1016/j.compstruct.2003.11.012>
- [18] Brischetto, S., “Hygrothermoelastic analysis of multilayered composite and sandwich shells”, *Journal of Sandwich Structures & Materials*, vol. 15, (2013), pp. 168–202. <https://doi.org/10.1177/1099636212471358>
- [19] Upadhyay, A.K., Pandey, R., Shukla, K.K., “Nonlinear flexural response of laminated composite plates under hygro-thermo-mechanical loading”, *Communications in Nonlinear Science and Numerical Simulation*, vol. 15, (2010), pp. 2634–2650. <https://doi.org/10.1016/j.cnsns.2009.08.026>
- [20] Ali, J.S.M., Alsubari, S., Aminanda, Y., “A Higher Order Theory for Bending of Cross Ply Laminated Cylindrical Shell under Hygrothermal Loads”, *Advanced Materials Research*, vol. 1115, (2015), pp. 509–512. <https://doi.org/10.4028/www.scientific.net/amr.1115.509>
- [21] Patel, B.P., Ganapathi, M., Makhecha, D.P., “Hygrothermal effects on the structural behaviour of thick composite laminates using higher-order theory”, *Composite Structures*, vol. 56, (2002), pp. 25–34. [https://doi.org/10.1016/S0263-8223\(01\)00182-9](https://doi.org/10.1016/S0263-8223(01)00182-9)
- [22] Ali, J.S.M., Bhaskar, K., Varadan, T.K., “A new theory for accurate thermal/mechanical flexural analysis of symmetric laminated plates”, *Composite Structures*, vol. 45, (1999), pp. 227–232. [https://doi.org/10.1016/S0263-8223\(99\)00028-8](https://doi.org/10.1016/S0263-8223(99)00028-8)

- [23] Brischetto, S. and Carrera, E., “Coupled thermo-mechanical analysis of one-layered and multi-layered isotropic and composite shells”, *CMES: Computer Modeling in Engineering & Sciences*, vol. 56(3), (2010), pp. 249–302. <https://doi.org/10.3970/cmcs.2010.056.249>
- [24] Khare, R.K., Kant, T., Garg, A.K., “Closed-form thermo-mechanical solutions of higher-order theories of cross-ply laminated shallow shells”, *Composite Structures*, vol. 59, (2003), pp. 313–340. [https://doi.org/10.1016/S0263-8223\(02\)00245-3](https://doi.org/10.1016/S0263-8223(02)00245-3)
- [25] Tauchert, T.R., “Thermally induced flexure, buckling, and vibration of plates”, *Applied Mechanics Reviews*, vol. 44, (1991), pp. 347–360. <https://doi.org/10.1115/1.3119508>
- [26] Khdeir, A.A., Rajab, M.D., Reddy, J.N., “Thermal effects on the response of cross-ply laminated shallow shells”, *International Journal of Solids and Structures*, vol. 29, (1992), pp. 653–667. [https://doi.org/10.1016/0020-7683\(92\)90059-3](https://doi.org/10.1016/0020-7683(92)90059-3)
- [27] Jin, Q. and Yao, W., “Hygrothermal analysis of laminated composite plates in terms of an improved C0-type global–local model”, *Aerospace Science and Technology*, vol. 63, (2017), pp. 328–343. <https://doi.org/10.1016/j.ast.2017.01.004>
- [28] Lal, A.; Singh, B.N., Anand, S., “Nonlinear bending response of laminated composite spherical shell panel with system randomness subjected to hygro-thermo-mechanical loading”, *International Journal of Mechanical Sciences*, vol. 53, (2011), pp. 855–866. <https://doi.org/10.1016/j.ijmecsci.2011.07.008>
- [29] Chao, W.C. and Reddy, J.N., “Analysis of laminated composite shells using a degenerated 3-D element”, *International Journal for Numerical Methods in Engineering*, vol. 20, (1984), pp. 1991–2007. <https://doi.org/10.1002/nme.1620201104>
- [30] Ali, J.S.M., Alsubari, S., Aminanda, Y., “Hygrothermoelastic analysis of orthotropic cylindrical shells”, *Latin American Journal Solids Structures*, vol. 13, (2016), pp. 573–589. <https://doi.org/10.1590/1679-78252249>

Impact of epoxy resin modification on its strength parameters

Andrzej Szewczak

*Department of General Construction; Faculty of Civil and Architecture; Lublin University of Technology;
Nadbystrzycka 40, 20-618 Lublin, Poland;
a.szewczak@pollub.pl; ORCID: 0000-0001-5933-0483*

Abstract: Modifications of polymer composites are one of the fastest developing fields of technology. Research is focused on two directions: obtaining new composites or modifying existing materials. The first group of tests uses methods for preparing new chemical formulas of polymers containing, as the main structural element: carbon (organic polymers) or silicon (inorganic polymers). In the second group, the research consists in seeking methods to modify the properties of polymers. In building construction, among the others types, the glues (adhesive polymers) are used. They are exerted to connect materials with different physical and mechanical properties. Under the influence of the factor initiating the crosslinking reaction (hardener or temperature), the polymers obtain a solid form. The strength of the glued joint depends on the initial parameters of the glue resin and the target substrate of its application. The glued surface is usually the weakest element in this connection in terms of the possibility of damage due to the effects of loads, therefore methods to improve the strength parameters of adhesives are sought.

The study presents the results of own research on methods of modification of a selected epoxy resin used in the technique as a glue. In order to ensure effective mixing of the adhesive with the fillers, ultrasound energy was used. After the resin had hardened, tests were carried out to determine the hardness and tensile strength of the obtained composites. Based on the results, SEM analysis and observation of the effect of ultrasound, the phenomena affecting the changes in the above mechanical properties were explained.

Keywords: epoxy resins, microsilica, carbon nanotubes, ultrasound

1. Introduction

Polymers are substances and chemical compounds based on cyclically repeating, single chemical sequences of atoms (so-called mers) and forming polymer chains [1][2]. In polymer chains structures, atoms and their individual sequences are connected with each other by means of different types of chemical bonds: ionic, coordination, polarized or hydrogen [2][3]. Depending on the chemical composition and type of existing bonds, polymers can have specific assignments. In the technique sciences, the usefulness of the polymer – epoxy adhesive in this paper/case – is determined by rheological, physic and mechanical properties: viscosity, final adhesion to the substrate, (concrete, steel) [4][5][6], hardness, tensile strength. Viscosity determines the possibility of spreading the adhesive on the target surface, filling the unevenness of the substrate with the glue and, finally, the adhesion of the resin after hardening. However, the durability of the glued connection depends on the adhesion of the resin after the crosslinking reaction and its resistance to loads. The process of the curing reaction largely depends on the presence of specific

polymer groups (phenolic, epoxy, ester), the type of reaction initiating factor (hardener/temperature) and the addition of possible substances (fillers) [1] [2] [3]. Polymer-based building glues harden after only a few hours, and after 2 days, they usually achieve full adhesion to the substrate [1].

The epoxy resins are oligopolymers which are reaction products of epichlorohydrin and bis-phenol [1] [2] [7]. Except for many favorable adhesive and strength properties, their additional features are: chemical resistance, non-absorption and dielectricity. The disadvantages include: low resistance to high temperatures and UV radiation.

The fillers this is a group of additives by means of which it is possible to obtain specific, other than initial, properties of resins [8]. Their quantity and type are selected due to the type of planned modification, polymer chemical composition, properties of filler particles (shape, chemical composition, specific surface) and the required final effect. Various substances are used as fillers, most often in the form of powders or liquids [9][10][11]. The role of the filler is also fulfilled by materials from the recycling process e.g. rubber, minced rock. The filler particle size is selected based on the known particle size of the polymer chain (nano- and microparticles). [12][13] The amount of filler usually depends on the weight of the resin (volumetric dosing is less accurate due to the change of resin density with temperature changes). In order to ensure regular and effective distribution of the filler in the volume of resin, in the technology of polymers the ultrasound are used [14][15][16][17]. Dynamic phenomena caused by ultrasound (high frequency vibrations, cavitation, pressure and temperature changes) cause the formation of temporary atomic bonds between the filler particles and the polymer chains. The degree of connection of the filler particles with the polymer and the filling of voids between the branches of the chain affects the mechanical properties of the hardened polymer. Then, the glue subjected to the hardening process obtains proper adhesion to the substrate.

The following paper presents the results of own research on the possibility of using epoxy resin modified with two fillers – microsilica and carbon nanotubes to improve the physical and mechanical properties of the glue. Exact mixing of fillers with the resin was achieved by the action of ultrasonic energy. The study contains results of research on the impact of fillers on the mechanical and strength properties of obtained composites – hardness and tensile strength. The tests were one of the stages of determining the impact of this kind of modification method thus adopted on the final adhesion of the adhesive to the substrate. The main reason in favor of the chosen topic is the lack of literature and research results focused on this type of modification in relation to epoxy resins. Microsilica is generally used in cement composites, nanotubes are widely used in electrical engineering and mechanics. Ultrasounds are abused as a factor which is activating the chemical sonoreactions [1]. The adopted method of changing resin parameters affects all their performance properties. In [16] [17] the results of research on rheological and adhesive properties are presented. It has been shown how ultrasound and fillers affect the viscosity, temperature and adhesive parameters (free surface energy measured by the Owens-Wendt method was used as the factor describing the adhesion of resin to the substrate). In order to accurately explain the effects caused by the introduced changes, SEM analysis was used. Obtained test results constituted the basis arguments for determining the effectiveness of the applied modifications in relation to their practical application, e.g. for reinforcing reinforced concrete structures or gluing the concrete elements. This is important from the point of view of striving to extend the durability of building structural elements by strengthening them.

2. Materials, devices and methodology of research

For the tests the Epidian 52 epoxy resin was used, by means of which it is possible to glue concrete, ceramics, wood or metal elements. Its basic parameters are:

- form/color – thick, yellow – brown liquid with a characteristic smell,
- flash point – 64°C,
- gel time (hardener Z-1) – 40min
- epoxy number [mol / 100g]: 0.51 – 0.55,
- density (at T = 22°C): 1.12 – 1.13g/cm³,
- viscosity (T = 22°C): 400 – 800 mPa·s,
- solubility: insoluble in water, soluble in ketones, esters, alcohols, aromatic hydrocarbons
- hardener: Z1 (triethylene tetrachloro amine)

The fillers used are: microsilica and carbon nanotubes. The amount of filler, determined experimentally, was related to the weight of the resin. The formulas of the tested composites are presented in table 1.

Table 1. Resin formulas used in research

Number of series	Series designation	Type of modification	Amount of filler [%]	Amount of hardener [%]
1	EP52	-----	-----	7.6
2	EP52+UD	sonication	-----	7.6
3	EP52+Mk	sonication + microsilica	0.5	10
4	EP52+NR	Sonication and carbon nanotubes	0.1	10

In the first stage of research, the initial parameters (viscosity and density) of unmodified resin at the temperature of 22°C were determined. Then the adhesive was subjected to three types of modification presented in table 1. The same time of ultrasound duration (3 min) was adopted for each recipe (the duration and power of ultrasound was determined experimentally based on observation and measurements of the temperature and resin viscosity). Due to the effect of ultrasound, consisting in heating the resin, further tests related to the preparation of the samples were carried out when the resin reached the initial temperature of 22°C. For hardness tests, samples were made in the form of discs with a diameter of 10 cm and a thickness of 1 cm (Fig. 2a). For testing strength properties, paddle-shaped samples were made (Fig. 2b), in accordance with Standards [18][19][20].

The UP 400S stationary sonicator emitting 24 kHz waves with adjustable power range from 0 to 400W was used as the source of ultrasound. Fig. 1 shows a test stand for applying modifications and measuring viscosity.



Fig. 1. Sonicator UP 400S (Andrzej Szewczak)

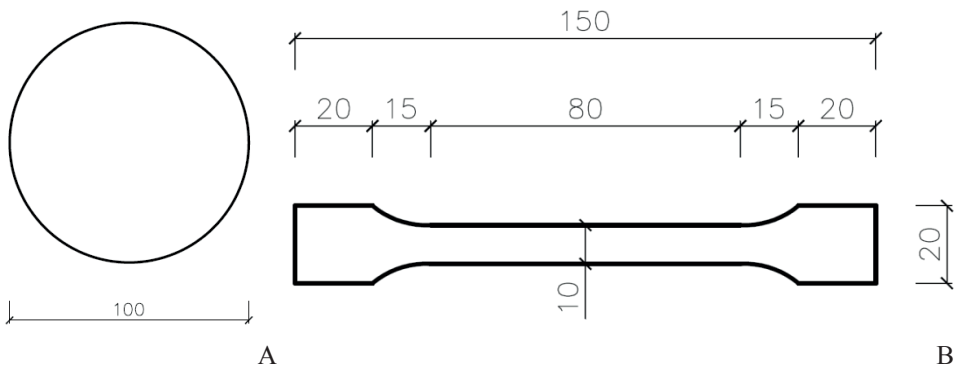


Fig. 2. Test specimen dimensions a) hardness, b) tensile strength (Andrzej Szewczak)

The hardness of the resins was tested using the Vickers method on a Zwick – Roell device assuming a base load of 10 N, and the diamond-shaped tip. Tensile strength tests were carried out on the MTS 810 testing press machine with an additional device with a load range up to 5 kN. All tests were carried out 14 days after sample formation and resin hardening. The end point of the research was SEM analysis to determine the changes in the internal structure of

the resins after the modifications carried out. All samples were stored in temperature 22°C in the time between their performance and research.

During sample preparation, it is important to follow several principles contained in the test Standards [18][19][20]. Paddle-shaped samples with specific dimensions must be subjected to mechanical pre-treatment to determine their uniform thickness of 4 mm, which necessitates the abrasion of the original surface layer (Fig. 3).



Fig. 3. Samples after the machining before tensile testing. (Andrzej Szewczak)

3. Results and conclusions

Table 2. The test results of resin mechanical properties, *results from [16] [17]

Series	1	2	3	4
Hardness HV10	20.35	21.4	20.6	21.03
Standard deviation	0.9	0.5	0.6	0.7
Tensile strength f_t [MPa]	36.97	42.53	29.67	29.44
Standard deviation	1.32	1.35	2.18	1.15
Viscosity* [mPa·s]	665.6	758.4	585.6	1977.6
Free surface energy* [mPa·s]	65.43	72.43	72.6	64.43

Obtained test results, considered together with the results presented in [16, 17] indicate fundamental differences in the mechanical properties of the described composites. Based on the research the following conclusions were made:

1. The modification method has a direct impact on the properties of the outer surface and the internal structure of the adhesive layer. Considering the viscosity (the parameter determining the adhesion of the non-hardened resin to the concrete substrate) and free surface energy (the parameter describing the adhesion of the resin to the substrate after its hardening), it was noticed that ultrasound causes the break of the primary structure of the polymer chains. In this way, free ends of mers are formed (Fig. 4 b), which can directly connect to the substrate or to filler particles, depending on its chemical nature.

2. The data presented in Table 2 show that the differences in the hardness of the resins (hardness is measured on the external surface) are small, at the limit of 1 – 5%, with the most favourable value for series 2. The addition of fillers significantly changed the obtained results. Also taking into account the viscosity results of the modified resins, each modification used should be considered separately. For the second series, it should be noted that the increase in ft value is due to disorganization of the adhesive structure during preparation of the resin under ultrasonic conditions. Re-crosslinking of the polymer structure after adding the hardener results in better distribution and packing of unit molecules and reduction of the distance between the chains.

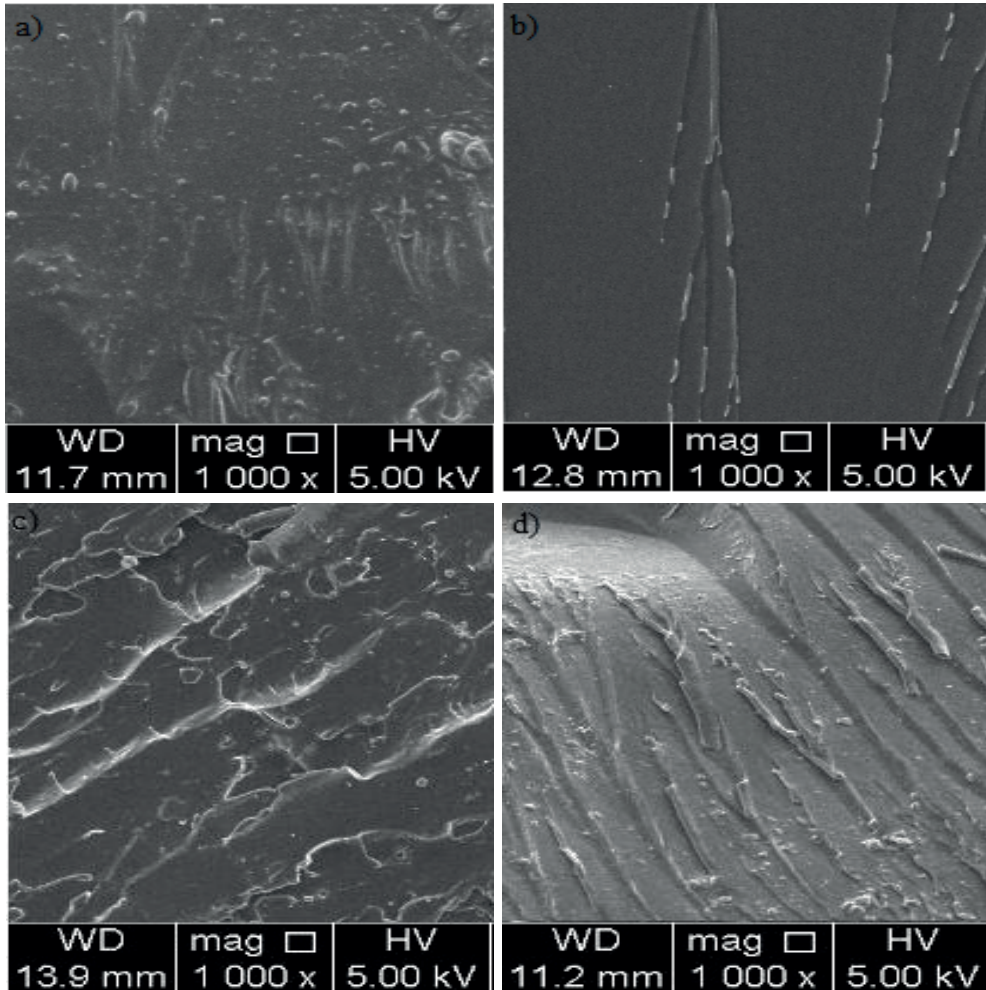


Fig. 4. SEM images of individual series of samples a) EP52, b) EP52+UD, c) EP52+Mk, d)EP52+NR (Andrzej Szewczak)

3. The addition of microsilia reduces the initial tensile strength. This is due to the introduction of spherical microsilia particles into the space between individual mayors. Considering the HV10 hardness results for this series, it was found that the outer layer,

which is in direct contact with the substrate, has an increased amount of microsilica particles that strengthen the external structure of the resin layer. However, their number in the internal structure is smaller. The connections between mers become less durable, but the material does not lose its deformability, it becomes more plastic.

4. For the last EP + NR series, with the addition of carbon nanotubes, it was found for similar conclusions, taking into account a few differences. Nanotubes, whose basic component is carbon, are more chemically compatible with polymer chains, they also have a similar branched structure during decomposition caused by ultrasound energy. Some connections between polymer chains are bound by nanotube particles, which makes them weaker than in series 1 without the addition of fillers. It is worth noting, however, that due to the large specific surface area of the nanotubes, the internal structure of the adhesive is compacted. At the same time, a similar phenomenon was observed as in the case of the EP52 + MK series – some nanotubes are concentrated on the surface layer of the adhesive, which does not cause significant changes in the hardness value.

4. Podsumowanie

At this stage of testing, it is already known that no explicit comparison and evaluation of composites should be carried out with only laboratory results in mind. They should also be referred to the conditions under which the gluing will occur (actual temperature, humidity), the required final effects, the type of glued materials and the parameters of the target surfaces, e.g. roughness. A similar research process can be applied to other construction adhesives, containing e.g. mineral fillers. The resin modified only by ultrasound, i.e. the modification method relatively easy to perform, obtained the best results for both adhesive and strength parameters. The addition of the described fillers has reduced the tensile strength, but taking into account the fact that the resin achieves the greatest adhesion in a thin layer of contact with the ground, this kind of modifications should not be rejected in advance. The addition of microsilica can improve the adhesion of the adhesive under conditions of lower real temperature at the time of its dispensing, and nanotubes may increase this adhesion at high temperature.

Acknowledgements

The research was financed from the funds awarded under the “Young Academic Staff 2017” subsidy.

References

- [1] Rabek J. F., *Modern knowledge about the polymers*, PWN, Warsaw 2015
- [2] Florjańczyk Z., Penczek S., *Polymer chemistry. Basic synthetic polymers and their applications*, Warsaw University of Technology Publishing House, vol. 2, Warsaw 2001.
- [3] Ehrenstein G. W., Brocka – Krzemińska Ż., *Polymer materials: structure, properties, application*, PWN, Warsaw 2016.
- [4] Sadowski Ł., Czarnecki S., Hoła J., 2016, “Evaluation of the height 3D roughness parameters of concrete substrate and the adhesion to epoxy resin”, *International Journal of Adhesion and Adhesives*, vol. 67, 2016, pp. 3 – 13. <https://doi.org/10.1016/j.ijadhadh.2015.12.019>
- [5] May I., Clayton A., *Epoxy resins. Chemistry and Technology*, Marcel Dekker Inc., New York, 2018.
- [6] Lokensgard E., *Industrial Plastics*. Cengage Learning, Eastern Michigan University, Ypsilanti, Michigan, 2016.

- [7] Fang-Long J., Xiang L., Soo-Jin P., “Synthesis and application of epoxy resins: review”, *Journal of Industrial and Engineering Chemistry*, vol. 29, pp. 1-11, 2015, <https://doi.org/10.1016/j.jiec.2015.03.026>
- [8] Wypych G., *Handbook of fillers*. ChemTech Publishing, Toronto, 2016.
- [9] Teh P.L. et al., “The properties of epoxy resin coated silica fillers composites”, *Materials Letters*, Vol. 61, Issues 11–12, 2007, pp. 2156-2158. <https://doi.org/10.1016/j.matlet.2006.08.036>
- [10] Park J. S., Jin. F-L., “Thermal properties of epoxy resin/filler hybrid composites”, *Polymer Degradation and Stability*, vol. 97, issue 11, 2012, pp. 2148-2153. <https://doi.org/10.1016/j.polyimdegradstab.2012.08.015>
- [11] Chikhi N., Fellahi S., Bakar M., “Modification of epoxy resin using reactive liquid (ATBN) rubber”, *European Polymer Journal*, vol. 38, issue 2, 2002, pp. 251-264. [https://doi.org/10.1016/S0014-3057\(01\)00194-X](https://doi.org/10.1016/S0014-3057(01)00194-X)
- [12] Sprenger S., “Epoxy resins modified with elastomers and surface-modified silica nanoparticles”, *Polymer*, vol. 54, nr 18, pp. 4790 – 4797, 2013. <https://doi.org/10.1016/j.polymer.2013.06.011>
- [13] Nakamura Y. et al., “Effects of particle size on mechanical and impact properties of epoxy resin filled with spherical silica”, *Journal of Applied Polymer Science*, vol. 45, issue 7, pp. 1281 – 1289, 1992. <https://doi.org/10.1002/app.1992.070450716>
- [14] Fic S., Szewczak A., Barnat – Hunek D., Łagód G., 2017, “Processes of fatigue destruction in nanopolymer-hydrophobised ceramic bricks”, *Materials*, no 1, vol. 10, 2017. <https://doi.org/10.3390/ma10010044>
- [15] Fic S., Szewczak A., Kłonica M., 2015, Adhesive properties of a low molecular weight polymer modified with nanosilica and disintegrated with ultrasounds for hydrophobization of building ceramics, *Polimery*, vol. 11-12, pp. 730-734, 2015, <https://www.doi.org/10.14314/polimery.2015.730>
- [16] Szewczak A., Szelaǳ M., Modifications of epoxy resins and their Influence on their viscosity, in: *IOP Conference Series: Materials Science and Engineering*, vol. 471, s. 1-9, 2019, doi: <https://www.doi.org/10.1088/1757-899X/471/2/022038>
- [17] Szewczak A. Szelaǳ M., Viscosity and free surface energy as parameters describing the adhesion of the epoxy resin to the substrate, *IOP Conference Series: Materials Science and Engineering*, vol. 484, nr 1, s. 1-7, 2019, doi: <https://www.doi.org/10.1088/1757-899X/484/1/012003>
- [18] PN-EN ISO 3673-2:2012, *Plastics – Epoxy resins – Part 2: Preparation of test pieces and determination of properties*
- [19] PN-EN ISO 527-1. *Determination of mechanical strength at static tensile. General rules.*
- [20] PN-EN ISO 527-2. *Determination of mechanical strength at static tensile. Plastic testing conditions.*

Wpływ modyfikacji żywic epoksydowych na ich parametry wytrzymałościowe

Andrzej Szewczak

*Katedra Budownictwa Ogólnego, Wydział Budownictwa i Architektury, Politechnika Lubelska
Nadbystrzycka 40, 20-618 Lublin, Polska;
a.szewczak@pollub.pl; ORCID: 0000-0001-5933-0483*

Streszczenie: Modyfikacje kompozytów polimerowych to jedna z najszybciej rozwijających się dziedzin techniki. Badania skupiają się na dwóch kierunkach: uzyskiwaniu nowych materiałów lub modyfikacji materiałów już istniejących. W pierwszej grupie badań stosuje

się metody sporządzania nowych wzorów chemicznych polimerów, zawierających główny pierwiastek strukturalny: węgiel (polimery organiczne) lub krzem (polimery nieorganiczne). W grupie drugiej badania polegają na poszukiwaniu metod modyfikacji właściwości polimerów. W budownictwie stosowane są m.in. są kleje (polimery adhezyjne). Wykorzystywane są do łączenia materiałów o różnych właściwościach fizyko – mechanicznych. Pod wpływem działania czynnika inicjującego reakcję sieciowania (utwardzacz lub temperatura) polimery uzyskują formę stałą. Wytrzymałość złącza klejonego zależy od parametrów wyjściowych kleju i docelowej powierzchni jego stosowania. Ponieważ takie złącze jest zazwyczaj najsłabszym elementem, to poszukuje się metod mogących pomóc w poprawieniu parametrów wytrzymałościowych klejów. W opracowaniu przedstawiono wyniki badań własnych nad sposobami modyfikacji wybranej żywicy epoksydowej stosowanej w technice jako klej. W celu zapewnienia skutecznego wymieszania kleju z wypełniaczami zastosowano energię ultradźwięków. Po stwardnieniu żywicy przeprowadzono badania mające na celu ustalenie twardości i wytrzymałości na rozciąganie uzyskanych kompozytów żywicznych. Na podstawie wyników, analizy SEM oraz obserwacji efektu działania ultradźwięków wyjaśniono zjawiska wpływające na zmiany w/w cech mechanicznych.

Słowa kluczowe: żywice epoksydowe, mikrokrzemionka, nanorurki węglowe, ultradźwięki

Liquid plastic films as a solution in terms of tightness problems and roofs aesthetics improvement – review

Barbara Ksit¹, Roman Pilch²

¹ *Faculty of Civil and Transport Engineering; Poznan University of Technology; Poland
barbara.ksit@put.poznan.pl; ORCID: 0000-0001-6459-8783*

² *Faculty of Architecture and Design; University of the Arts Poznan; Poland
grafitpilch@wp.pl; ORCID 0000-0002-6780-1350*

Abstract: Liquid plastic films are understood as single- or two- or multi-component polymer or polymer bitumen mixtures. Liquid plastic films must meet the requirements for waterproofing insulation, which means, among others, that they must protect the roof from mechanical damage and have resistance to weather conditions. Suitability for use as waterproofing must be confirmed by an ETA (European Technical Assessment) certificate. The article presents the advantages and disadvantages of waterproofing coatings. The application and division of sealing compounds with a brief description of individual solutions are presented. It was also pointed out that the roof aesthetics would be improved due to the use of renovation solutions in the form of plastic films.

Keywords: liquid films, waterproofing masses, sealings

1. Introduction

Ready-made masses for waterproofing are most often used to secure foundations and basement walls. Many of them are also intended for sealing bituminous roofing materials. They are also used for waterproofing on terraces and balconies. Some of them are also used for insulation in bathrooms and other rooms with high humidity [1]. Because the material adapts to the geometry of the substrate, it allows to incorporate even complex extensions into the surface, such as through elements, dome skylights or roof drains, and adheres to the roof of almost any shape, which prevents water damage. These properties enable sealing architecturally diverse objects with the highest requirements. Existing roofing often suffers damage during assembly work (e.g. air conditioning devices, antenna masts, advertising stands or roof skylights) [2]-[5]. These devices are placed on the bases fixed to the ceilings, which may result in perforations of the roof slope. After completing the assembly work, it is necessary to thoroughly seal the damaged areas to prevent water from entering the building [Fig. 1]. The use of liquid foil in such cases turns out not only convenient, but often the only reliable solution.

Hard-to-reach places, roof outlets with complex shapes, tight spaces between walls, etc are extremely difficult to seal with bitumen roofing. Its thickness, which is usually an advantage, turns into a disadvantage. The ideal material suitable for insulating such places (but also entire roof slopes) are so-called liquid waterproofing foils.



Fig. 1. Crucial areas in flat high-volume rooftops. Source: B. Ksit

2. Division of materials on the construction market

On the domestic market, the following sealing materials are used for roof surfaces:

Reactive systems:

- methacrylic resins
- (UP) unsaturated polyesters
- polyurethane resins

Dry systems:

- products based on pure water dispersion
- polymers or copolymers acrylics part of the styrene acrylate group.

Single-component bitumen masses. They are used mainly for maintenance and repairs of bituminous roofing materials, especially roofing felt damage. They can also be used to make independent, seamless bitumen coatings. They contain organic solvents, so they should not come in contact with expanded polystyrene and extruded polystyrene.

Two-component bitumen masses. They are used to obtain a thick film with high flexibility. Two-component bituminous masses are suitable for damp insulation and waterproofing. They are used for all mineral materials. They are recommended for vertical and horizontal insulation. They do not damage the foam, so they can be used to fix foam boards to foundations.

Asphalt-resins masses. They are semi-liquid ready waterproofing compounds with excellent adhesive properties. They are made of moisture insulation, and after applying 3-4 layers – also heavier waterproofing. They are also used for gluing roofing felt and maintenance of bituminous roofing materials. Asphalt-resin compounds are not recommended for insulation

inside the house. They have a destructive effect on expanded polystyrene and extruded polystyrene. Instead, they penetrate well into the porous structure of the substrate. They are applied with a brush or roofing brush.

Asphalt-rubber masses – can be **solvent** or **dispersion** (water-thinnable). The former contain asphalt, artificial rubber (latex), fillers and organic solvents. The dispersion masses contain asphalt emulsion, rubber latex, mineral fillers, water and vulcanizing agents. After application they form a flexible, rubbery coating. They are suitable for vertical and horizontal insulation against moisture and water. They are used indoors and outdoors. Some are enriched with reinforcing fibers, which can be applied to slightly damp substrates. Bentonite clay is also added to some. Styrofoam and other polystyrene products can be glued with dispersion masses. There are also masses of asphalt-rubber available which can be applied at any temperature.

Asphalt-polymer masses have the consistency of a dense paste [12]. They are recommended for vertical and horizontal damp-proof insulation, less often for waterproofing. They can be applied to slightly damp surfaces. Because they form a permanently elastic coating, they can be applied to substrates that are exposed to shrinkage and the formation of scratches and cracks. Asphalt-polymer masses do not damage expanded polystyrene and extruded polystyrene. New are the bitumen-polymer mass containing granules of expanded polystyrene. These granules facilitate even distribution of the mass on the insulated surface.

Asphalt-aluminium masses are liquid masses, they contain an aluminium pigment that tints the surface of the insulated layer silver during desiccation. They are used for regeneration of the bitumen rooftops. The exceptions are tar-based coverings. Thanks to the shiny surface that reflects sunshine, the roof preheats less. They are perfect to protect the slate coverings against dust (dust contains harmful asbestos fibers). The masses are also appropriate to seal in the works connected with tinwork on the roofs. The asphalt-aluminium masses are not appropriate to use indoors because they contain harmful substances.

Asphalt solutions – they are used for priming masonry surfaces, before applying the proper waterproofing layer. Asphalt solutions are also used for gluing roofing sheets and maintenance of corroded concrete surfaces. Some of them are suitable for lightweight moisture insulation. Asphalt solutions are also recommended for corrosion protection of metal structures. They are solvent-ready masses for waterproofing. They should not be used to glue expanded polystyrene and extruded polystyrene, as these materials could then dissolve. Asphalt solutions are flammable substances.

Asphalt emulsions – these are suspension of asphalt molecules in the water [13]. water constitutes up to 50% of their volume. Predominantly, they are used as a primer for other insulating materials or as light damp-proof courses. Producers offer two kind of such emulsions:

- **anionic emulsions** –they have a long bonding time – approximately 6 hours. They can be used not only for sealing and priming the bed before the application of the insulating material but also to apply the Styrofoam boards. They can be applied outside the building only if the weather is good, but they can be applied on a wet bed. They are vapour-permeable and odourless.
- **cationic emulsions** – they bond faster and they can handle even very low temperatures. They are not readily available on the market as few producers offer them.

In addition to asphalt emulsions, **latex emulsions** are also available on the market. They have a long setting time. They are resistant to chemicals. They can be used for gluing foamed polystyrene. They are suitable for indoor and outdoor use. They are also used for roofing maintenance. They should be applied to dry, possibly slightly moist substrates.

Polyurethane masses – they are two-component complete masses for hydro-insulation based on polyurethane resins [14]. The polyurethane masses have a semi-liquid consistency. They are suitable for indoor and outdoor use, as horizontal waterproofing and damp-proof courses. They are appropriate for swimming-pools, terraces and balconies insulation. They enable the creation of flexible layers resistant to the chemicals (acids, bases, chlorine, salt and lime solution). Moreover, other than insulating, they fill in small scrapings visible on the surface. They cannot be used to fill in the deeper imperfections of the bed. Bitumen cements – **they are complete masses for the hydro-insulation used pro tem to fix the smaller damages visible on the insulation layers.**

Liquid polymer foils – they are water dispersion of plastics polymer binder, fillers and modifiers. Except for the water-dilutable foils they are also liquid foils containing organic solvents. The polymer foils are mainly used to create the water resistant protection for ceramic siding. They can be applied to create vertical and horizontal insulation. Some of them can be used only inside the rooms and the others can be applied outside the house. They are applied for insulating the walls and the floors of the bathrooms, terraces and balconies just before a glaze or a terracotta application. They can also be used to glue Styrofoam boards. The liquid foils can be applied on the dry and wet surfaces. Additionally, they fill in any imperfections, cracks and scratches visible on the bed. They create a flexible layer resistant to the chemicals. They hinder concrete corrosion. They are marked by a high resilience to the chemicals and the UV light.

Liquid sealants are the products of a structural chemistry based on resins, for example: a flexible unsaturated polyester resins (**UP**), elastic polyurethane resins (**PUR**) and flexible reactive polymethyl methacrylate (**PPMA**). The liquid sealants are appropriate materials for protection in accordance with the requirements of the European Technical Assessments, they are applied as a liquid material (as their name suggests and they are enhanced with a polyester geotextile).

Single-component sealants are ready to use directly after opening the container, they gel when they come into contact with wet air. Multi-component products always have to be mixed together directly before the application on the bed. There is a chemical reaction in these products when the components blend together. Each of these materials gel and they become homogenous sealings without the connections.

3. Liquid foils – general characteristics

3.1. Advantages and disadvantages

Liquid plastic films adhere tightly to the sealed surface, without the need for mechanical fixing. They are seamless coatings and accurately fill all kinds of uneven surfaces. In contrast to bituminous felt or plastic membranes, liquid waterproofing films have excellent water vapor permeability. The advantage in this case is that moist surfaces to which a liquid film is applied can dry over time. When sealing the entire roof slope, there is no need to install ventilation stoves. In most cases, it is unnecessary to remove the old coating, because the load on the sealed surface is incomparably small and is usually about 3–3.5 kg / m², while the thickness of the finished waterproofing coating (in accordance with the requirements of ETAG 005 for liquid films[6]) is about 2.5 mm.

Advantages:

- tight filling
- installation on virtually any surface

- diversified colour palette (reduces heating of horizontal surfaces)
- easy installation in hard to reach places
- very good insulating parameters
- high efficiency
- high level of coverage aesthetics
- **high UV resistance** – the coating does not age, no cracks after years
- **resistance to weather conditions** – coating extremely resistant to snow, rain, extreme thermal loads – frost and high temperatures, air pollution, etc.

Disadvantages:

- a small group of qualified fitters
- high price compared to traditional methods
- difficult to remove

The usage of the liquid foils is diverse:

- a damp-proof protection of the concrete slabs and the walls connected with the ground without exposure to water pressure
- the damp-proof protection of the internal rooms without exposure to water pressure
- the damp-proof protection of the external usable surfaces without an exposure to water pressure
- the damp-proof protection of the concrete slabs and the walls connected with the ground in case of water pressure and permeant waters
- unevenness of the old coating and deformation of the undercoat can be leveled with a flexible and sufficiently thick **intermediate layer**, e.g. made of polyester or glass fiber

3.2. Restoration

Liquid foils are ideal for renovating old coatings and protecting surfaces against environmental degradation. For example, in order to preserve the original stone character of the domes, the still-fresh surface (Kemperol PUR) is sprinkled with quartz sand with a grain size of 0.4-0.8 mm in natural color.



Fig. 2. The roof after the restoration with the use of the plastic foil. Higher level of aesthetics. Source: R. Pilch

4. Pro-ecological use – cool roofs

The Cool Roof Rating Council originated in the United States of America in 1998 (CRRC) – and its main goal is the measurement of the roof features. It is a non-profit organization. [11] The council oversees laboratory tests that are designed to classify products used in roofing. Resins based and polyurethane based masses can be used as a cold coating. The material itself is not ecological, but thanks to its advantages it improves thermal emissivity parameters, i.e. the ability of the surface to return absorbed energy. The modern materials have the emissive ability approximately 0,89 and the reflection factor of approximately 0,78. In case of the traditional covering the reflection factor for the typical materials used to cover the roofs hovers around 0,10 to 0,25. The higher factor lengthens the technical lifetime of relevant materials [15], [16].

5. Summary

Materials used on construction sites should have ecological parameters [17] – such as dispersion masses. These materials are made in the form of aqueous dispersions. When the agent is applied to the atmosphere, no harmful gases are emitted, only water vapor. The basic material presenting an ecological approach is asphalt rubber. An additional material is decorative and covering mass, which can also serve as maintenance and protection of metal surfaces, especially roofing made of galvanized sheet. Liquid foils can also work as cold roofs, reducing the greenhouse effect of large cities and as environmental load reducers. The use of plastic film materials results in obtaining a smooth surface and a uniform color, resulting in improved aesthetics of the roof surface.

References

- [1] Ksit B., “Dachy balastowe jako przykład przystosowania standardowego dachu do wymogów zimnego dachu” in Proceedings – Forum *Nowoczesne budownictwo*, 02.2018.
- [2] Byrdy A., “Pokrycia dachów płaskich z folii z tworzyw sztucznych”, *Izolacje*, vol. 10/2008. <http://riad.usk.pk.edu.pl/~abyrdy/artykuly/Pokrycia.pdf>
- [3] Francke B., “Część C: Zabezpieczenia i izolacje, zeszyt 1: Pokrycia dachowe”, ITB Warszawa 2019.
- [4] Ksit B., Szymczak-Graczyk A., “Rare weather phenomena and the work of large-format roof coverings”, *Civil and Environmental Engineering Reports*, vol. 30(3), 2019, pp. 123-133. <https://doi.org/10.2478/ceer-2019-0029>
- [5] Ksit B., Monczyński B., *Zabezpieczenie dachów płaskich i tarasów*. Verlag Dashofer, 2012.
- [6] ETAG 005-06: In Form einer flüssigen Versiegelung aufgetragen. Besondere Rückstellungen für flüssige Folien auf Polyurethanbasis.
- [7] Adamoski J., Matkowski Z., *Materiały do wykonywania warstw hydroizolacyjnych w dachach płaskich*. Medium, 2016.
- [8] Coster M., Chermant J., “Image analysis and mathematical morphology for civil engineering materials”, *Cement and Concrete Composites*, vol. 23, 2001, pp. 133-151.
- [9] Grębiszewski M., “Gotowe masy do hydroizolacji”. Available: <https://budujemydom.pl/> [Accessed: 20 Jan 2020]
- [10] DIN EN 1350 1–5 Klassifizierung von Bauprodukten und Bauarten zu ihrem Brandverhalten.
- [11] Klatt R., *Wtyczne do projektowania i wykonywania dachów z izolacją wodochronną- wtyczne dachów płaskich*, DAFA DP 2.01, 2011.

- [12] PN-EN 13707:2013-12. Elastyczne wyroby wodochronne – Wyroby asfaltowe na osnowie do pokryć dachowych – Definicje i właściwości.
- [13] PN-EN 13956:2013-06. Elastyczne wyroby wodochronne – Wyroby z tworzyw sztucznych i kauczuku do pokryć dachowych – Definicje i właściwości.
- [14] Leszkowski K., *Synteza właściwości jonowo przewodzących materiałów poliuretanowych*, Phd dissertation, Faculty of Chemistry, Gdansk University of Technology, 2011.
- [15] Pilch R., "Charakterystyczne elementy współczesnej sztuki budownictwa" in *UNESCO, MAN AND THE BIOSPHERE, URBAN SYSTEM*. Zimowski L. ed., Uczelniane Wydawnictwo WSG, Bydgoszcz, 2011.
- [16] Laks I. et al., "Hydraulic and legal conditions for buildings in floodplains-case study of Kalisz city (Poland)". *IOP Conference Series: Materials Science and Engineering*, vol. 471 (2019), 102050. <https://doi.org/10.1088/1757-899X/471/10/102050>
- [17] Trechsel H.R., *Moisturecontrol in buildings*. ASTM Manual Series, Philadelphia. 1994.

The wooden architectural complex of the city and royal residence of the John III Sobieski in Kukizów

Mykola Bevz

*Department of Build Conservation; Faculty of Civil Engineering and Architecture;
Lublin University of Technology; Nadbystrzycka st. 40, 20-618 Lublin, Poland;
Department of Restoration of Architectural and Artistic Heritage; Institute of Architecture and Design;
Lviv Polytechnic National University; Bandera St. 12, 79013 Lviv, Ukraine;
m.bevz@pollub.pl; ORCID 0000-0003-1513-7045*

Abstract: The palace in Kukizów of King of Poland John III Sobieski is known only to a narrow group of architecture and art historians. The palace and park complex ceased to exist in the 19th century. The architecture of the palace is known especially from the descriptions in the inventory documents from the early 18th century. Although the authorship of the palace design belongs to the well-known artists of the era – Augustyn Wincenty Locci and Piotr Beber, its architecture has not yet been reconstructed. A specific feature of the royal residence in Kukizów was the construction of royal buildings and town buildings in a wooden material. The intention to create a city complex and an entirely wooden residence was a unique experiment in the field of European architecture and urban planning of the 17th century. In the paper we present the results of our research on the architecture of the palace and town for the end of the 17th century.

Keywords: royal residence, Kukizów town, John III Sobieski, palace, park, 17th century

1. Introduction

As Zbigniew Wójcik, the author of the book about John III Sobieski, rightly writes, the king “added splendor to his rule by building a number of monuments of both secular and sacred architecture. The most famous work of his patronage is undoubtedly the beautiful palace in Wilanów near Warsaw...” [40, p. 392]. Some of his initiatives implemented in Ruthenia and the Lublin region include the reconstruction of the castle, palace, and park in Jaworów, renovation of the castle and park in his hometown Żółkiew, the extension of the castles in Złoczów, Olesko, Pomorzany, and manors in Żółtańce, Wysock, and Pilaszkowice. In Żółkiew, the king transformed the castle buildings, added bathrooms in the park and expanded the hunting court in Garaj [21, p. 183]. He also rebuilt his tenement house on the Market Square in Lviv. It is not without reason that historians believe that the king liked his hereditary possessions the most in Rus’ (Ruthenia) region – Żółkiew and Jaworów, where he most often stayed [40, p. 397–398].

This is also proved by the little-known fact of building a royal summer residence in the late 80s of the 17th century with a palace and garden in the town of Kukizów, near Lviv and Żółkiew. The above-mentioned objects in Rus’ lands, liked and nurtured by the king, belonged to the headquarters of the elders and were rebuilt and adapted to the new needs of the royal court. The only newly built object, entirely built on behalf of the John III, was the palace complex in Kukizów. We can conventionally assume that it was the “Wilanów” in

the Ruthenian lands (Rus' or Ruthenia – the name of the east part of the Polish state in the 14-18th century). John Sobieski's full title was – King of Poland, Grand Duke of Lithuania, Ruthenia, Prussia, Mazovia, Samogitia, Livonia and in Kyiv, Smolensk, Siversk and Czernihiv lands: *Dei Gratia Rex Fidei Defensor Poloniae, Magnus dux Lithuaniae, Russiae, Prussiae, Masoviae, Samogitiae, Livoniae, Smolenscie, Kijoviae, Volhyniae, Podlachiae, Severiae, Czernichoviaeque*) [17]. However, while the palace complex in Wilanów is often referred in scientific literature and recent years this object has been carefully restored together with the façades of the palace, its interiors, garden quarters, the palace complex in Kukizów ceased to exist in the 19th century and only lives in scientific literature, thanks to the few publications of historians. But, e.g., Zbigniew Wójcik [40, p. 619], the author of an excellent biography of King John III, published in 1983, when writing about the King's stays in Rus' region, unfortunately, makes no mention of his Kukizian period of life or the design and construction of a palace with a park in Kukizów. The lack of this information is also noticed on numerous websites devoted to King John III [17, 20].

2. Analysis of previous studies

The Kukizów royal palace is known only to a narrow group of experts in the field of history of architecture and art. Art historians who devoted attention to this are: Tadeusz Mańkowski [24, p. 133–138], Mieczysław Gębarowicz [13, p. 231–245], and in recent years Jerzy Kowalczyk [21, p. 183–189]. The first two authors reconstructed the history of the palace and its main features. Kowalczyk more precisely set the date of the palace and garden creation, narrowing down the construction for 1687–1694. He also proved the authorship of the project of Augustyn Wincenty Locci and justified that the palace was built by Piotr Beber. In his dissertation, Kowalczyk also performed a graphic reconstruction of the palace plans, based on an analysis of the inventory from 1741. Due to the fact that the palace in Kukizów did not survive to our times, Kowalczyk's work is the only and unique attempt to bring knowledge of this object in the form of planning reconstruction. It also encourages further search for information about the Kukizów residence that would complement its history, being a clue to the detailed reconstruction of architecture and urban planning.

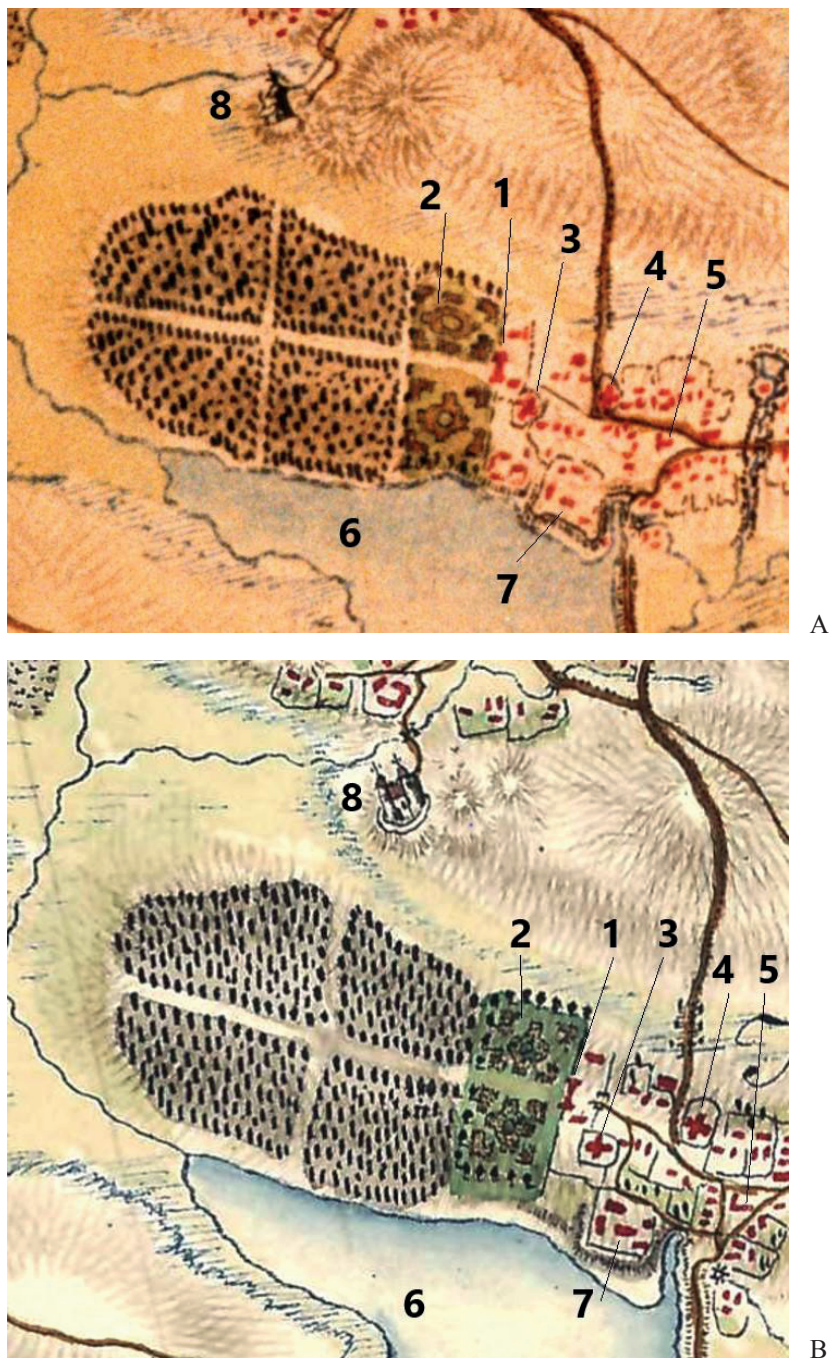


Fig. 1. The town of Kukizów on the map of F. von Mieg: A) drawing of the town plan from the period of the first map editing from 1781 (negative print; photo by the author taken in Kriegsarchiv in Vienna) [26]; B) drawing of the city map from the period of the second map editing (so-called “fair copy” of the map) from 1782 (from the internet publication of the map on the “The Mapire.eu” website [25]). Numbers indicate: 1 – palace, 2 – park, 3 – wooden Greek Catholic church, 4 – wooden Catholic church, 5 – Market Square with a wooden town hall, 6 – lake, 7 – old castle, 8 – wooden church in the village of Remeniv

Archival information about the palace complex in Kukizów is very poor. In the Lviv archives, materials regarding the town's history have been preserved, but unfortunately there are no documents about the royal residence. The most important source remains the inventory of the palace and garden from 1741, from the archive in Warsaw (published by M. Gębarowicz [13, p. 231–245]). A new, very important source for clarifying the location of the palace and recreating the complex planning system was the map of Friedrich von Mieg, made in 1779–1782, and kept in the military archive in Vienna. Although the map was made by hand in a scale of 1:28800, Kukizów is drawn on it with extreme precision [26]. Based on the map analysis, the complex plan reconstruction was successfully completed and published in 2006 [10, p. 64-65]. Major analyses of the palace and town were made in our publication in 2016 [11].

3. Purpose of the paper

In this work, we try to recreate the planning and spatial structure of the Kukizów town during the construction of the royal residence and determine the exact location of the palace by reconstructing the complex planning system of the residence with the park and fortifications. It needs to be pointed out that there was no single building (palace) in Kukizów. An unique architectural and urban complex, characteristic of the Baroque era, was created. Studies on the urban context of the residence have not yet been carried out. The issues of linking the palace with the garden and fortifications are not fully displayed.

4. Presentation of research results

Professor J.Kowalczyk tried to determine the hypothetical location of the palace and garden on the basis of the cadastral map from 1854 [21, p. 188]. It should be noted that this map shows the small remains of the former complex (fragment of the garden without the palace) after its major transformations in the 18th and the early 19th century. Our field research and observation of small traces of palace foundations allowed for a more accurate indication of its location.

To reconstruct the planning structure of the royal residence built at the end of the 17th century in Kukizów, we must first analyze the conditions of its creation and the earlier nature of the settlement, answering the questions of what the motivation was for choosing the site of the palace and park complex and how its surroundings were shaped.

4.1. Reconstruction of earlier development stages of Kukizów

The Kukizów urban development is divided into several individual phases.

4.1.1. *The first phase, dated to the 15th century, when the settlement and a small castle were located here*

The first mention of the Kukizów town was recorded in December 1440, in the record of the postponement of the court case about the ownership of the pond in Kukizów between Stefan and John (Stephanus, Iohannes) from Lviv and Gregorius (Georgium de Kukyziv) from Kukizów [5, ark. 44]. The information about the pond is very important. The pond and the picturesque surroundings were later factors shaping the town's development.

The name was given from the surname Kukiz, which may have oriental linguistic origins (Turkish-Tatar) [18]. Karaites origin cannot be excluded: "kok" – blue, "koz" – eye

[9, p. 336-337]. The owners of the settlement were the Kukizowski family, and the above-mentioned Gregorius from Kukizów – its representative [5, p. 19].

4.1.2. The second phase can be dated to the 16th-17th century

Already at the end of the 15th century, the village belonged to the Herbut family [8, p. 606], who bought it from the Kukizowski family [33, p. 176]. In 1502, Aleksander Jagiellończyk as a reward for the faithful service of Frederick of Kniehnicz (de Knyahunicze) Herbut, transferred the village from Polish and Ruthenian law to the Magdeburg law [8, p. 854]. According to the author's hypothesis, the Herbut castle (on a square plan with semicircular bastions or towers in the corners) was located in the southwestern part of the downtown, in today's "tower". It was probably built at the end of the 15th or the beginning of the 16th century on a small hill above the pond on the town's border.

To this day, older residents of Kukizów remember the toponym "tower", which they call the territory to the left of the road, at the entrance to the city through a dam on the pond (near the mill). The remains of the fortifications were leveled after World War II [41, p. 500]. We have no doubt that the remains of the tower (or towers) of the older castle were called so. Confirmation of oral tradition can be found on the map of F. von Miega from 1779, where between the downtown and the pond, quite carefully, traces of earth embankments after two towers or bastions (Fig. 1a) [26] were drawn.

Traces of one more manor (or small castle) were identified outside the city (fig. 2), in the western part of the settlement – on an artificial island, in the middle of a large pond, in the "castle", at the small settlement in Leszczów (Leszczów). The castle was located on an area increased by 3-4 m above the pond, on an island with a diameter of about 100-125 m (fig. 2). It was surrounded by a ring of rampart and ditch (still partially preserved to this day) among the wide, swampy valley of the Remenowski Potok River. From north to southwest, this valley was cut by a dam, which served as an entrance road to the castle. Its relics are preserved to this day. The object itself was found on a map from 1890 (Fig. 3) [22]. The artificial islet with a rampart and moat was leveled in the 1980s as a part of the agricultural work of the local kolkhoz. Quite recently, this place was entered into the provincial register of archaeological monuments as a "late medieval castle" [35, p. 56].

As part of the field reconnaissance, a significant amount of archaeological material was collected from the surface. First of all, the finger-bricks of various sizes were found, as well as profiled gothic bricks (which can be testified to the building from the 14th-16th century), remains of stove tiles and pottery, metal objects, fragments of stained glass with a diameter of 8.5 cm, and a ball stone with a diameter of 10-12 cm. Historians and conservators date this material from the 15th to the 17th century [2, p. 1-8]. The oldest unwashed tiles have gothic features. Some ceramics probably come from the ceramic center in Potylicz. A huge heap of bricks testifies to the existence of brick buildings here in the past.

The small castle on the island was probably built by the Herburts (as evidenced by dating some archaeological materials) and used as a hunting lodge.

After 1502, when Kukizów moved from Polish and Ruthenian law to the Magdeburg law, the city began to transform from a rural settlement to an urban type. There was a market square and a regular street plan, fortifications (downtown defense shaft from the west and east, with a moat dug) and three gates. The privilege confirming the town rights from 1538 of Zygmunt I Old also introduced a weekly market and two fairs a year [8, p. 607]. The city's coat of arms was a key on a red background, symbolizing the key of St. Peter.



Fig. 3. A fragment of the map of 1890 with a castle near the Leszczów forest (Kriegsarchiv Wien. H 76-133, F. Map of 1890 of Galicia [22])

At the turn of the 16th and 17th century, Kukizów became the property of the hetman Stanisław Żółkiewski. In the erection act of the church in Żółkiew of January 12, 1623, Jan Żółkiewski defines himself as “heir in Żółkiew, Jaryczów, Nahaczów, Dziedziłów, Kukizów...” [4, p. 213]. After the death of the son of the hetman, the goods went to the daughter Zofia, and then to her granddaughter Teofila, who married Jakub Sobieski. John III Sobieski inherited the town from his mother [13, p. 231]. He made the town his residence and built a palace, which was finished in 1690 [21, p. 184–185]. After him, the son Konstanty took over and renewed the Magdeburg rights (privilege of May 20, 1699) [3, p. 113]. In this document, Kukizów was also called the Krasny Ostrów. After the death of Konstanty, Kukizów fell to the eldest son of John Sobieski, Jakub. In 1740, his daughter Maria Karolina sold the town to Michał Radziwiłł [20, 18].

The mention of the existence of a orthodox church in Kukizów from 1560 is noted in the document regarding the donation of the processional cross of artistic work by a shoemaker from Żółkiew [34, p. 77–108]. An independent Catholic parish was established in Kukizów before 1600. The date of establishment is unknown. The first church was to be very modest, without any foundation [19]. In the Sobieski era, a Karaim colony was established in Kukizów, consisting of five families brought from Troki [7, p. 26–28], which had their kenasa (synagogue) here [16].

4.1.3. The third phase of the town's development is dated to the second half of the 17th and the beginning of the 18th century

The next, most interesting from the urban point of view, stage of city development is associated with the Sobieski family. We can assume that John III Sobieski was attracted to this place because of the picturesque location and good hunting conditions. The swampy valley of the river flowing from Kulików, with numerous bends, was an ideal place for hunting wild birds. The presence of an old hunting castle next to a large pond and a small forest increased the attractiveness of the place. Located near Żółkiew and Lviv, the wooden town was perfect for a summer stay and rest in the countryside. There is no doubt that the older downtown castle and Herburt's hunting castle were used by Sobieski for this purpose, although they were small and outdated buildings, not really suitable for the new needs. The requirements of running the royal court necessitated the design of a new residence. Its architecture, taking into account the character of the town, was to be made of the traditional material (wood), but made in a modern style, combined in a compositional way with the town's buildings and blended into the park.

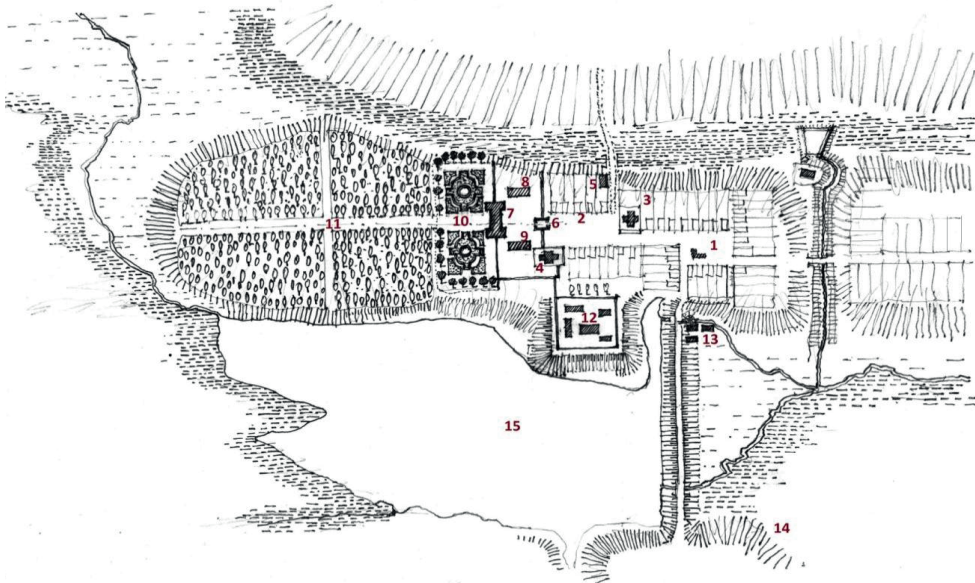


Fig. 4. Preliminary reconstruction of the planning and functional structure of Kukizów from the second half of the 18th century based on the analysis of the original “fair copy” of the F. von Mieg map from 1782: 1 – market square with the town hall; 2 – square-esplanade in front of the royal residence; 3 – Roman Catholic church; 4 – Greek Catholic church of St. Nicholas; 5 – brickyard; 6 – entrance gate to the former residence; 7 – palace; 8 – kitchen; 9 – chancellery; 10 – one-story bed garden; 11 – walking sticks; 12 – court buildings at the site of the older castle; 13 – mill; 14 – Karaim cemetery; 15 – pond (author Mykola Bevz, 1996 [10, p. 150])

After the decision to build a summer residence in Kukizów was made, preparatory and design work began. The concept envisaged the creation of a new palace and park complex in the western part of the city, next to the downtown and the old castle. The design of the new complex, according to Mieczysław Gębarowicz, was initially made by the famous Dutch architect Tylman of Gameren [13, p. 232]. The architect's archives included designs of wooden palaces, one of them signed as "the design of a multi-story wooden manor for the king" [28, p. 274]. Thus, the version about the participation of Tylman of Gameren in the birth of the idea of architecture of the new wooden palace of John III Sobieski may be true. How the project was played out is unfortunately not known. Eleven drawings of the aforementioned Tylman's project were lost during World War II, so we cannot connect and compare design decisions with the urban and topographic situation in Kukizów.

Jerzy Kowalczyk proved that the design of the palace was created with the participation of the architect Augustyn Locci, who is described as the author of the design in documents created during the construction of the building [21, p. 182]. The builder of the palace is Piotr Beber – the architect who realised most of the royal buildings in Rus, the author of, among others, the extension of the town hall tower in Kraków, the Korniaкта tower in Lviv, the town hall and synagogue in Żółkiew, the castle in Nowy Jaryczów and others [27, p. 397]. The construction of the palace lasted until 1693. Then the park was designed (in Italian style?) and the town was tidied up. It was also mentioned that the king himself was directly involved in the work next to the gardener [21, p. 234].

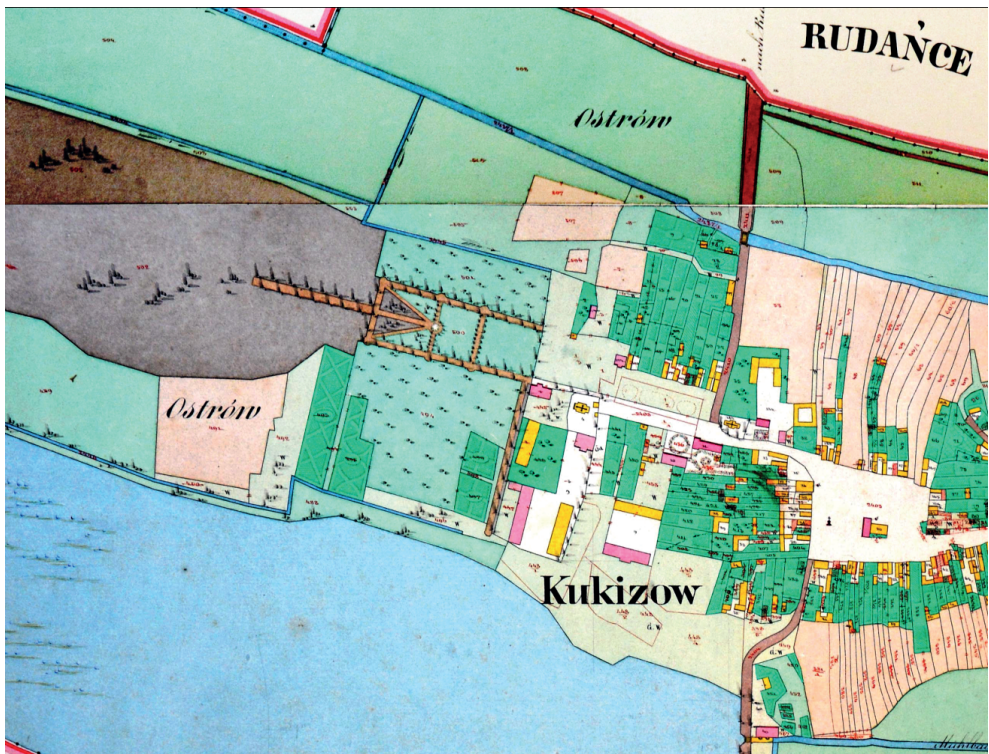


Fig. 5. Kukizów on the cadastral map from 1854 (Tsentrалnyi Derzhawnyi istorycznyi archiv Ukrainy v misti Lvovi, Fond 186, opys 5, sprava 330. – Kukyziw. Kadastrova karta, 1854. – Ark. 3, 8 [36])

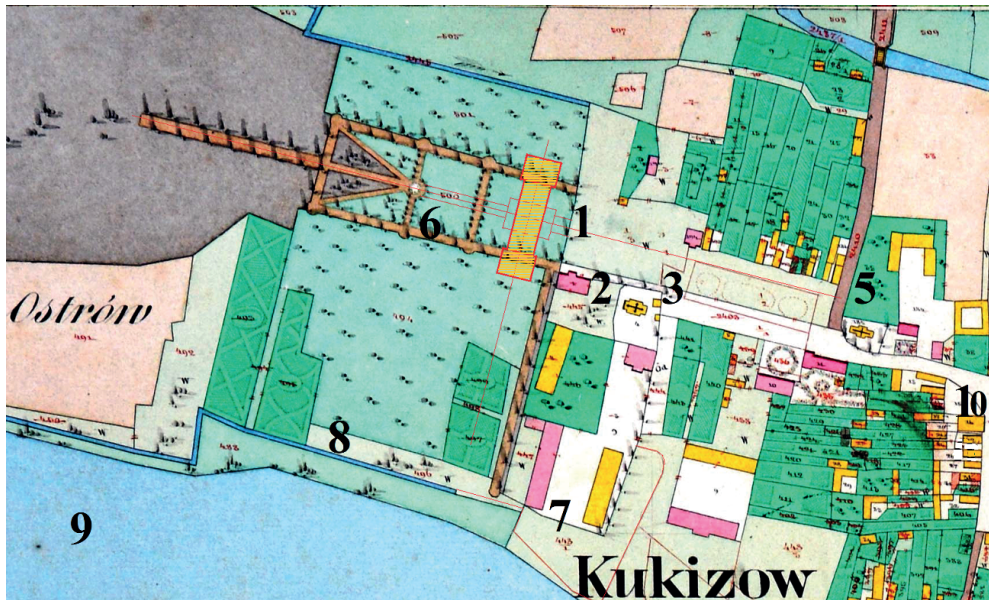


Fig. 6. Hypothetical reconstruction of the palace location on the base of the cadastral map of Kukizów from 1854: 1 – the hypothetical place of the palace; building configuration; 2 – the building of former chancellery; 3 – Greek Catholic church; 4 – the building of former kitchen; 5 – the Catholic church; 6 – park; 7 – remains of south bastion; 8 – the canal; 9 – the lake; 10 – the building of kenasa

According to the inventory of June 20, 1741, the park occupied an area of approximately 17,000 square fathoms (62,000 m²). Part of the park was planned in a regular-quarters style (there were rows of clipped plantings, there were a large number of medicinal plants, a special gardener's house was built) [21, p. 234]. It is assumed that the second part of the park was shaped in the form of alleys marked out in the existing forest, so that its natural environment can be included in the garden. The main garden avenue also cut west through the forest and lengthened towards the castle on the pond by a long wooden bridge made of oak piles. Remains of piles were removed after World War II, after the liquidation of the pond [29, p. 78].

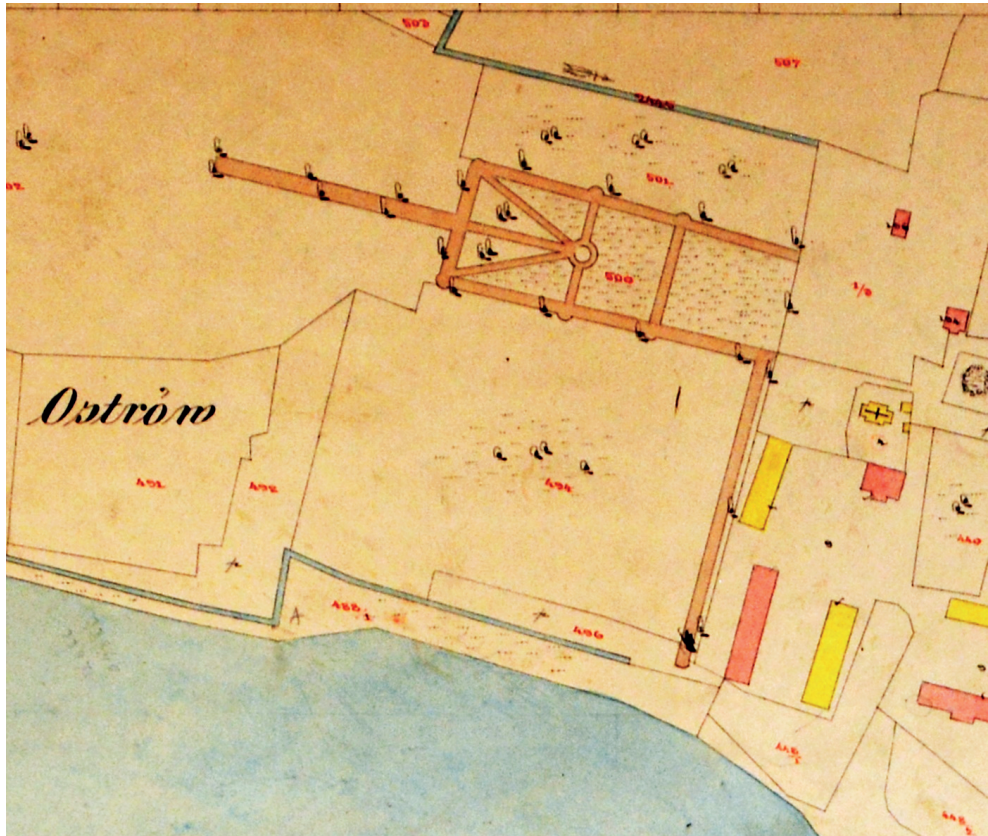


Fig. 7. Kukizów on the cadastral map from 1870 (Tsentralnyi Derzhavnyi istorycznyi archiv Ukrainy v misti Lvovi, Fond 186, opys 5, sprava 331. – Kukyziw. Kadastrova karta, 1870. – Ark. 8) [37]

The palace was located in the western part of Kukizów, behind the ukrainian church grounds (Fig. 5, 6, 7), on the border with the downtown area. The complex of residence was also built: kitchen, granary, bakery, basement, barn, dock at the pond, as well as the building of chancellery [21, p. 244].

The name “Zwierzyniec” was also found mentioned in archival documents (referred to in the letter-request of the townsmen of Kukizów to C.K. Governor of October 29, 1814) [29, p. 103–104]. Although the case concerns a dispute from the beginning of the 19th century, this mention is considered to be an important fact, indicating the existence of a zoo in the royal park in the past. Knowing King John III’s preference for hunting, it can be undoubtedly said that the introduction of the zoo took place in parallel with the establishment of the park. At the beginning of the 20th century, the area above the pasture was referred to as “the pond” (on the cadastral map of 1854 this place above the pond is marked as *islat* – “Ostrów”) (Fig. 5, 6, 7).



Fig. 8. Kukizów on the cadastral map from 1927 (Tsentralnyi Derzhavnyi istorychnyi archiv Ukrainy v misti Lvovi, Fond 186, opys 5, sprava 335. – Kukyziw. Kadastrova karta, 1927. – Ark. 8 [38])

4.2. Hypothetical reconstruction of the architecture of the Royal Palace

Art historian Jerzy Kowalczyk presented the reconstruction of the palace plan (based on the reading and interpretation of the palace inventory from 1741) as a rectangular building with a six-column portico in the main eastern facade (Fig. 9). The palace was extended on the north-south line [21, p. 184-185], a newer version can be sketched, specifying the general scheme of the palace plan, combining Kowalczyk's concept with the analysis of the palace plan on the map of F. von Mieg and cadastral maps of Kukizów from 1854, 1890 and 1927 [15, 26, 36, 37, 38, 39]. According to the drawing on the map, it can be concluded that the palace as an elongated rectangular in the plan, had two projections on its sides (where, as we know, there were offices: the king in the south and the queen in the northern part, alcove on the first floor and wardrobes on the ground floor).

Figures 10a and 10b present the author's version of the reconstruction of the palace plan. projections are added protruding beyond the façade line on the main and garden facades from the plan of F. von Mieg (Fig 1a). The presence of projections also results from the palace's descriptions in the inventory from 1741, where it was noted that in the corners of the roofed floor there were helmets covered with sheet metal with pinnacles made of wood and white metal. The architectural solution of helmets in the corners of such a small palace was exceptionally possible with the existence of projections, when the helmet structure protruded outside from the main body of the roof. In a letter of August 29, 1690, of Piotr Beber, the builder of the palace, to Andrzej Wolski, writer of the goods of Żółkiew [21, p. 184], he talks about the crowning of the four corner cabinets with "pinnacles with tin knobs and wooden elements, which are to be made by the carpenter according to the model prepared by Beber".

The author's version of the palace plan develops slightly the hypothesis of Jerzy Kowalczyk (compare Fig. 9 and 10). The difference is mainly in adding projections. The second important factor is the length of the building. Based on Mieg's map, the plan is reconstructed in different proportions – the building is longer and each room has a square plan (which was characteristic of a wooden building). Inside the building there was the gallery-balcony, which surrounds the great hall at the height of the second floor; it had a rounded plan. The six-column portico supported on the main and garden façades was, in the author's opinion, two stories high and crowned with a triangular gable (Fig. 10, Fig. 11).

After the palace was built in 1693, works on decorating its facade continued for some time, as well as the construction of the gate, walls around the residence, buildings “for the convenience of the court” and the garden [21, p. 185].

The palace was decorated with the participation of a German stucco master (sculptor?) sent from Warsaw [6, p. 33]. His participation in the works was noted in letters to Andrzej Wolski from 1696. The artistic decoration of the palace was also made by master Tymofij. In 1690 he came to Kukizów after being paid from the castle cash in Żółkiew for the paper “for painting abrasions to Kukizów” [6, p. 60]. It can be assumed that these were palace interior decoration designs.

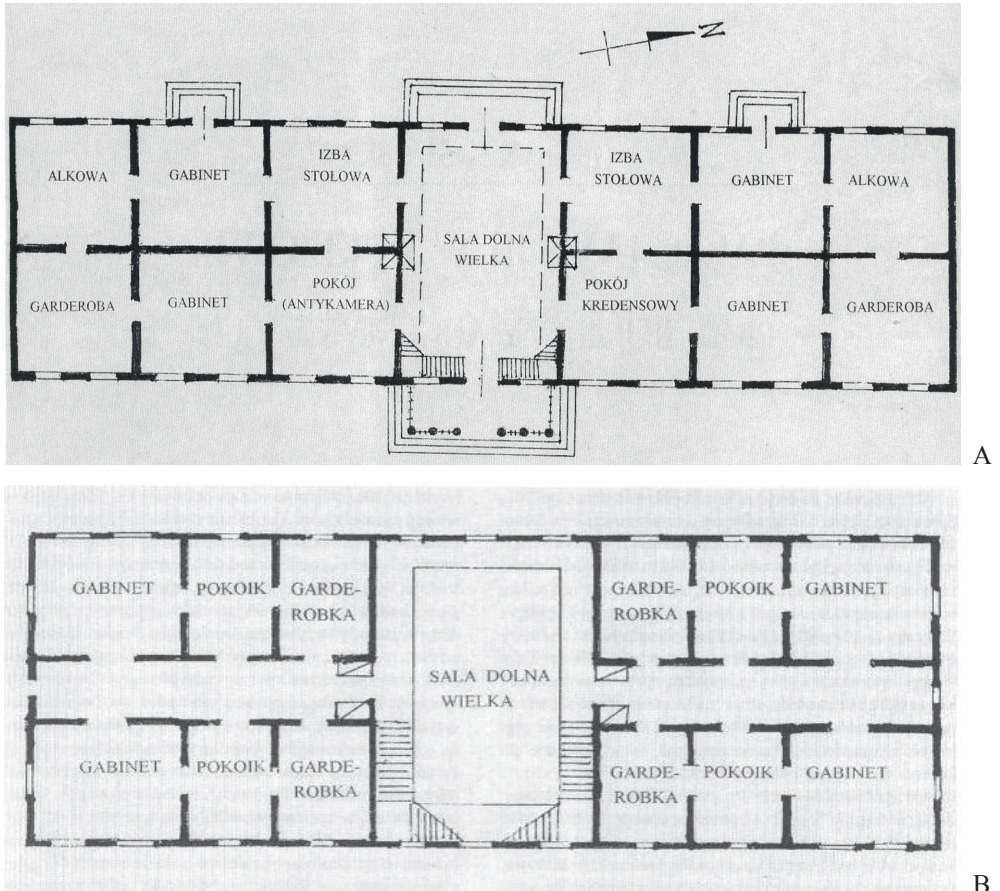


Fig. 9. A, B – Hypothetical reconstruction of the planning structure of the palace of John III Sobieski in Kukizów by J. Kowalczyk (*Kowalczyk J. Pałac Jana III w Kukizowie: Piotr Beber czy Augustyn Locci? // Arx Felicitatis. – 2001. – S. 183-189* [21])

Mieczysław Gębarowicz believes that painting works in the newly built wooden Kukizów residence began in June 1690 [13, p. 245–247]. An unknown group of contractors took part in the works. Piotr Poznański and Udnowski [6, p. 61], as well as journeyman Karaim, were mentioned in the accounting books, without giving his name. In 1692, the painter Tymofij worked on ceiling decorations [6, p. 61]. It is known from the inventory of 1741 about the ceiling painted on canvas in the king's bedroom (in the alcove) and in the table room, where it was painted on plaster (“alfresco”) [13, p. 237]. The note of August 29, 1695 gives information about “a painter devoted to master Tymofij, how to paint on the headliners in the Kukizów palace, sent in a tin box from Warsaw” [6, p. 61].

The palace was built using special technology of wood cut to the format of a brick and bonded on a lime mortar (like the bathrooms in Żółkiew). From the outside, the walls were painted red, imitating a “brick thread” [13, p. 238].

In summary, drawing information from various sources, here is an attempt to recreate the image and calendar of the royal residence.

Palace: a two-story building with a third floor hidden in the roof; tops of four corner cabinets with pinnacles and wooden elements (according to the Beber's model); large windows on the ground floor and smaller on the first floor, with fittings and shutters; the size of the glass is different (French windows in the royal apartments); in 1692, 460 straight glass panes were prepared for the palace; inside, works completed in 1693; in 1694, the outside walls were still in a raw state, without developing the facade; the work outside was not completed during the king's life (1696); inside there were furnaces from the workshop in Sieniawa (the order of John III to make tiles by craftsmen of the pottery guild in Sieniawa dates back to 1693 [23, p. 114]); the palace architecturally beautiful and unusual; in 1711 one side of the palace (main) was ready in terms of both painting and woodcarving; in 1739, interior decorations (paintings and goldsmiths) were led by Antonio Castelli (for the new owner – Gozdski) with the participation of Bazyli Petranowicz.

In November 1693, the king personally, accompanied by the architect, measured the location of the gate and other buildings for the convenience of the manor [24, p. 137]. These facilities were to be built quickly, within one season.

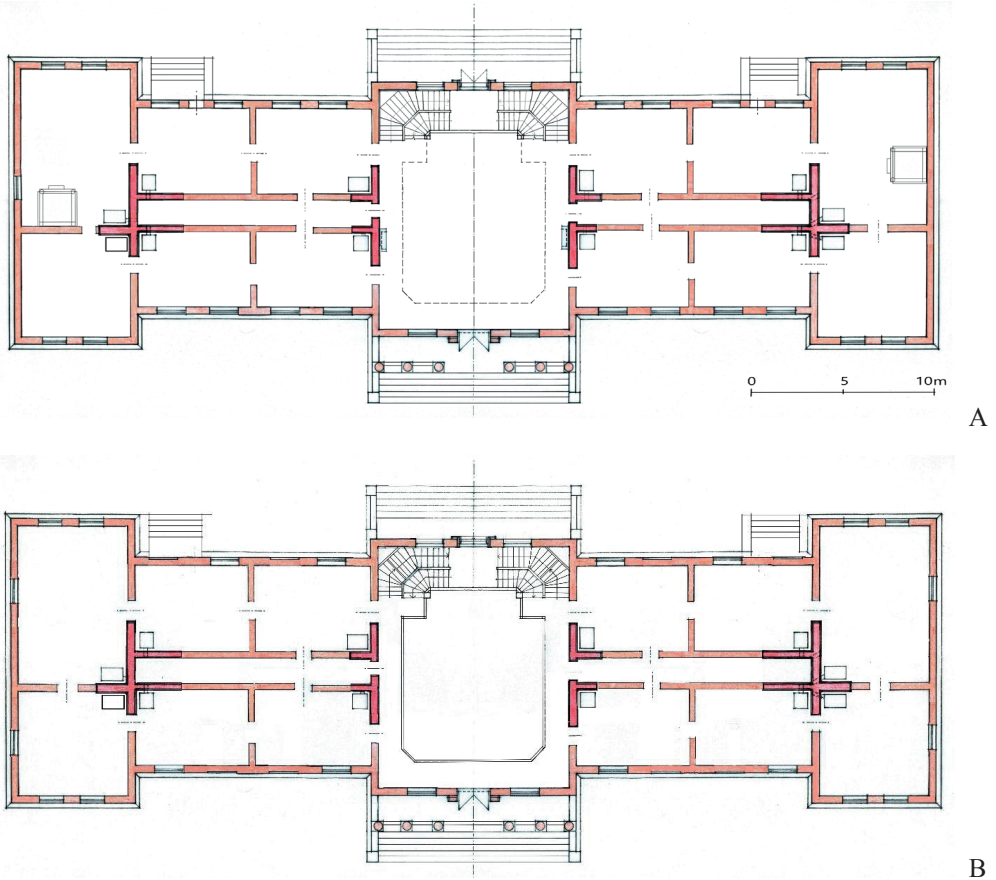


Fig. 10. A hypothetical reconstruction of planning structure of the palace of John III Sobieski in Kukizów for the period from the end of the 17th century made based on analyzes of the original 1781 F. fon Mieg map and the cadastral map from 1854 (Mykola Bevz, 2019): a) parter; b) the first floor

In the inventory from 1741, on the occasion of the writing of a lease contract by Gozdski, the object was described as follows:

- the palace built of wood;
- the palace has the three-story form (third floor fused into the attic);
- the plan of the story – is the arrangement on a mirror principle (plans illustrated by J. Kowalczyk; Fig. 9a, b) and our version (Fig. 10a, b);
- the palace has the six-column portico on the axis of the main and rear elevations; the entrance on the main facade has a carved portal;
- a two-story floor is in the center of the building; above the first floor there is a second one in the attic;
- a large upper hall with seven windows is above the lower hall; next to is a confectionery with three windows and four doors;
- corner upper offices topped with a roof with domes (helmets);

- dormers in the roof with two windows;
- shingled roof;
- the palace has a regularly divided façades: in the front facade 17 axes of windows (and doors) and 19 in the garden facade;
- windows for two and four quarters each; lower windows on the first floor;
- facades decorated with pilasters;
- the corners of the palace enclosed in wooden rust decoration “ad instar hewn stones” [13, p. 242] (one vertical row on the ground floor had 14 tiles; in total there were 505);

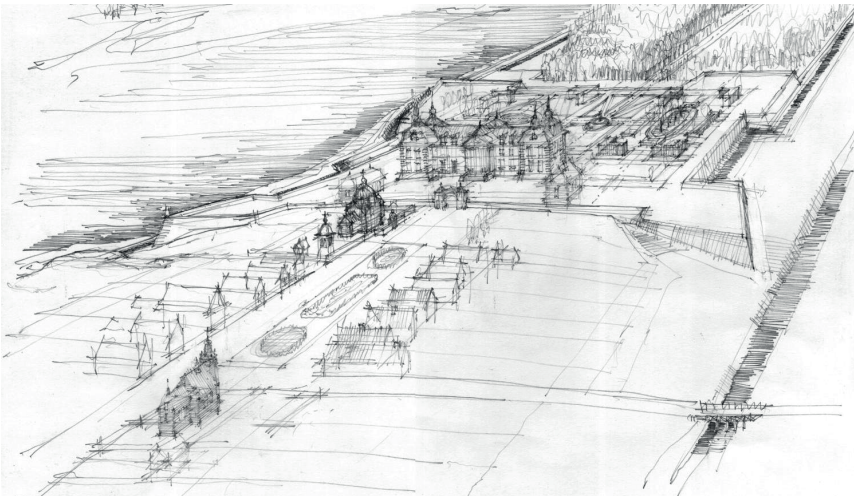


Fig. 11. A hypothetical reconstruction of the palace and park complex of John III Sobieski in Kukizów for the period from the end of the 17th century, aerial drawing (by Mykola Bevz, 2014)

- to give the building the appearance of a brick building, the palace was painted red, “in a brick” [13, p. 242] (on a plaster base?);
- portico in the facade on six columns, between which there are banisters, above the door the “texture of wood carving work” (lintels carved, profiled, decorated with cartouches and figurines of carved melons);
- Sculpture decoration “Melusine holding the shield with gilded crown” [13, p. 242] is on the façade from the side of the garden above the central door;
- “domes covered with white sheet metal and four iron studs with white metal shields on four corner cabinets” [13, p. 242] above the first floor; the rooftops on the corners of the building differed from the roof of the body; the corner tops had not a mansard broken form with shingle sheathing, but were made in the form of a helmet and covered by white (zinc) sheet; each helmet was finished with a needle iron pinnacle, to which a zinc shield (painted and gilded?) was attached – the Sobieski’s family emblem);
- the palace built on a brick pedestal (with a basement in the north-east corner from the side of the kitchen).

In 1840, the palace ceased to exist. Its iconography is unknown. After the finish of the palace build, the park was founded (in Italian style) and the town was cleaned up. In cooperation with the gardener, the king himself took part in the works [13, p. 234].

Garden: after the Kukizów acquisition in 1810, Gerwazy Strzelecki describes the garden (the palace does not exist) as follows: the “Lord’s garden” at the pond (new) and the “Italian garden from Fossa” (royal) [21, p. 189]:

- the gardens covered an area of around 17,000 square fathoms (62,000 m²); new garden – 1/6 of the area; part of the royal park in the style of regular housing [13, p. 234], part in the form of a forest with marked paths (fig. 12);
- not very extensive assumption, limited from the west with a “thrust” or defensive fortifications (?); the entrance to the garden led from Ostrów through a drawbridge;
- axial composition: a central alley and two parallel sides, between which linden coolers (cabinets) were located in the corners and four of them – in the middle “with sofas and a marble table”;
- terrace garden, with turf stairs;
- quarters surrounded by boxwood and filled with ‘various herbs’;
- fruit trees between the quarters and on the sides of the garden [13, p. 244-245].

Jerzy Kowalczyk believes that the garden designer was Jakub Kochanowicz – administrator of the royal gardens in Ruthenian estates in the years 1681–1688 [21, p. 188]. A gardener’s house was built in the park, as well as the abovementioned economic facilities of the residence.

The planning structure of the city during the existence of the royal residence consisted of two main parts connected to each other: a palace and park complex with a ring of bastion fortifications and downtown with a market square in the center. The panorama of the town next to the palace is dominated by the silhouettes of three temples: the church, the Orthodox church, and the Karaim kenasa. The downtown consisted of a market square with a wooden town hall and three main streets (Fig. 12). The city had its fortifications, and thanks to its excellent location on the hill, it was surrounded by water on all sides.

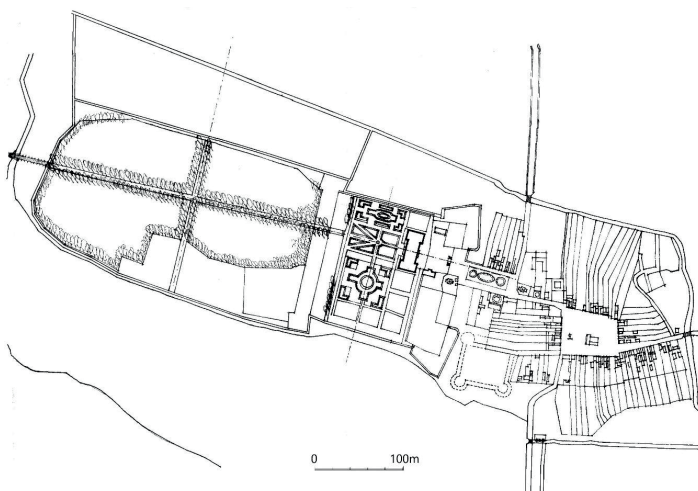


Fig. 12. Reconstruction of the planning structure of the town, palace and park complex of John III Sobieski in Kukizów; author’s version, drawing by Mykola Bevz

A wide esplanade led to the residence from the market, which was a continuation of the street from the northwest corner of the square. The composition of the esplanade was oriented on the main axis of the palace building. In the eastern and southern spans of the esplanade buildings, wooden buildings of the church and orthodox church appeared as dominants.

Reconstructing the old planning scheme of the palace complex of the John III Sobieski, let's analyze the historical maps of Kukizów. At first glance, the park plan presented on the cadastral map from 1854 does not agree with the previous plan on the map of F. von Mieg (Fig. 1 and 6). It also does not correspond with historical descriptions of the park from the time immediately after John III Sobieski (from the 1741 inventory).

The map of F. von Mieg was made in two editorial versions [32, p. 18], which differ partly in content. In the context of the presentation of Kukizów's plan, they should be analyzed as the original and a copy (fair copy) of the map, made between 1779 and 1782 (Fig. 1a and 1b). The copy is poorer with important details. The original drawing (Fig. 1a) shows in more detail the old Herbut castle, which was located by the pond at the entrance to the town from Lviv.

The monastery buildings on the former bastion, south of the church (they were drawn on the copy) were shown precisely. The market square was drawn more accurately in the form of a square (the copy of the market square is irregular). On the first and second versions of the map, the plans of the palace gardens are fundamentally different. On the original, two-quarters of the garden are drawn in different sizes. The southern section is larger, square in plan, with a cross flower bed in the center. The northern, however, smaller, rectangular, has the form of an oval flower bed, cut off, without wings. These right and left parts that vary in size, as well as the clear asymmetry of the garden plan concerning the main avenue, also appear on the cadastral map from 1854.

On the newer version of the map of F. von Mieg, the garden plan has been "improved" and drawn as the symmetrical layout with even quarters. Of course, there is a situation when in the first version the unknown author sketched the plan of the palace and park foundation by nature, passing on correctly perceived details, and in the second version (made based on the first, in cozy conditions) the second author mistakenly "improved" the configuration of the garden quarters for more regular and symmetrical.

The plan of the palace on the map of F. von Mieg was drawn very precisely – in a rectangular form with four corner projections. We can even approximate the proportions of his plan. The border of the manor and its fence was shown. From later photos of the church, published by Yaroslav Taras and Ryszard Brykowski [12], we can assume that the fence was made of brick. From the photo (Fig. 13) we even read the brick thread – in the order the head and cart layers, which proves the authenticity of the wall from the 17th century. An interesting thing is an entrance to the church from the north shown in the photo. Standard solutions provide for the arrangement of the entrance to the church from the west and rarely from the south, never from the north. Violation of this rule was caused by the need to connect the entrance to the church with the pre-palace esplanade.



Fig. 13. The Greek Catholic Church of st. Mykola from 1708 in Kukizów. Photo from the beginning of 20 century (the holdings of the Museum of Ethnography in Lviv [12, p. 165])

The entrance gate to the royal residence was to be located on the longitudinal axis of the rectangular esplanade, laid out between the downtown and the palace complex. The gate axis from the opposite side of the square visually closed on the main facade of the church. When the residence was still there, all the buildings on the esplanade square were wooden – a Catholic church, a Greek Catholic church (Fig. 13) and residential buildings (fig. 14). Roofs and other finials had shingle roofs. It is known from the documents that the king went to the forest with the architect, to choose wood for the construction of the gate [21, p. 187]. We can conclude that the architecture of the gate also had elements in a wooden structure. Behind the gate was a small pre-palace square, framed on two sides with symmetrical wooden chancellery and kitchen buildings. The gate axis “closed” on the six-column portico of the palace.

4.2. Reconstruction of town planning

The town square was built up with wooden buildings according to the one pattern [3, p. 113–115]. In the center of the square, a wooden town hall building with beautiful architecture was erected.

The entire downtown urban complex with the buildings of residents (Ruthenians, Poles, and Karaites), town hall, kenasa, church and orthodox church was connected to the complex of buildings of the royal residence – a palace with a large, beautiful, orderly, two-part garden, office buildings and kitchens – all in wooden construction. Together, they created an urban complex of a city residence, unique to Poland and abroad. It is believed that the complex created in Kukizów was also unique due to the accepted compositional and urban principles as a town-baroque residence.



A



B

Fig. 16. A – The old buildings in the northern frontage of Rynek square in Kukizów.

Photo by Mykola Bevz, 1986

B – The old buildings of Rynek square in Kukizów, the beginning of 20 century.

Drawing by A.Hrechylo, from the book of A.Persowski [31]

Cadastral maps, although younger than Mieg's maps, complement our knowledge of the residence complex. The oldest cadastral map is dated to 1854 (Fig. 8) [36]. The palace and some of the residence buildings no longer existed. The map accuracy and precision in the presentation of details made it possible to read on it the remains of ancient fortification lines – two bastions with rounded ears (presumably Italian-style, which can be an additional argument for the authorship of the design of Augustyn Locci), connected to a partially preserved network of moats and water channels from the lifetime of the residence. Noteworthy are two

artificial water channels framing the garden from the south and north. Undoubtedly, they formed the boundary of the complex, and their form indicates a connection with two bastions in the eastern part of the residence. According to the author's hypothesis, these bastions did not have a defensive function, but they were a standard decoration of the royal palace. The cadastral map confirms the asymmetry of the garden composition with respect to the main axis of the entire assumption (this also results from the map of F. von Mieg).

On the cadastral map small remains of the park are noticeable: two green side quarters are presented, but without one-story compositions with flowerbeds. The central, rectangular part of the pre-palace lawn has been preserved, from which the main avenue begins (indicating the course of the compositional axis of the former assumption). This avenue began in the round form of the square with accompanying, diagonally running, two side avenues (Fig. 6, 12).

The planning details discovered on the maps have been adapted to reconstruct the plan of the entire assumption (Fig. 11 and 12). The justification for this scheme is given below.

The location of the palace can be hypothetically drawn on a cadastral map, between two main alleys, along the axis of the round square and the central lawn, along the axis of the alley entering the forest. We can assume the width of the palace, remembering that the side elevations of the garden facade descended into the garden (this information from the inventory of 1741 was highlighted in the publication of J. Kowalczyk and presented on his reconstruction of the palace plan). It seems logical that the aforementioned stairs from the palace were oriented on two side alleys (Fig. 6, 10 and 12). The combined diagram of the two avenues on the cadastral map indicates that the distance in the axes between them is about 30 m. Based on the palace plan reconstructions of Jerzy Kowalczyk, we can assume that the length of the palace was about 40–42 m. It should be assumed that the width in the projection section was about 14 m. The palace building of this size presented on our planning reconstruction of the complex (Fig. 6, 12). The reconstructed plan also took into account the existence of a small square with chancellery and kitchen buildings between the gate, church, and palace. The location of the facilities and the planning layout of the square are obtained from the data of the map of F. von Mieg and the cadastral map.

The first mention of the existence of a church in Kukizów refers to 1560. It is the author's opinion that, during the creation of the residence, a new church building in the Baroque style was also built (photo on Fig. 13). The catholic church in wooden frame construction, like the orthodox church, had façades in the Baroque style. The late transmission says about the foundation of a new church dedicated to Saint Stanisław in 1668 by Mikołaj Giedziński, which was to be burned by the Tartars. In 1730 another wooden church was erected in Kukizów, dedicated to Saint James the Apostle, from the foundation of Prince Jakub Ludwik Sobieski [19].

In the 17th century the Market Square was called the Karaim Market. We know about the invitation of the Karaims by John III Sobieski [31, p. 46]. After 1831, they moved from Kukizów to Halycz [34, p. 854]. The mill in the southern part of the city existed from the beginning of the city's history.

5. Conclusions

The main conclusions from the presented research are as follows:

- In Kukizów in earlier times, before the palace complex was founded by John III Sobieski in the 1680s, there were two fortified mansions (castles): The older one

was located at a distance west of the city, on an island, in the middle of the swampy valley of the Dumna River and Remenowski Stream (remnants of wall foundations with fragments of the Gothic bricks, traces of embankment and moat in the form of a circle; it was a building from around the 15th and 16th centuries). The second castle, on a rectangular plan with semicircular bastions in the corners (founded probably in the 16th century), was located on the bank of the pond, southwest of the town center and was connected with city ramparts.

- The residence with the palace of John III Sobieski was built in a new place, irrespective of the previous two castles, in the western part of the urban settlement, on the extension of the street running from the northwest corner of the market square.
- The palace complex of John III Sobieski was surrounded by a bastion line of fortifications, the traces of which are still legible on historical cartographic materials from the late 18th and mid-19th centuries. This allows us to perform a graphic reconstruction of the planning structure of the object. Answers to the question about the functions of the bastion line: to what extent was it military or only ceremonial, should be sought in future studies.
- The park and garden part of the complex consisted of five main buildings: 1. a palace square from the city side (combined with the church and orthodox church buildings); 2. a one-story garden adjacent to the west facade of the palace; 3. a regular housing garden on subsequent park terraces; 4. the forest and park part, running west, on the continuation of the main axis of the residence; 5. a small hunting castle on the island, adapted to new needs, in the middle of the pond.
- Downtown and the palace-park complex, including the woods, were located on a conventional island, surrounded by water from all sides: from the south and west – by ponds, and in the east and north – by the bank of the river.
- The planning scheme of the residence, garden, and town complex shows the author's professional qualifications and his great experience in designing urban compositions. In our opinion, the complex concept belongs to an Italian school. The question of whether it is the urban composition of the object by Tylman of Gameren (the general scheme of the assumption resembles essentially his plan of residence in Przeclaw, designed for the Rej), or the palace architect – Augustyn Winsente Locci, or its builder – Piotr Beber, remains unresolved, but does not seem particularly important: probably all of the mentioned persons, including John III Sobieski, took part in the creation of the residence.
- The analyzed palace and park complex in Kukizów, as well as the entire town, require further thorough archival and field research.
- The urban complex of the royal residence in Kukizów – an outstanding and little-known work of Baroque architecture, was one of the greatest examples of wooden architecture of the 17th century in Poland and Europe.

The residence in Kukizów was a charming rural residence, corresponding to the 17th-century ideals of life, according to which summer holidays had to be spent in a quiet place where there was no rigid etiquette and life seemed simpler. The image of the reconstruction of these assumptions justifies the new name of Kukizów – Krasny Ostrów, created after the implementation of John III Sobieski foundation.

The implementation of the complex of the royal residence and the city in the form of a wooden architecture presents an unique experiment in the space of Baroque architecture in Europe, where dominate exuberant, rich stucco decorations of artificial stone, fanciful

forms of buildings separated by rustication, projections, belts of multiple cornices and pilasters. Wooden material was also the most suitable for receiving forms of the imposing baroque architecture.

References

- [1] Aftanazy R., *Dzieje rezydencji na kresach dawnej Rzeczypospolitej*. – Warszawa: Ossolineum, 1999. – T. 7.
- [2] Archive of the Department of Architecture and Conservation, Lviv Polytechnic National University: Bevz, Mykola, Materials of field survey of the old castle in Kukizów-Leshchiw, sygn. 2016-PM-01, p. 1-8.
- [3] AGZ. – T. I. – Warszawa: 1868. – S. 113-115. (przywilej z 1699 p.) [in] http://www.europeana.eu/portal/record/92033/Bibliographic_Resource_3000053548350.html [Access: 19 Dec 2018]
- [4] AGZ. – T. X. – Warszawa: 1884. – S. 213. Dokument erekcyjny kościoła w Żółkwi. Available: http://www.europeana.eu/portal/record/92033/Bibliographic_Resource_3000053548350.html [Access: 19 Dec 2018]
- [5] AGZ. – T. XIV. Najdawniejsze zapiski sądów lwowskich. 1440-1456. – Warszawa: 1889. – S. 19 (dok. 137). Available: http://www.europeana.eu/portal/record/92033/Bibliographic_Resource_3000053548350.html [Access 19.12.2018].
- [6] Aleksandrowycz W., “Ukrajinski malarii pracijuczi na dworci Jana III Sobiesko”, in: *Chronika 2000. - Ukrajina-Polszcza: dialog uprpdowz tysiaczolit*. Kyiv, 2012, pp. 17-151.
- [7] Balaban M. “Karaici”, in: *Studia historyczne w Polsce*. pp. 26-28.
- [8] Baliński M., Lipiński T. *Starożytna Polska pod względem historycznym, geograficznym i statystycznym opisana*. Warszawa, 1845. pp. 606-607.
- [9] Baskakov N.A., Zajączkowski A., Šapšal S.M. *Karaimsko-russko-polskiy slovar'*. Moskva, 1974, pp. 336–337.
- [10] Bevz M., “Problemy reheneratsiyi zapovidnykh terytoriy istorychnykh mist”, *Visnyk Natsionalnoho Universytetu „Lvivska politechnika“*. Arkhitektura. L'viv, 2001. №429, pp. 146-155.
- [11] Bevz M. “Pałac królewski Jana III Sobieskiego w Kukizowie: próba rekonstrukcji urbanistyczno-krajobrazowej”, in: *Władza i architektura. Rezydencje monarchów i siedziby władz państwowych w Europie – formy i funkcje (XV-XXI w.)*, Materials of the 1st PRE international scientific conference in the Royal Castle in Warsaw, 9-11 April 2014, ed. Anna Czarniecka, Przemysław Deles, Angela Soltys, Zamek Królewski w Warszawie-Muzeum, pp. 261-281.
- [12] Brykowski R. *Cerkwie drewniane na kresach*. Warszawa, 2001. pp. 77.
- [13] Gębarowicz M. *Szkice z historii sztuki XVII wieku*. Chapter 3: Pałac w Kukizowie. Toruń: 1966. pp. 231-245.
- [14] Janusz B., “Karaici i ich cmentarzysko w Kukizowie”, *Ziemia*, 1911, vol. 11, p. 3.
- [15] Cadastral Maps and Landowner Records from Kukizow. Available: <http://www.geshergalicia.org/towns/kukizow>. [Access: 20 Sep 2019]
- [16] Cracovia Leopoldis, DUBLANY / JAMNA / JAREMCZE / KUKIZÓW / SOKAL / WOROCHTA. Available: <http://www.cracovia-leopoldis.pl/index.php?pokaz=art&id=1499> [Access: 21 Apr 2015]
- [17] Wikipedia.org, Jan III Sobieski. Available: https://pl.wikipedia.org/wiki/Jan_III_Sobieski [Access: 10 Mar 2020]
- [18] Wikipedia.org Kukizów. Available: <https://pl.wikipedia.org/wiki/Kukiz%C3%B3w> [Access: 20 Apr 2019]

- [19] Kościół parafialny pod wezwaniem Św. Jakuba Apostoła w Kukizowie. Available: <http://www.rkc-skowyra.com/publ/7-205-2//Dekanat Żółkiew> [Access: 20 Sep 2019]
- [20] Szlak Sobieskiego. Available: <http://szlaksobieskiego.pl/publikacje/1/1.pdf> [Access: 20 Apr 2015]
- [21] Kowalczyk J., „Pałac Jana III w Kukizowie: Piotr Beber czy Augustyn Locci?”, *Arx Felicitatis*, 2001, pp. 183-189.
- [22] *Kriegsarchiv Wien*. H 76-133, F. Mapa 1890 r. Galicya.
- [23] Kuśnierz K. Sieniawa. Krakow, 1999. p. 114.
- [24] Mańkowski T., „Mecenat Jana III w Żółkwi”, *Prace Komisji Historii Sztuki*, 1948. pp. 133-138.
- [25] Galizien und Lodomerien (1779–1783) - First Military Survey, Available: <https://mapire.eu/en/map/firstsurvey-galicia/?layers=144&bbox> [Access: 20 Apr 2019]
- [26] F. Von Mieg map. *Osterrachisches Staatsarchiv. Kriegsarchiv*. Sygn. B IX A, ark. 265.
- [27] Milobędzki A., *Architektura Polska XVII wieku*. PWN, 1980. p. 397.
- [28] Mossakowski S., *Tylnianin z Gameren. Architekt polskiego baroku*. Wrocław, Warszawa, Kraków, Gdańsk: Zakład Narodowy imienia Ossolińskich, 1973. 350 s.
- [29] Mychailo P., *Pamijatajemo tebe. Meminimus Tui. Z istorii Kukezowa*. Lviv, 2014, pp. 77-108.
- [30] Gębarowicz M., „Opisanie pałacu Kukizowskiego die 24 Juni 1741 Anno. Inwentarz pałacu, ogrodu, folwarku i ratusza w Kukizowie z archiwum Jana Tarły” in: *Szkice z historii sztuki XVII wieku*. Chapter 3. Toruń: 1966, pp. 236-245.
- [31] Persowski F., *Osady na prawie ruskim, wołoskim i niemieckim w ziemi Lwowskiej*. Lwów, 1924, p. 46.
- [32] Petryszyn H., *Karta F. von Miega” (1779 -1782) jak dzerelo do mistoznavstva Halyczyny*. Lviv Wydawnictwo Nacionalnoho uniwersytetu “Lwiwska Politechnika”, 200, p. 290.
- [33] Uruski S., *Rodzina. Herbarz szlachty polskiej*. Vol. VIII, 1911, p. 176.
- [34] Sulimierski F., Chlebowski B., Walewski W., *Słownik Geograficzny Królestwa Polskiego i innych krajów słowiańskich*. Warszawa, 1883, vol. IV, p. 854.
- [35] Sweszniuk I.K., *Dowidnyk z archeologii Ukrainy. Lwiwska oblast*. Naukowa dumka, Kyiv, 1976, p. 56.
- [36] *Kukyziv, kadastrova karta, 1854 r.*, ark. 3, 5, 7, 8. *Tsentralnyj derzhawnyj istorycznyi archiw Ukrainy w misti Lwowi*, fond 186, opys 5, spr. 330.
- [37] *Kukyziv, kadastrova karta, 1870 r.*, ark. 8. *Tsentralnyj derzhawnyj istorycznyi archiw Ukrainy w misti Lwowi*, fond 186, opys 5, spr. 331.
- [38] *Kukyziv, kadastrova karta, 1927 r.*, ark. 3, 5, 7, 8. *Tsentralnyj derzhawnyj istorycznyi archiw Ukrainy w misti Lwowi*, fond 186, opys 5, spr. 335.
- [39] *Kukyziv, karta 1890 r.* – ark. 44, (1440). *Tsentralnyj derzhawnyj istorycznyi archiw Ukrainy w misti Lwowi*, fond 9, opys 1, spr. 1.
- [40] Wojcik Z., *Jan Sobieski: 1629-1696*. PIW, Warszawa 1983.
- [41] Zdybel B., „*Kukyziv jakyj ja znaju I jakyj ja czula*”, in: Mychailo Padura. *Pamijatajemo tebe. Meminimus Tui. Z istorii Kukezowa*. Lviv, 2014, pp. 500-505.

The possibility of DIC system application in numerical models updating

Barbara Turoń¹, Bartosz Miller²

¹ *Department of Structural Mechanics; Faculty of Civil and Environmental Engineering and Architecture;
Rzeszow University of Technology; Powstańców Warszawy 12, 35-959 Rzeszów, Poland
bturon@prz.edu.pl; ORCID: 0000-0002-7013-6304*

² *Department of Structural Mechanics; Faculty of Civil and Environmental Engineering and Architecture;
Rzeszow University of Technology; Powstańców Warszawy 12, 35-959 Rzeszów, Poland
bartosz.miller@prz.edu.pl; ORCID: 0000-0003-3318-4339*

Abstract: The paper presents the results of updating of numerical models of the rectangular steel plate members in a plane state of stress, the updated parameter was a support length. Three different members loaded in a static or dynamic way were analyzed. The article shows examples of purely numeric updating. The data used to the update of numerical models was obtained from numerical simulations and it corresponds to the data, which can be measured by using the Digital Image Correlation (DIC) system. The main aim of the paper is to check the possibilities of the DIC system application in updating of numerical models.

Keywords: Digital Image Correlation, DIC system accuracy, optimization, updating of numerical models

1. Introduction

Reproduction and simulation of the behavior of real structures using numerical models is an invaluable source of information for engineers. The possibility of numerically generating a structure response may significantly shorten the design and the experimental research processes. It can also help to avoid high costs and technical difficulties connected with a performance of experimental measurements. The creation of precise models of structural elements, element connections and complete structures is a paramount issue, both in analyzes of conditions of real structures and in the design of the structures. Numerical models are continuously being improved thanks to technological progress, development of the computing power of computers and the development of advanced procedures for engineering calculations. Nevertheless, inaccuracies still appear in numerical models. The inaccuracies can be caused by a variety of factors. For example, they can be associated with the modeling of support conditions or they can appear as a result of the material heterogeneity. To eliminate the inaccuracies, numerical models can be updated. It means they can be corrected and improved on the basis of the results of the experimental research (the comparison of the results of the experimental research carried out on the real structure with the results of numerical simulations of the model of the structure which is used to change and to improve the numerical models) [1].

2. Digital image correlation – the method and its accuracy

2.1. Characteristics of the Digital Image Correlation method

Digital Image Correlation (DIC) is a full-field image analysis method, based on high-resolution grey value digital images of an object under a load. The images are recorded during a change of shape and/or location of the examined object. This method is used for the determination of contours, displacements and strains of investigated objects. This method allows for measurements in two-dimensional (2D) or three-dimensional (3D) spaces. Compared to the traditional measurement methods, DIC gives a possibility to acquire in a very short time a very large amount of data on displacements and strains of the tested object from its entire surfaces, or in case of a larger element, from surface fragments, moreover in a non-contact way [2-4].

During the measurement process, the image of the investigated object is taken before the deformation process and series of images are recorded after applying the load to the object. Digital Image Correlation uses the correlation algorithm for the data evaluation. To achieve a successful correlation between the two images, it is necessary to apply random speckle patterns on the object surface by spraying the white-and-black pattern onto the sample surface. One of the recorded images is selected as reference (most often it is an image of the object taken before its loading). A regular grid with equidistant grid points is laid over the image of the reference camera (if there is more than one camera, only one is selected as reference) at the reference step. Each grid point defines the center of a squared image region in the reference image. This square area around the grid point is called a facet (see Fig. 1). The correlation algorithm uses facets in order to identify the corresponding area of another image. It locates every facet of the reference image in subsequent deformed images. For 3D DIC the image correlation algorithm uses these facets for determining the 3D-position and tangential plane of the underlying object surface for each of the grid points. The correlation algorithm is based on the tracking of the grey value pattern in small local Adjacent facets so each facet must contain a characteristic part of the pattern with good contrast features. The minimal size of the facet is limited by the size and roughness of the stochastic pattern on the object surface [2-6].

The DIC measurement results in a determination of the contour and the deformation of the investigated object and obtaining data of the strain state of the object. The direct measurement result of DIC are displacements of the object in two or three directions. The calculations of strains are based on the value of displacements. The measurement quality relies on exact knowledge of the parameters of the DIC system, the determination of these parameters is made in a process called calibration. The calibration is obtained by recording images of a unified calibration target under different perspective views. A bundle-adjustment algorithm is used to determine the DIC parameters. This knowledge of the parameters allows to evaluate the geometry of the object from captured camera images. An object point is identified in the images of the two cameras by applying the correlation algorithm and finding homologous points. Taking the imaging parameters into account, the contour of the object can be calculated. Calculating the transformation parameters for images under different conditions of loading, both the displacement vector and deformation for each facet can be determined. Considering the object curvature, the strain can be calculated by the parameter of the affine transformation and by the gradients of the deformation [2-6].

The application of the image correlation method in mechanics dates back to the 1980s [7-9], however, only in recent years, intensive research has allowed for significant development and improvement of this method, among others by using high-resolution digital

cameras in measurements. An example of a measuring system based on the digital image correlation method is the Dantec Dynamics Q-450 system. The basic elements of the system are two high-speed digital cameras, the control computer with Istra 4D software, the Timing Box synchronizing multiple sensors and ensuring that the images are recorded at the same time, and calibration targets. The measurement carried out using Q-450 system consists of several stages: the sample preparation for the test by creating a random pattern of points on its surface, the preparation of the measurement set-up and the hardware configuration, the system calibration by using special calibration targets, the proper measurement i.e. the images registration during sample loading, the analysis of saved images based on correlation, and the visualization of obtained results [3, 6].

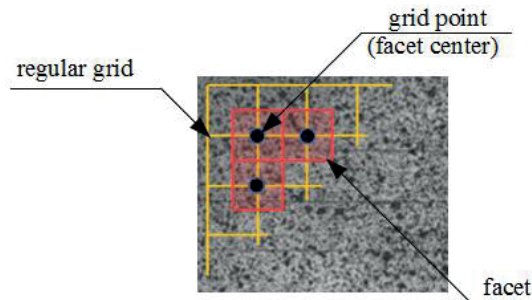


Fig. 1. Virtual grid of points and facets grid

2.2. DIC system accuracy on the example of the Q-450 system

Accuracy of the measurement system is a very important issue in the research and planning of the tests. Over the past few years, the accuracy of DIC has been investigated by many researchers. For example, Guoqing Gu et al. [10] studied the influence of the non-uniform intensity images on the measurement accuracy of DIC (influence of non-uniform illumination was analyzed through the comparison of experimental results of DIC by the use of speckle patterns with both uniform and non-uniform intensity distributions, and a new correctional method was proposed). Hack E. et al. [11] described a simple reference material for establishing the minimum measurement uncertainty of optical systems for measuring 3D surface displacement fields in deforming objects, as well as its use. Lutowski Z. et al. [12] decided to verify the accuracy of the displacement detection of the DIC method by comparing the results with real displacement, and performed the tests on a special system for fatigue properties testing of micro-objects (MFS), which allowed to estimate the measuring errors for the DIC method. Zappa E. et al. [13] discussed the DIC uncertainty assessment in dynamic applications and evaluation and improvement of DIC uncertainty in dynamic conditions. Krawczyk Ł. et al. [14] also wrote about the inaccuracies of the DIC system. The estimated measurement of the inaccuracies for the Aramis system and gave some practical information about determining compatibility between the crack width measured traditionally and by the Aramis. They also discussed the influence of the facet size on the crack width.

Herein, the accuracy of the digital image system is presented on the example of the Q-450 System from Dantec Dynamics with Phantom v341 cameras. Phantom v341 has the possibility of image recording with a frequency of up to 130 kHz. The full image resolution is 2560 x 1600 pixels. The maximum speed of the camera at full image resolution is 800 frames per second [15]. The cameras of the Q-450 System and the system scheme is shown in Figure 2.

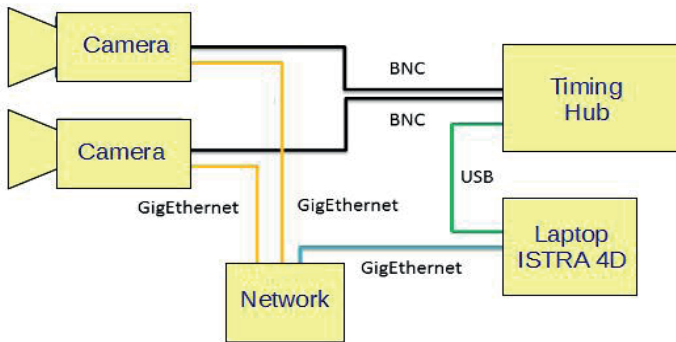


Fig. 2. Q-450 System [6]

The system accuracy regarding the displacements measurement given by Dantec Dynamics is better than 0,01 pixels [3, 12, 16]. This value was verified during experimental research. The investigated object was a plane, a two-story portal frame (see [17]). The horizontal and vertical elements of the frame were made of I-beam (IPE80) and S355 steel. The length of the elements of the frame was 1.6 m. For the accuracy test, the area located in the middle of the lower beam of the frame was chosen (see Figure 3). This area had a dimension of 100 mm x 50 mm and it was located centrally to the symmetry axis of the frame. The image resolution corresponding to the selected part 100 mm x 50 mm was 1516 x 758 pixel. Thus, 1 pixel had an approximate dimension of 0,066 mm. In reference to the system accuracy given by Dantec Dynamics, the measurement error should be smaller than 0,00066 mm. The error size of the displacement [mm] for five points located on the selected surface was measured. The points were in four corners of the surface and in the middle of the surface. A thousand images were registered during the research, and therefore 1000 values of the uncertainty at each point were obtained from ISTR4 software. The average value was calculated, and the result was 0,00046 mm. The maximum error value obtained from measurements was 0,00081 mm and the minimum error value was 0,00019 mm (see Figure 4).

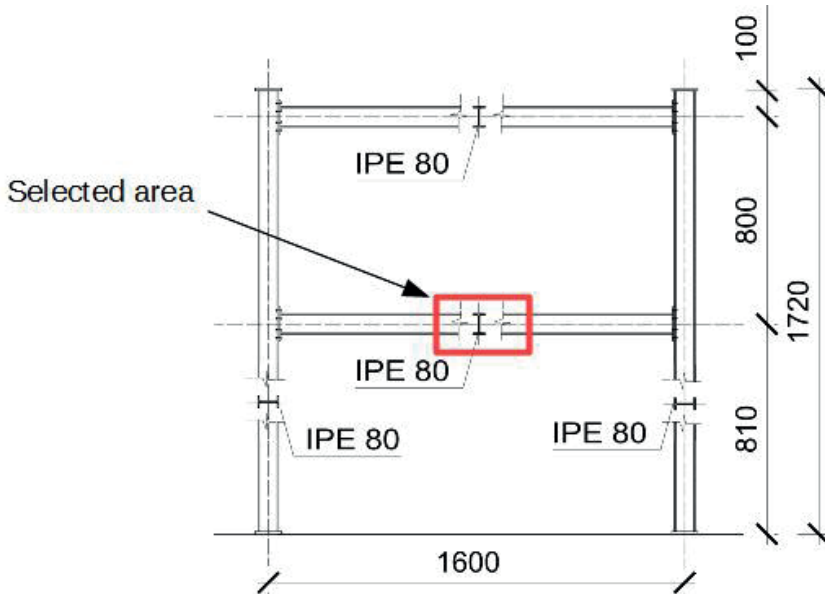


Fig. 3. Area of the frame selected for the accuracy test [17]

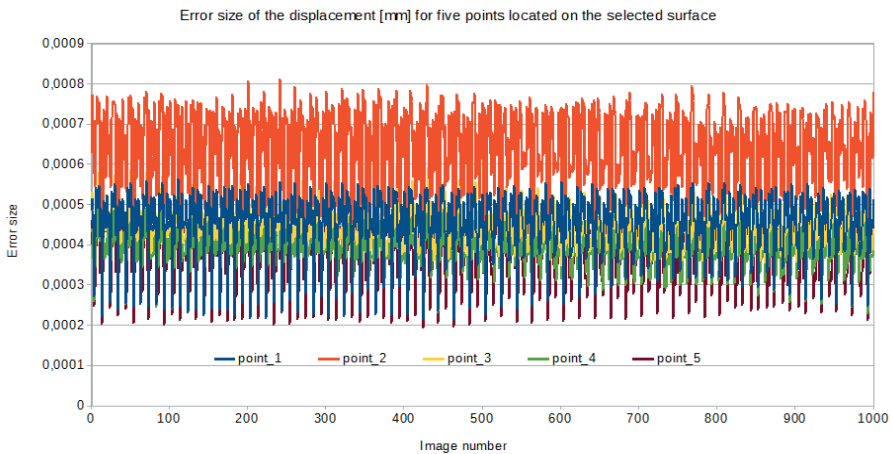


Fig. 4. Measurement errors

The size of measurement errors is closely related to the size of the measurement field. The larger measurement field, the bigger measurement errors and the smaller measurement accuracy. The size of measurement errors is also connected with the resolution of the digital image. The higher the image resolution, the smaller the measurement error. This dependence is very important in planning DIC measurements. The relationship between the measurement field size and the error size for the system Q-450 assuming 1600 pixel x 1600 pixel image resolution is presented in Table 1 (1600 pixel is the biggest pixel number at the height of the image for camera Phantom v341 [15]).

Table 1. Accuracy of Q-450 System with Phantom v341 cameras

Measurement field size [mm]	Measurement error size [mm]
16 x 16	0,0001
32 x 32	0,0002
48 x 48	0,0003
64 x 64	0,0004
80 x 80	0,0005
96 x 96	0,0006
112 x 112	0,0007
128 x 128	0,0008
144 x 144	0,0009
160 x 160	0,0010
1600 x 1600	0,0100

3. Affine transformation and affine parameters

The affine transformation (also called the affinity) is a geometrical transformation that preserves the parallelism of lines but not the lengths and angles. It means that sets of parallel lines remain parallel after the affine transformation, but this transformation does not necessarily preserve angles between lines or distances between points, though it does preserve ratios of distances between points lying on a straight line. In general, an affine transformation allows for rotations, translations and scaling (different scaling in two directions).

The affine transformation can be represented with the following matrix:

$$\begin{bmatrix} a_0 & a_1 & a_2 \\ b_0 & b_1 & b_2 \end{bmatrix} \begin{bmatrix} a_0 & a_1 & a_2 \\ b_0 & b_1 & b_2 \end{bmatrix} \quad (1)$$

where:

$\begin{bmatrix} a_0 \\ b_0 \end{bmatrix}$ is the translation vector, it simply moves the points,

$\begin{bmatrix} a_1 & a_2 \\ b_1 & b_2 \end{bmatrix}$ is a rotation matrix. This matrix defines the kind of transformation that will be performed, scaling and rotation.

If x and y are the coordinates of a point, the transformation can be done by a simple multiplication:

$$\begin{bmatrix} X \\ Y \end{bmatrix} = \begin{bmatrix} a_0 & a_1 & a_2 \\ b_0 & b_1 & b_2 \end{bmatrix} \begin{bmatrix} 1 \\ x \\ y \end{bmatrix} \begin{bmatrix} X \\ Y \end{bmatrix} = \begin{bmatrix} a_0 & a_1 & a_2 \\ b_0 & b_1 & b_2 \end{bmatrix} \begin{bmatrix} 1 \\ x \\ y \end{bmatrix} \quad (2)$$

The parameters $a_0, a_1, a_2, b_0, b_1, b_2$ are called the affine ones. They can describe precisely how the figure consisting of three points is transformed after changing the positions of these points [18-20].

The pseudo-affine transformation (bilinear transformation) was used in this article. This transformation does not preserve lengths and angles, and as opposed to the affine transformation, it does not preserve parallelism. However, it still preserves collinearity and incidence. The pseudo-affine transformation can be represented as the transformation of an arbitrary quadrangle (i.e. a system of four points) into another one.

The pseudo-affine transformation can be represented with the following matrix:

$$\begin{bmatrix} a_0 & a_1 & a_2 & a_3 \\ b_0 & b_1 & b_2 & b_3 \end{bmatrix} \begin{bmatrix} a_0 & a_1 & a_2 & a_3 \\ b_0 & b_1 & b_2 & b_3 \end{bmatrix} \quad (3)$$

where:

$$\begin{bmatrix} a_3 \\ b_3 \end{bmatrix} \begin{bmatrix} a_3 \\ b_3 \end{bmatrix} \text{ is the distortion vector.}$$

If x and y are the coordinates of a point, the transformation can be done by the simple multiplication:

$$\begin{bmatrix} X \\ Y \end{bmatrix} = \begin{bmatrix} a_0 & a_1 & a_2 & a_3 \\ b_0 & b_1 & b_2 & b_3 \end{bmatrix} \begin{bmatrix} 1 \\ x \\ y \\ xy \end{bmatrix} \begin{bmatrix} X \\ Y \end{bmatrix} = \begin{bmatrix} a_0 & a_1 & a_2 & a_3 \\ b_0 & b_1 & b_2 & b_3 \end{bmatrix} \begin{bmatrix} 1 \\ x \\ y \\ xy \end{bmatrix} \quad (4)$$

In the case of the pseudo-affine transformation there are eight affine parameters as follows: $a_0, a_1, a_2, a_3, b_0, b_1, b_2, b_3$ (Fig. 5).

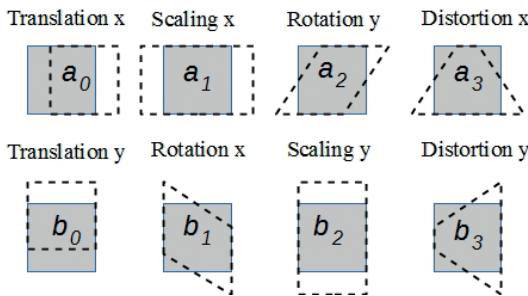


Fig. 5. Affine parameters [21]

Knowing the coordinates of four points before and after the load application, the affine parameters determining the transformation of the rectangular region defined by the four points can be calculated [19-21].

4. The aim of the paper

The aim of this paper is to check numerically the possibility of using the DIC system in updating simple numerical models. The paper contains the examples of a purely numeric updating, the data used to update were obtained from numerical simulations and they correspond to the data which can be measured by using the DIC system. Various variants of using the DIC in measurements were considered, i.e. using the system with one camera, two cameras or four cameras. The most beneficial location and size of the area from which data for model updating were obtained were being looked for. The type of data giving the best updating results was being investigated.

In this paper, the models of three steel plate members in a plane state of stress were investigated. The members were loaded statically or dynamically. The updated parameter was a support length of the members, based on the displacement difference or the difference of the affine parameters obtained for pseudo-experimental models. In the case of the static load,

differences between the displacement values of selected nodes of the models were minimized, in the case of the dynamic load, differences between the affine parameters for selected quadrangular fragments of the models were minimized. The displacements obtained from models corresponding to the experimental research were cut off to the theoretical accuracy of the DIC Q-450 system.

In the article, the DIC Q-450 system and its accuracy are presented. Then the affine transformation and affine parameters are described. The updated models of steel plate members conducted numerical analyzes and their results are shown. Finally, the conclusions are formulated.

5. Investigated objects and updating their models

5.1. Investigated steel plate members

The subject of updating were models of steel plate members. Three plates in plane stress were analyzed. The first analyzed plate *A* had dimensions of 100 mm x 50 mm and a thickness of 5 mm, the second plate *B* was 1000 mm x 200 mm x 20 mm, the third plate *C* was 1000 mm x 1000 mm x 20 mm (see Figure 6). All members were partially fixed along their bottom edge. The length of the fixed support varied from 1/20 of the plate length to the whole length. All plates were loaded by one concentrated force acting vertically in the right upper corner of the plate. For all created models two types of loads were defined, a static load and a dynamic load with a varying maximal value (from 1 kN to 10 kN with step 1 kN), with the time history of the dynamic load shown in Fig. 7. The time step assumed as 0,005 sec and the total load time assumed as 1 sec.

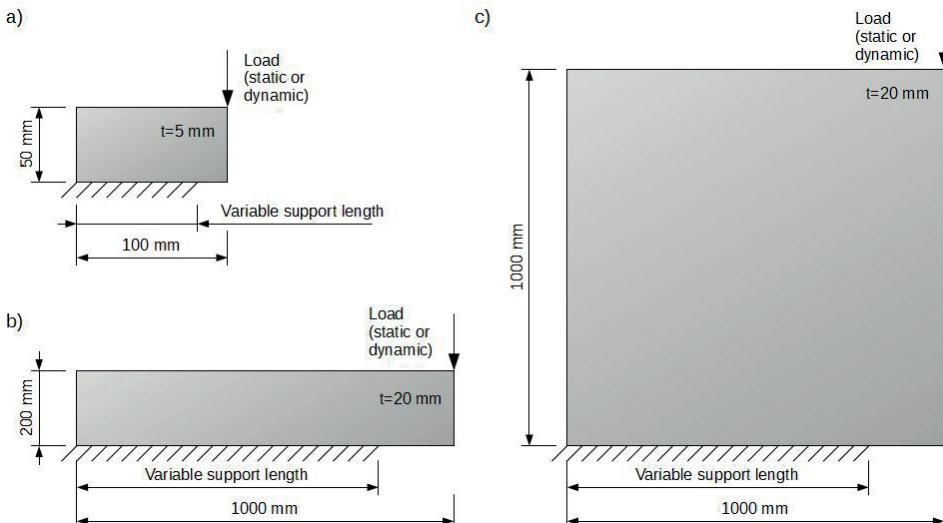


Fig. 6. Analyzed plate members: a) *A* 100x50x5 mm, b) *B* 1000x200x20 mm, c) *C* 1000x1000x20 mm

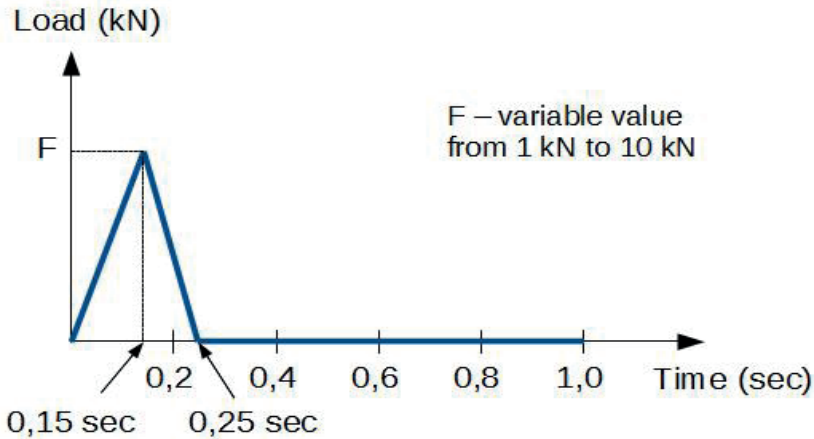


Fig. 7. Time history of the impact load [22]

5.2. Numerical models

For each of the three analysed structures, two Finite Element (FE) models were built. For each plate, one of the two models played the role of the pseudo-experimental model. It was the model with a larger number of finite elements, and it was named herein as a *Dense Model* (DM), the decision on the number of finite elements was preceded by an analysis of this number on the results obtained. The second model was named as a *Sparse Model* (SM), a significantly smaller number of finite elements introduced some inaccuracies into the results obtained from this model. The numerical models of the structures were created by using the MATLAB R2018a program. Four node plane stress elements (built as a combination of four general-purpose linear triangular plane stress elements) called *planqe* in Calfem was used [22]. Material parameters used in the numerical models are as follows: Young's Modulus $E = 205$ GPa, Poisson's Ratio $\nu = 0,30$, density $\rho = 7860$ kg/m³.

For the first analyzed member *A*, two numerical models were built – the *Sparse Model A1* and the *Dense Model A2*. Model *A1* consisted of 1250 finite elements i.e. 50 finite elements in the horizontal direction and 25 elements in the vertical direction. The model *A2* corresponded to the experimental research. The model *A2* consisted of 5000 finite elements i.e. 100 finite elements in the horizontal and 50 elements in the vertical direction. For the second analyzed plate *B*, the model *B1* consisted of 1000 finite elements i.e. 100 elements x 10 elements. Model *B2*, corresponding to the experimental research, consisted of 4000 finite elements i.e. 200 elements x 20 elements. For the third analyzed plate member *C*, the *Sparse Model C1* consisted of 100 finite elements i.e. 10 elements x 10 elements. Model *C2*, corresponding to the experimental research, consisted of 400 finite elements i.e. 20 elements x 20 elements.

In *Sparse Models* i.e. *A1*, *B1*, *C1* fixed support along the bottom edge on the selected fragment of the edge was modeled. The length of the fixed support was treated as unknown and denoted by x . This length x was updated. For pseudo-experimental i.e. *Dense Models A2*, *B2*, *C2* support length was accurately determined and denoted by SL . The value of x was updated to SL and different SL values were considered (from 1/20 of the plate length to the whole plate length). The selection of the parameters treated as unknowns was related

to the previous experience of the authors, which shows that in real cases, the numerical modeling of the supports often has a decisive impact on the compatibility of experimental and numerical models.

5.3. Updating of numerical models

The pseudo-experimental models had four times as much finite elements than the updated models, which resulted in a structure error between the results obtained from both models. The displacements values obtained from models corresponding to the experimental research were rounded to the accuracy that can be obtained from DIC measurements.

The updated parameter of the sparse model was chosen so to minimize the differences between the values of selected magnitude obtained from the calculations performed for the updated model and the ones obtained from the calculations performed for the pseudo-experimental model. In the case of the static load, differences between displacement values of selected nodes of the models were minimized. In the case of the dynamic load, differences between affine parameters for selected quadrangular fragments of the models were minimized. It was being checked if using such parameters for updating models will give better results than using displacement values caused by the static load.

The numerical procedure used to update the numerical models solves nonlinear least-squares curve fitting (nonlinear data-fitting) problems of the formula [22]:

$$\begin{aligned} \min_x \|f(x)\|_2^2 &= \min_x (f_1(x)^2 + f_2(x)^2 + \dots + f_n(x)^2) \\ \min_x \|f(x)\|_2^2 &= \min_x (f_1(x)^2 + f_2(x)^2 + \dots + f_n(x)^2) \end{aligned} \quad (5)$$

with lower and upper bounds lb and ub on the components of x .

A value of the support length of the *Sparse Model* x was updated. The numerical procedure started at the point x_0 and found a minimum of the sum of squares of the difference of the displacements for static cases or difference of the affine parameters for the dynamic cases. The lower and upper bounds were defined so that the solution was always in the range $lb \leq x \leq ub$. For the *A1* model the lower bound was 0,005 m and the upper bound was 0,09 m. For the *B1* and *C1* models the lower bound was 0,05 m and the upper bound was 0,90 m. For all models the starting point x_0 was chosen randomly from the range between the lower bound and the upper bound.

6. Results of updating of numerical models

For the first updated *Sparse Model A1*, two cases of updating were considered. In the first case, the updated support length of the Model A was chosen to minimize the differences between the displacements caused by the static load (case 1). For the updated model the displacements of all nodes were taken into account. For the *Dense Model A2*, the displacements of the nodes in which locations were the same as the location of the nodes of the updated model were only taken into account. In the second case, the differences between the affine parameters' values for the quadrangular fragment of the models were minimized (case 2). It was decided to analyze the quadrangle of the highest possible length. Thus, four points of the most distant from each

other were chosen. The selected fragment was determined by four points with the coordinates (x, y) [m]: (0,002; 0,048), (0,098; 0,048), (0,002; 0,002), (0,098; 0,002) (see Fig. 8).

It was assumed that in the case of experimental tests the whole plate will be observed by the DIC system using one camera. To take into account the accuracy of the DIC system, the displacements obtained for *Dense Model A2* were rounded to 0,00001 m.

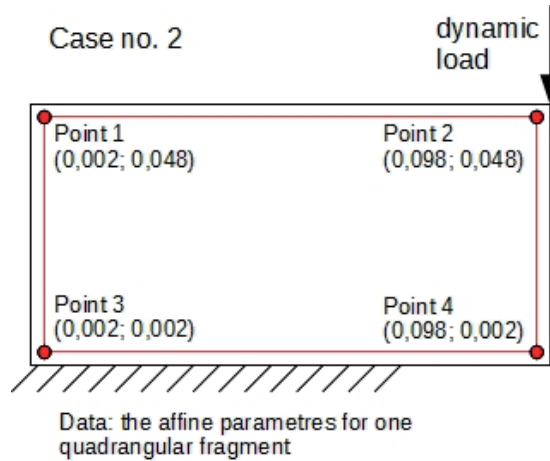


Fig. 8. Data for updating of numerical model *A*, case no. 2

The updating of the model *A1* was repeated 50 times for each considered case and for each value of the load from 1 kN to 10 kN to estimate a statistical description of the result of the model updating by calculation the following values: standard deviations, absolute errors, relative errors and the average value of each type error. The exemplary values of relative errors and their average value obtained from 50 calculations preformed for dynamic load 10 kN is shown in Fig. 9.

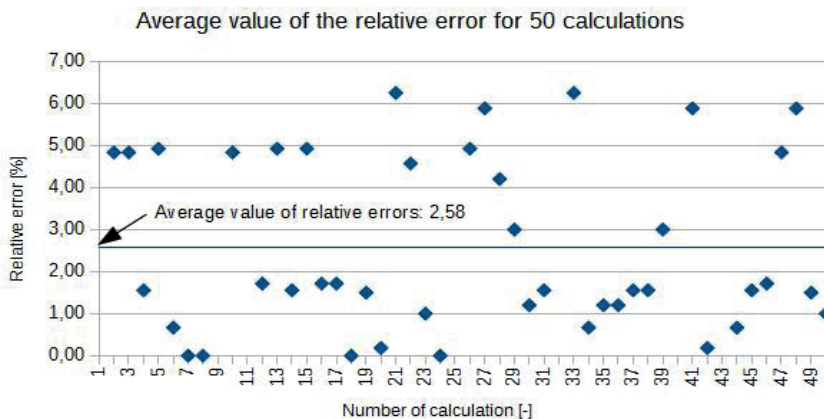


Fig. 9. The average value of relative error for the dynamic load 10 kN

The final results of updating of the numerical model *AI* for the static load and the dynamic load (from 1 kN to 10 kN) are shown in Fig. 10.

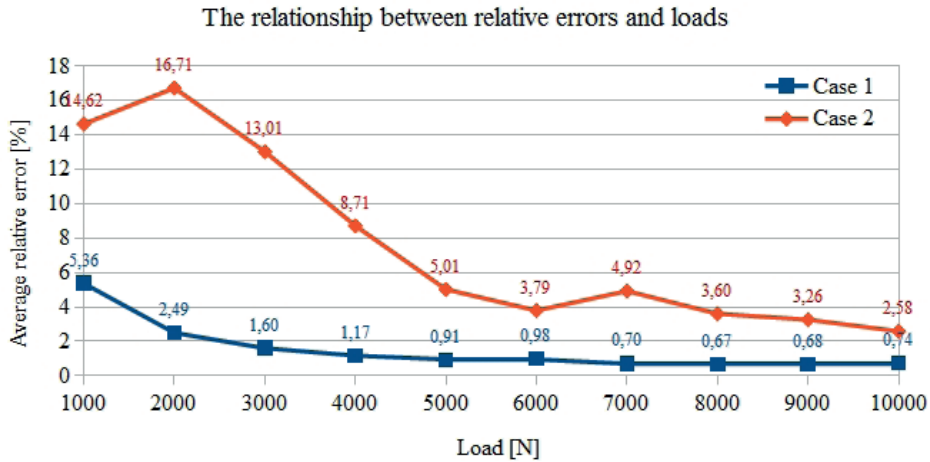


Fig. 10. Average values of the relative errors of updating the model *AI*

For the second updated *Sparse Model B1*, five cases of updating of the numerical model were considered. The considered cases from 1 to 5 are as follows:

- 1) the differences between the displacements caused by the static load for all nodes of the model *B1* and corresponding nodes of the *Dense Model B2* were taken into account,
- 2) the differences between the displacements caused by the static load for selected nodes of the model *B1* and corresponding nodes of the *Dense Model B2* were taken into account, the selected nodes were located on the selected fragment (100 mm x 100 mm) of the model as shown in Fig. 11,
- 3) the differences between the affine parameters values for the quadrangular fragment of the models were minimized, the selected fragment was determined by four points with the coordinates (x, y) [m]: (0,91; 0,14), (0,99; 0,14), (0,91; 0,06), (0,99; 0,06) as shown in Fig. 12 a,
- 4) the differences between the affine parameters values for the quadrangular fragment of the models were minimized, the selected fragment was determined by four points with the coordinates (x, y) [m]: (0,50; 0,14), (0,99; 0,14), (0,50; 0,06), (0,99; 0,06) as shown in Fig. 12 b,
- 5) the differences between the affine parameters values for the quadrangular fragment of the models were minimized, the selected fragment was determined by four points with the coordinates (x, y) [m]: (0,01; 0,14), (0,99; 0,14), (0,01; 0,06), (0,99; 0,06) as shown in Fig. 12 c.

In case no. 1, it was assumed that the experimental tests will be performed on the whole surface of the plate by the DIC Q-450 system using one camera. In order to take into account the accuracy of the DIC system, the displacements obtained for the *Dense Model B2* were rounded to 0,0001 m. In the cases no. 2 and 3 it was assumed that the experimental tests will be

performed only on the selected fragment of the plate element i.e. 100 mm x 100 mm by using one camera. In order to take into account the accuracy of the DIC system, the displacements obtained for experimental model *B2* were rounded to 0,00001 m. In the cases no. 4 and 5 it was assumed that the experimental tests will be carried out with the use of two cameras, one camera will record images of the two left points of the selected quadrangular fragment and the second camera will record images of the two right points of the selected quadrangular fragment. In order to take into account the accuracy of the DIC system, the displacements obtained for *Dense Model B2* were rounded to 0,00001 m.

The updating of the model *B1* was performed 50 times for each case and for each value of the load. For each value of the updated parameter, a relative error and an absolute error were calculated and average values of every type of the errors. The final results of updating of the numerical model *B1* are shown in Fig. 13.

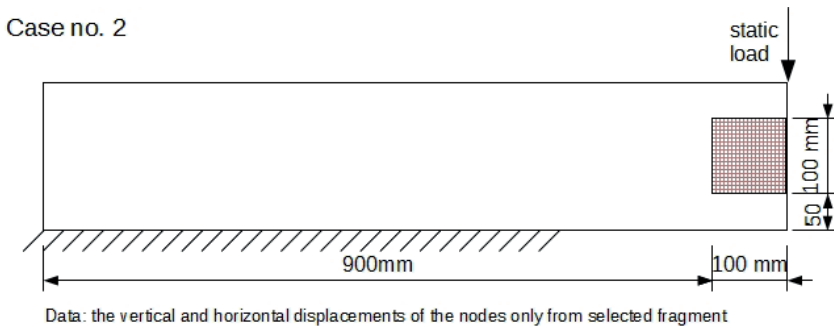


Fig. 11. Data for updating of numerical model *B1*, static load, case no. 2

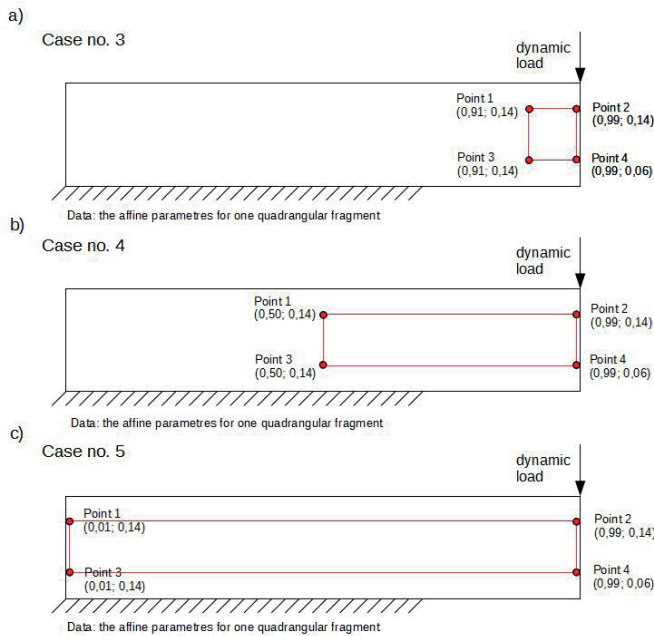


Fig. 12. Data for updating of numerical model *B1*, dynamic load: a) case no. 3, b) case no. 4, c) case no. 5

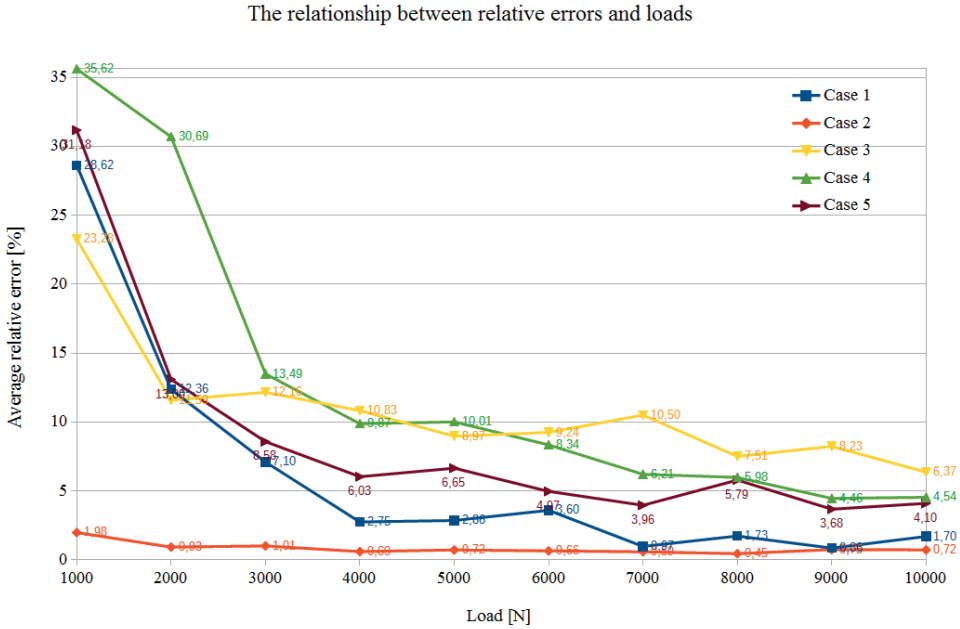


Fig. 13. Average values of the relative errors of updating the model *BI*, case no. 1-5

For the third updated *Sparse Model C1* of the plate, at first, the updated support length of the model *C1* was chosen to minimize the differences between the displacements caused by the static load for all nodes of the model *C1* and for corresponding nodes of the *Dense Model C2* (case 1). It was assumed that in the case of experimental tests the whole plate will be measured by the DIC Q-450 system using one camera. In order to take into account the accuracy of the DIC system, the displacements obtained for the *Dense Model C2* were rounded to 0,0001 m. Then the differences between the displacements caused by the static load for selected nodes of the model *C1* (located on the 100 mm x 100 mm fragment in the lower right corner of the plate) and corresponding nodes of the *Dense Model C2* were taken into account (case 2). In this case, the displacements obtained for dense model *C2* were rounded to 0,00001 m and it was assumed that one camera will be used.

Next the updated support length of the model *C1* was chosen so as to minimize the differences between the affine parameters calculated on the basis of displacements caused by the dynamic load for three cases. The considered cases marked as 3, 4, 5 are as follows:

- case 3 – the differences between the affine parameters for the quadrangular fragment determined by four points with the coordinates (x, y) [m]: (0,10; 0,90), (0,90; 0,90), (0,10; 0,10), (0,90; 0,10) were minimized, see Fig. 14 a,
- case 4 – the differences between the affine parameters for the quadrangular fragment determined by four points with the coordinates (x, y) [m]: (0,10; 0,40), (0,90; 0,40), (0,10; 0,10), (0,90; 0,10) were minimized, see Fig. 14 b,
- case 5 – the differences between the affine parameters for the quadrangular fragment determined by four points with the coordinates (x, y) [m]: (0,60; 0,40), (0,90; 0,40), (0,60; 0,10), (0,90; 0,10) were minimized, see Fig. 14 c.

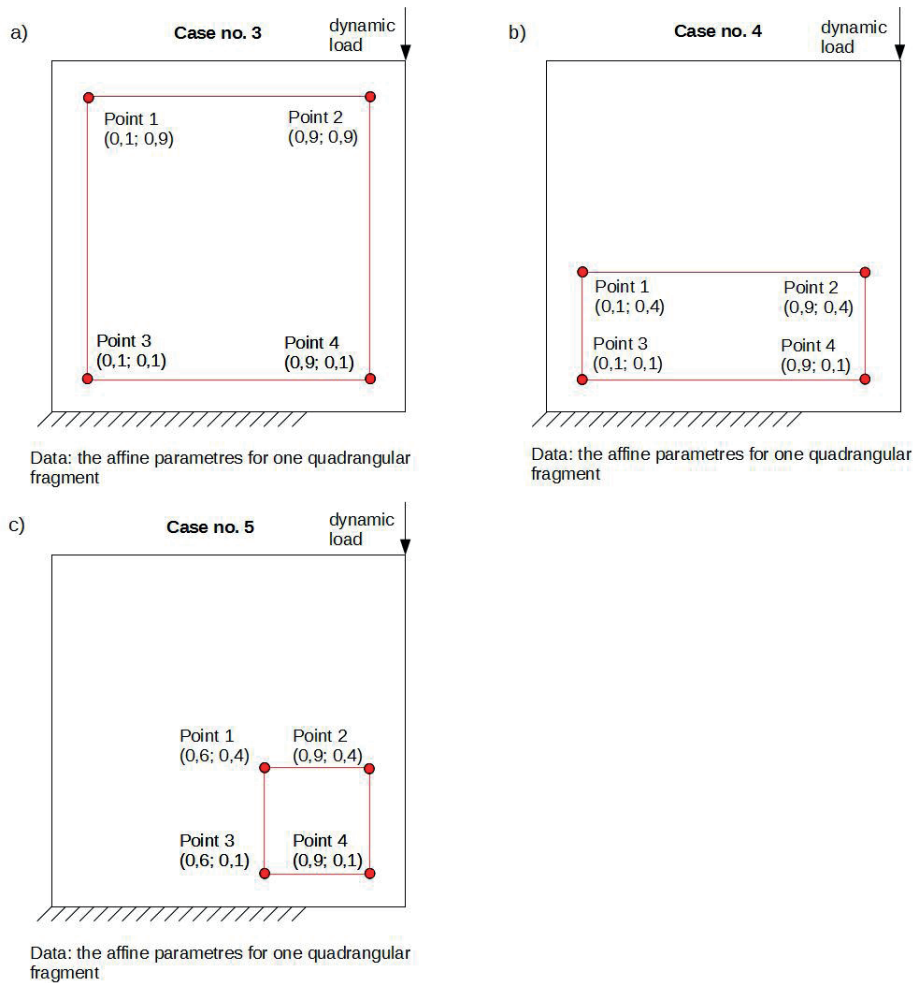


Fig. 14. Data for updating of numerical model *CI*: a) case no. 3, b) case no. 4, c) case no. 5

In cases 3-5 it was assumed that the experimental tests will be carried out in four parts of the plate with the use of two cameras or four cameras. In research with 2 cameras (it is the basic number of cameras in the DIC Q-450 system), the measurements will be made as follows: first the cameras will be set to the left of the plate and the measurements will be made on the left part of the plate in such a way that every camera will record images of one left point of the selected quadrangular fragment, next the cameras be moved to the right side and every camera will record images of one right point of the selected quadrangular fragment. In research with 4 cameras, the measurements will be made as follows: every camera will record images of one point of the selected quadrangular fragment. In order to take into account the accuracy of the DIC system, the displacements [m] obtained for the *Dense Model C2* were rounded to 0,00001 m.

The updating of the model *CI* was performed 50 times for each case and for each value of the load. For each value of the updated parameter errors are calculated. The final results of updating the numerical model *CI* are shown in Fig. 15.

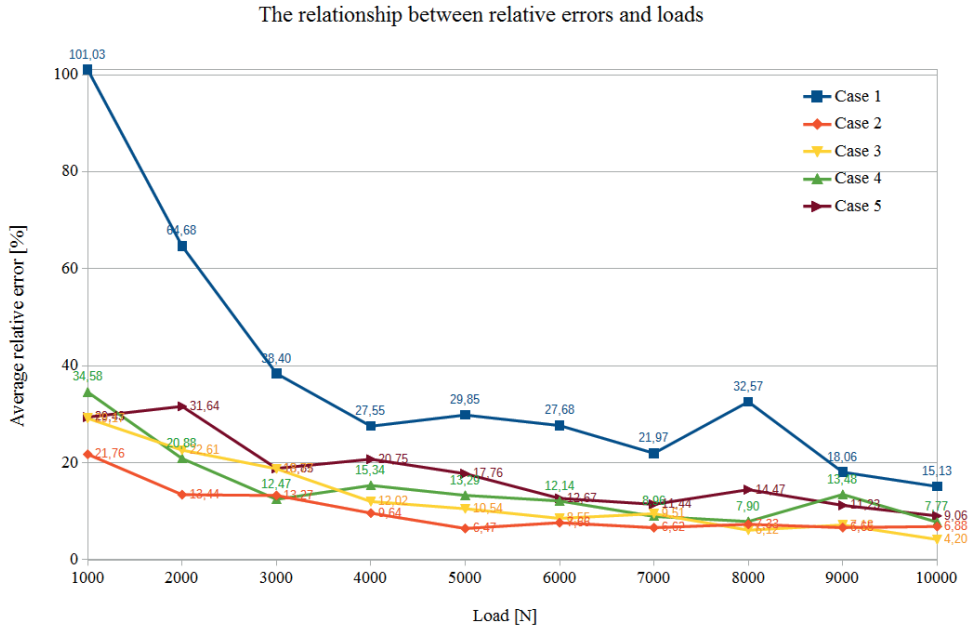


Fig. 15. Average values of the relative errors of updating the model CI , case no. 1-5

For more detailed analysis the results obtained for the load of 10 kN were selected. For all analysed plates, i.e. A , B , C , average values of relative error were compared. In Table 2 there are presented individual updating cases, types of loads, types of data used for updating, and accuracy of DIC system included in the calculations and an expected number of cameras that were simulated in the experimental research.

As shown in Table 2, for member A the better result was obtained in case 1. For the plate B , the better results of updating models were obtained for the cases with a static load. The best result was obtained in case 2. Comparing the first two cases, it can be noticed that the DIC system's accuracy has a significant impact on the updating results. Comparing all cases with a dynamic load, it can be noticed that the best procedure taking into account the affine parameters was one used in case 5. The selected fragment for which the affine parameters were calculated, determined by four points in the corners of the plate (four points create the quadrangle with the possible longest sides) was the most advantageous. As shown in Table 2, the best result of model updating for the plate member C were obtained in case 3. In this case the updating procedure considered affine parameters obtained for the square fragment of the plate member. The selected fragment of the area was determined by four nodes located close to the corners of the plate members. As would be expected, analyzing the cases with a static load it can be noticed that the DIC accuracy is very important in research – the greater accuracy, the better result of updating. The results obtained for updating procedures considering the dynamic load i.e. cases from 3 to 5 are similar to the result obtained in case 2.

Table 2. Summary of results for plates *A*, *B*, *C*

Plate	Updating Case	Load type	Data type using for updating	Accuracy of DIC system included in the calculations	Expected number of cameras in the research	Updating result for load 10 kN (average value of the relative error)
<i>A</i>	1.	static	displacements	0,00001 m	1	0,74%
	2.	dynamic	affine parameters	0,00001 m	1	2,58%
<i>B</i>	1.	static	displacements	0,0001 m	1	1,70%
	2.	static	displacements	0,00001 m	1	0,72%
	3.	dynamic	affine parameters	0,00001 m	1	6,37%
	4.	dynamic	affine parameters	0,00001 m	2	4,54%
	5.	dynamic	affine parameters	0,00001 m	2	4,10%
<i>C</i>	1.	static	displacements	0,0001 m	1	15,13%
	2.	static	displacements	0,00001 m	1	6,88%
	3.	dynamic	affine parameters	0,00001 m	2 or 4	4,20%
	4.	dynamic	affine parameters	0,00001 m	2 or 4	7,77%
	5.	dynamic	affine parameters	0,00001 m	2 or 4	9,06%

As shown, for larger plates the use of the procedure with affine parameters can give better results than the procedure using the displacements caused by the static load. However, attention should be paid to the number of cameras that are expected to be used. More cameras mean more time-consuming and more complicated research, for example, due to the camera calibration or data analysis. For larger plates, the use of the procedure with affine parameters may be a better option, but there should be considered the difficulty of measurements by means of DIC system with several cameras. Moreover, in this paper for dynamic load, there were considered the cases with only one quadrangular fragment for which the affine parameters' values were calculated. However, the procedure can use a much larger number of affine parameters. The parameters can be obtained for at least as many quadrangles as they can be built on the nodes of the sparse model.

7. Conclusion

On the basis of the numerical analyses, the following some conclusion can be formulated:

- the DIC system can be helpful in updating of numerical models of structural elements,
- the DIC accuracy has a significant influence on the updating results,
- for larger members, the updating procedure taking into account the affine parameters in dynamics can give better results than the procedure based on displacements values caused by the static load.

The results of numerical simulations and statistical analyzes show that the DIC can be used for updating numerical models of steel plates in plane state of stress. For different size members, it is possible to create the test procedure that allows updating the numerical models in a quick and non-contact way. The presented procedures of numerical models updating were verified only in a numerical way. The next step of the work will be to check the proposed procedures with different unknown parameters and in an experimental way by carrying out research on the real elements by using the DIC Q-450 system and by using measurement data to update the numerical models.

References

- [1] Miller B., “Nieniszczące badania konstrukcji: dostrajanie modelu oraz identyfikacja obciążenia powodującego częściowe uplastycznienie”, *Zeszyty Naukowe Politechniki Rzeszowskiej, Budownictwo i Inżynieria Środowiska*, no. 243, 45 (2007), pp. 125-134.
- [2] Wang Y. H. et al., “Whole field sheet-metal tensile test using digital image correlation”, *Experimental Techniques*, vol. 34, no. 2 (2010), pp. 54-59. <https://doi.org/10.1111/j.1747-1567.2009.00483.x>
- [3] *Digital Image Correlation (DIC)*. Available: <http://www.dantecdynamics.com/digital-image-correlation> [Accessed: 20 Dec 2019]
- [4] Sutton M.A., Ortu J.J., Schreier H.W., *Image Correlation for Shape, Motion and Deformation Measurements: Basic Concepts, Theory and Applications*. New York: SPRINGER (2009), ISBN: 978-0-387-78746-6, e-ISBN: 978-0-387-78747-3. <https://doi.org/10.1007/978-0-387-78747-3>
- [5] Szymczak T., Kowalewski Z. L., Brodecki A., “Metoda cyfrowej korelacji obrazu w badaniach materiałów i elementów”, *Dozór Techniczny*, vol. 4 (2016), pp. 22-31.
- [6] Q-450 SYSTEM Operation Manual, Dantec Dynamics (2013)
- [7] Chu T. C., Ranson W. F., Sutton M. A., “Application of digital-image correlation techniques to experimental mechanics”, *Experimental Mechanics*, no. 25 (1985), pp. 232–244. <https://doi.org/10.1007/BF02325092>
- [8] Peters W. H. et al., “Applications of digital image correlation methods to rigid body mechanics”, *Optical Engineering*, no. 22 (1983), pp. 738–742.
- [9] Peters W. H., Ranson W. F., “Digital imaging technique in experimental stress analysis”, *Optical Engineering*, no. 21 (1982), pp. 427–431. <https://doi.org/10.1117/12.7972925>
- [10] Guoqing Gu et al., “Non-uniform illumination correction based on the retinex theory in digital image correlation measurement method”, *Optica Applicata*, vol. XLVII, no. 2 (2017), pp. 199-208. <https://doi.org/10.5277/oa170203>
- [11] Hack E., Lin X., Patterson E. A., Sebastian C. M., “A reference material for establishing uncertainties in full-field displacement measurements”. *Measurement Science and Technology*, vol. 26, no. 7 (2015). <https://doi.org/10.1088/0957-0233/26/7/075004>
- [12] Lutowski Z., Marciniak B., Marciniak T., Bujnowski S., “Precision of Sub-Pixel Image Displacement Measurements”. *Journal of Machine Construction and Maintenance*, vol. 4 (2017), pp. 21-26.
- [13] Zappa E., Matinmanesh A., Mazzoleni P., “Evaluation and improvement of digital image correlation uncertainty in dynamic conditions”, *Optics and Lasers in Engineering*, vol. 59 (2014), pp. 82–92. <https://doi.org/10.1016/j.optlaseng.2014.03.007>
- [14] Krawczyk Ł., Gołdyn M., Urban T., “O niedokładnościach systemów cyfrowej korelacji obrazu”, *Journal of Civil Engineering, Environment and Architecture*, vol. XXXIV, no. 64 (2017), pp/ 259-270. <https://doi.org/10.7862/rb.2017.120>
- [15] *Kamera szybka Phantom v341*. Available: http://www.ects.pl/produkty/c84_kamery-szybkie/p264_kamera-szybka-phantom-v341 [Accessed: 20.12.2019]
- [16] Lord J. D., *Digital Image Correlation (DIC)*. Modern Stress and Strain Analysis. A state of the art guide to measurement techniques. BSSM Technical Editors: J. Eaton Evans, J. M. Dulieu-Barton, R. L. Burguete (2009), pp. 14-15.
- [17] Turoń B., Ziaja D., Miller B., “Wykrywanie uszkodzeń węzłów ramy stalowej z wykorzystaniem metody cyfrowej korelacji obrazu”, *Journal of Civil Engineering, Environment and Architecture*, vol. XXXIV, no. 64 (2017), pp. 185-198. <https://doi.org/10.7862/rb.2017.91>
- [18] *Affine and Projective Transformations*. Available: <https://www.graphicsmill.com/docs/gm/affine-and-projective-transformations.htm> [Accessed: 20.12.2019]

-
- [19] Heckbert P. S. *Fundamentals of Texture Mapping and Image Warping*. Master's thesis, University of California at Berkeley, Department of Electrical Engineering and Computer Science, Berkeley 1989.
- [20] Wang Y. *Video Processing & Communications. Two Dimensional Motion Estimation (Part I: Fundamentals & Basic Techniques)*. Available: http://eeweb.poly.edu/~yao/EL6123old/motion2d_part1_new.pdf [Accessed: 20 Dec 2019]
- [21] Trebuňa F., Huňady R., Bobovský Z., Hagara M., "Results and Experiences from the Application of Digital Image Correlation in Operational Modal Analysis", *Acta Polytechnica Hungarica*, vol. 10, no. 5 (2013), pp. 159-174.
- [22] CALFEM. A finite element toolbox. Version 3.4 (2004), ISBN: 91-8855823-1

Houses of the Polish-Belarusian borderland as areas of value

Magdalena Sulima

*Faculty of Architecture; Bialystok University of Technology; Oskara Sosnowskiego Street 11,
15-893 Bialystok, Poland*

mssulima@poczta.onet.pl; ORCID: 0000-0002-0807-9417

Abstract: Nowadays, as a result of globalization processes, the sense of identity and relationship between humans and their place of living is increasingly losing its importance. Today's thinking about the house as a centre of the world is becoming less obvious in comparison to the symbolism of a house in the folk culture. Wooden houses on the Polish and Belarus border are an example of a temporal continuum – both in the spatial and in the spiritual aspect. Because of their architecture, decoration on facades and spatial layout, they are a distinctive feature of the local landscape, and ethnic communities inhabiting them, to this day have maintained a strong identification with their own roots and place of residence. The greatest threat to the continuity of local tradition as well as wooden architecture of borderland villages is their progressive extinction. That is why the issue of protection of the cultural heritage and the generational memory of local residents is one of the key issues in maintaining the identity of those areas. The aim of the article which is based on ethnographic sources and field researches is to present the symbolism of traditional wooden houses in the villages of the north-eastern Poland as areas of material and spiritual values and to bring attention to the need of protecting them in the context of contemporary civilization changes.

Keywords: borderland, wooden houses, protection, cultural heritage, intergenerational transmission

1. Introduction

At the turn of the twenty-first century, inevitable globalization processes in the contemporary world have shown how fragile and unstable terms such as tradition, religion, and identity have become. These terms, once very important to one's idea of self, have gone into oblivion, losing their rank. Such changes in civilization have also had influence on something particularly important to human beings: their place of residence.

In folk culture, the relationship between man and home was based on strong foundations such as the father's faith and intergenerational relationships, causing people to strongly identify with the space they occupied. Nowadays, thinking about home as the most important place on earth, as a refuge from the fast-paced world and a community for the people living in it (families), is less obvious when compared to the symbolism attached to traditional ways of living. Our lives, in contrast to past periods, seem to be detached from the cycle of generations as a way of measuring time [1, p.200]. The transformation and deepening crisis in terms of adherence to traditional values has become a subject of twentieth century philosophical thought¹. Anthony Giddens stated that the modern world is a very different place compared to the world our ancestors lived in. For

¹ Martin Heidegger, Gerardus van der Leeuw, Emmanuel Levinas, Gaston Bachelard, Mircea Eliade and Józef Tischner, among others, wrote about the recession of traditional values.

them, religion and customs passed down from generation to generation were integral determinants of norms regulating social behavior, and order in the world was determined by thinking about the world through the prism of faith. The doctrine of modernity has achieved success by breaking down traditional ideas about lifestyle, community, and a lack of authority [1, p.8-9].

Advancements in civilization, economic progress, and the spread of mass culture have left their mark not only in the socio-cultural sphere and the nature of life in urban agglomerations, but also on the cultural life of the countryside. These changes are noticeable both in the cultural landscape of rural areas (where new and modern forms are being introduced) and in the field of spiritual culture (where the human bond with the place of his birth – one of the most important and the most lasting existential values – is slowly passing away and is moving into non-existence). Analysis of the phenomenon of the home, and its role in social culture, is an activity that is very important and relevant nowadays, since the home contains both material (building) and psychological (emotional) components.

An example of the existence of a temporary continuum – both in architectural and spiritual aspects, are the wooden houses of the Polish-Belarusian borderland close to Białowieża Forest². These homes, with their form (building material, construction, façade decoration) and placement in the rural setting, constitute a distinctive feature of the local landscape. The ethnic communities that inhabit this region are made up of people with affiliations in terms of nationality (most declare themselves as Belarusians) [4, p.114], religion (most are members of the Orthodox Church), linguistics (speaking a combination of Polish, Belarusian and Ukrainian languages) and space.

The eastern borderland of Poland are areas where Polish culture meets eastern cultures, i.e. Belarusian, Lithuanian, Ukrainian and Russian [5, p.9]. This refers to the penetration of both national as well as civilizational elements – this is the borderland between the Latin and Byzantine cultures [6, p.298]. Interestingly, in these sites the sense of religious affiliation is also often a criterion for determining national belonging. That is why the communities describe themselves as “local”, “Orthodox”, “Russian” or “Belarusian” [7, p.80, citing: 41]. This “*socio-cultural phenomenon*” [8, p.23] of the dependence of Orthodoxy and Belarusian heritage, historically and currently exert a colossal impact on the entire life of the inhabitants [9, p.508]. These ethnic groups, in opposition to modern society strongly connected with urban culture, to this day have a strong connection with local tradition, their roots and place of residence. This is visible in the preserved architecture of houses and in activities connected not only with day to day living, but also to holidays. This shows how multifaceted the issue of wooden architecture is.

The aim of this paper, based on ethnographic sources and field studies, is to present the symbolism attached to traditional wooden architecture found in the villages of the north-eastern part of Poland (Bielsk Podlaski, Czyże, Hajnówka and Narew communes), as areas of both material and spiritual value and bring attention to the need of protecting them in the context of contemporary civilization changes.

² According to sociologist Andrzej Sadowski, the term “borderland” defines the area, zone, territory on which two or more ethnic and cultural groups come into contact [2, p.17], the consequence of which is the inevitable penetration and assimilation of certain elements of the culture (including language, religion, customs). In terms of geography in Poland, three borderlands can be distinguished: southern, eastern and western. Sadowski included: Podlaskie, Warmian-Masurian, Eastern Mazovian, Lubelskie and Podkarpackie Voivodships [3, p.27] in the eastern borderland areas. The phenomenon of the eastern borderland in the socio-cultural aspect is a frequent subject of analysis by many researchers, including Włodzimierz Pawluczuk, Grzegorz Babiński, and Marek Barwiński.



Fig. 1. Location of the research area (Bielsk Podlaski, Hajnówka, Czyże, Narew communes) within the borders of the Podlaskie Voivodeship; source: author based on the map of Poland according to the administrative division

2. The cultural landscape of the borderland village

The villages of eastern borderland Poland, located on the border with Belarus, are characterized by a settlement system created in the 16th-century. It is the result of a great agrarian reform carried out by Queen Bona Sforza in the years 1558 – 1561³. The layout and proportions of the plots are very similar in that they are very elongated. They begin with the residential house set sideways with its peak to the main road (after WWI, when they were built with the roof ridge parallel to the road), the road being the axis around which the whole village was built. The outbuildings were built in a row behind the residential house. The arable fields were located even further from the main road, across a smaller road which ran behind the barns. After later transformations in agriculture, arable fields were also located much further away from inhabited areas (phot. 1).

³ During the reform almost all lands belonging to Queen Bona were measured. The scale and enormous size of the enterprise is demonstrated by the number of measured lands in Podlasie, Lithuania and Belarus. According to Marian and Wojciech Pokropek, by the 1566-67 there were about 1231 hectares measured [10, s.104].



Photo 1. Satellite map of a fragment of Deniski village (Bielsk Podlaski commune), scale 1: 12000; source: google maps

The distinctive features of the local rural landscape are undoubtedly the original wooden houses and their specific characteristics. They were built over a period of hundreds of years through natural development of the region, and in accordance with traditional patterns. A flower garden, which first appeared in the 1920's – 1930's, usually occupies the front lawn, where a cross has been placed to show gratitude, and a bench to permit for social gathering among older residents of the village (phot.2-4).

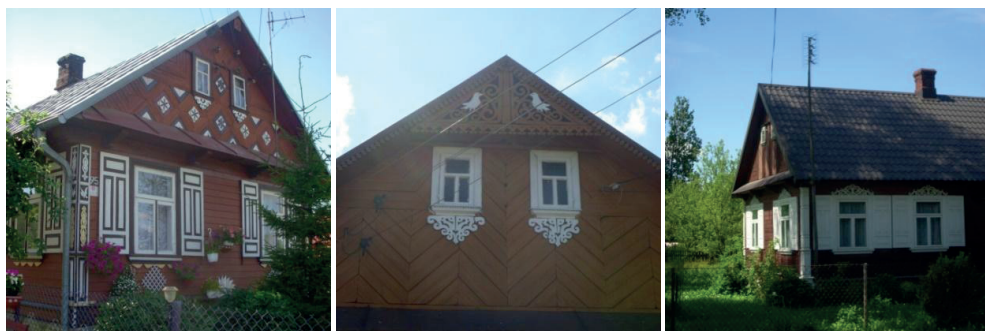


Photo 2-4. Phot.2. Plutycze village (Bielsk Podlaski commune), Photo 3. Stare Berezowo village (Hajnówka commune), Photo 4. Kojły village (Czyże commune), All photos by the author

Until the end of the 19th century, the cottage consisted of one room that was heated with a massive “Russian” clay stove located in the corner of the room, next to the door. Its corner-wall location was also found in Belarus, Ukraine and Russia [11, p.37, citing: 42, p.147]. Cottages were either detached houses or were connected with livestock buildings and covered with a common thatched roof. Over the years (starting in the interwar period), houses were built in two-way

systems with gabled roofs. During the same time period, the facades of the houses began to be decorated with ornaments cut out of wood. Windows, shutters, corners, peaks, porches and verandas were decorated with plant and animal motifs (phot. 5-7). The colorful walls of the buildings, with their bright ornaments, create a folk, fairy-tale, magical climate that is unique on a national and international scale⁴. The decorations should not, however, be treated only as products of folk art created by local craftsmen. The symbolism attached to this form of architecture runs much deeper, combining religious themes with the community's common imagination about the world going back to pagan times [12, p.13]. The external source of inspiration was primarily the surrounding nature. Motifs appearing on the houses in the form of twigs, birds, hearts, suns – derive from the world of fauna and flora, as well as religious-cosmic compositions. For example, the motif of pigeons symbolised love, clover – life, and sun – happiness. Therefore, each decorative element had a different, sometimes not entirely rational meaning, emphasizing the strong relationship of its place on earth with transcendent forces [13, p.107].

Residents are mostly Orthodox and this religion, apart from the theological aspects, represents a particular lifestyle which is also reflected in the cultural and moral layer [14, p.41], [13, p.95-108]. The essence of this religion is the cult of spirituality and mysticism. Orthodoxy, as Eastern Christianity compared to Western Christianity, is more mystical and “*out of this world*” [15, p.168]. It is based on symbols and characterized by sensual and intuitive knowledge of God. The Eastern Church has always been open to the phenomenon of folk religions, therefore religion in the villages is very often a cluster of specifically understood dogmas of the church, traditions passed down from generation to generation and folk traditions that bordered on what could be called magic [13, p.111], [16, p.577]. The strong dependency between the religious and the cultural system allows for the use of the concept “*religious society*” in relation to the people living there [17, p.12. citing: 43]. Religion was, and remains, one of the most important and enduring aspects of life for inhabitants, and provides the canon for creating, arranging, and decorating a home and its surroundings, as well as defines and regulates acceptable behavior and habits in terms of the use of its space.



Photos 5-7. Phot.5-6. Czyże village (Czyże commune), Photo 7. Nowoberezowo village (Hajnówka commune), All photos by the author

⁴ To this day, the ornamental elements on the houses are made by local carpenters living in these areas. In the village of Cieluszki (Zabłudów commune) it is done by Jan Szarkiel, in Kaniuki (Zabłudów commune) Włodzimierz Naumiuk is the local carpenter and sculptor, and in the village of Plutycze (Bielsk Podlaski commune) until recently it was done by Michał Grygoruk and Jan Onopiuk. However, this is the last generation involved with this profession.

3. The home in traditional borderland culture

Historically, in the culture of the countryside, the word “home” had a basic and constitutive meaning. The traditional vision of the world had not so much a historical, but rather a cosmological character [18, p.17]. In folk consciousness, the house of man on earth was to be a reflection of the house of God, and its construction was to be identical with the creation of the world, as a reconstruction of the time of creation [19, p.46]. This conviction was already evident during the preparation and laying of the foundation of the house, which had to be carried out according to strictly defined rules, dictated by tradition. Various rituals at different stages of the build were important here: such as choosing a plot that had been indicated by sacred powers, marking it with a cross, the making of offerings to bring happiness and prosperity to the inhabitants of the space, cutting down the right trees, and the customary behavior of the craftsmen. The decision about the area on which the future cottage was to be erected was governed by many rules, and the area had to be uncontaminated and ritually cleaned [19, p.16], [20, p.443]. Only then could the foundations, walls, doors, windows be installed and covered with a roof. At the end of construction, the house was decorated with colorful ribbons, paper and a sprig of spruce placed on the last rafter (so called “wianek”), and the completion of the construction (in the local dialect was called “winkowe”) was celebrated with dance and music. The house was compared to a tree: in the basement it had its roots, and the roof was crowned with a crown [21, p.308], and through its opening (chimney) was a link with the world of sacrum. From the first moments of existence there was a strong bond between man, home and God. This is also reflected in the activities carried out during the next stages of the build, such as sprinkling the foundations with holy water, referring this to the gesture of God creating the world, or walking around the building with a holy image as a sign of taming and taking possession of the space. The home, built on such a solid foundation, could accompany a person throughout their life, and constitute a framework for the subsequent stages of their existence. The home was therefore a birthplace: the view from the windows was a person’s first view of the world; they matured here, and eventually passed away in this space [22, p.43]. By saying: “I am from here”, “I am from this house”, “this is my land” – people identified with their surroundings. This attachment to one’s space had primarily a spiritual and psychological value, but also an intimate one.

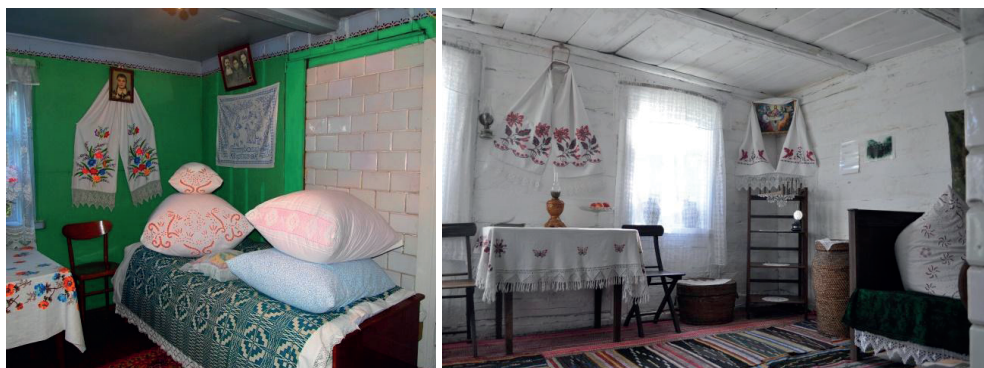
The home was treated by village residents as a space of value in which a person grew up, took root and was bound to for years. This symbolic relationship was revealed most during the celebration of annual holidays and in important moments in a person’s life, such as birth, weddings or funerals, in which the ritual activities performed within this space were symbolically “*created and recreated again*” [23, p.58]. It is worth mentioning the custom of laying a newborn child on the stove, which is meant to strengthen the relationship between the person and their home, or knocking of the coffin on the doorstep of the house, as a sign of the last goodbye of the deceased with the house in which he was born, worked and died. Therefore, the house was connected to man from the beginning, until the end of his life.

The bond between the home and the fatherland was not broken within the culture of the countryside. This bond, as a heritage of fathers, had both earthly and spiritual connotations [24, p.9]. The area acquires the meaning of the fatherland when a given community refers to it in a certain way, thus shaping its image [25 p.18]. On the Polish-Belarusian borderland, the concept of home is not autonomous in relation to mental and emotional attitudes. Here, the family home has been compared to a private and intimate homeland, the most important place on earth. A home that was metaphorically called a family nest or the land of childhood, was inevitably associated with the motif of cradle and childhood, a synonym of shelter, safety and joy [26, p.223], [18, p.22]. The image of the parents constitutes the multitude of references showing the home environment as a happy place [26, p.224]. The mother – a woman who has given birth to a child, a caregiver . The

father (patrimony) – a symbol of stability and refuge. Stanisław Ossowski wrote that *“the family land is the land where you come into the world. At the same time, the family land is etymologically associated with the concept of family and ancestry”* [27, p.44]. The cult of ancestors who lived and died there was therefore the most durable link that unites the family land and the home. *“Through the parents, the fatherland is the land of fathers, the land to which fathers were bound by birth and a long chain of experiences; through blood they gave this relationship to their children”* [27, p.27]. The villagers’ awareness of past generations and the emotional attachment towards their place on earth have become distinctive features of their moral attitudes.

The home, in the whole system of folklore, was undoubtedly made up of the community of people living in it. As a hierarchical institution, the home connected generations: grandparents, parents and children [22, p.46, citing: 44]. Such a traditional home also had its own psychic temporal extension: here lived the past, present and future. The home gave its inhabitants an opportunity to look back at events and situations in the past and, at the same time, it was also a place to dream about the future [26, p.224-225]. The very sense of belonging to the family community and intergenerational memory – merged and grounded the home. This is confirmed by Jerzy Bartmiński, who wrote that, according to popular belief, the aspect of communality dominates over location [28, p.36].

Even today, in many houses of the eastern borderland one can encounter traces and memorabilia of the past, which are a confirmation and a preserved piece of the history of people living there and a tangible record of fragments from their lives. These items constitute the foundation of the identity of a given family built over the years by the history of the ancestors. Memories belonging to the home, however, are not only tangible objects, but also non-material – such as sounds, songs, and smells (pastries prepared by housewives), annual holidays designated by the Julian calendar, as well as family celebrations (baptisms, weddings or funerals) formerly took place in the home and were accompanied with music and song, with the whole household engaged, utilizing specific items found in the home. Even today, in many Orthodox homes, the corners of the interior are decorated with sacred images – patron icons decorated with small aprons, small curtains or towels, which, according to their belief, protect the living space and its household from danger. The floors are decorated with hand-sewn carpets. There are huge embroidered cushions displayed on the beds in guest rooms (photos 8-9). These cushions were passed down from generation to generation as a dowry of the bride. Thanks to these memorabilia and memories that have been cultivated over time, these spaces acquire symbolic importance and become rich in meaning.



Photos 8-9. Soce village (Narew commune), photos by M. Dekutowska, P. Jungiewicz (students of the Faculty of Architecture at Białystok University of Technology)

In the analysis of borderland homes, apart from their architectural (visual) value, it is not possible to omit the “*humanistic coefficient*” [29, p.36, citing: 45, p.50]. “*The home as an interiorised space, as Hanna Buczyńska-Garewicz wrote, can be experienced and felt and, undoubtedly, it is a common and fundamental experience (...) it unifies many different types of egos. Conscious and subconscious, intellectual, emotional and volitional experiences intertwine with one another, different needs of the soul come to the fore. Memory is connected with a dream*” [26, p.220, 224]. In the rural tradition, the home was undoubtedly a space of cultural significance, a space for passing down traditions and material artifacts through generations. Behaviors learned from the family home, ethical and moral values, attitudes toward one’s surroundings, prayers, songs, repeated gestures, are all evidence of how strong the connection is between inhabitants and their place of residence.

4. Present day

The cultural landscape of the eastern villages of Podlasie is a very broad topic. Being a spatial record of the history of previous generations and a reflection of the relationship between people and their living space, it contains many themes and references that penetrate the dependencies between the material and the spiritual. On the one hand, the preserved spatial arrangement of the plot, the wooden architecture, the façade decoration, as well as the interior decoration, evoke the past of the ethnic communities who have lived here. On the other hand, it shows a “*cultural and visual reality*”, and “*a unique image of their lives*” [30, p.45], presenting the local culture and how they experience their space.

Interestingly, the houses of the eastern Polish borderland to this day shape the character of these lands, constituting their identity. The houses are a tangible and indirect link with history. In addition to the typical utility function – as a space for living, they also have a symbolic dimension – they contain a compilation of meanings, spiritual and sensual: the memory of generations with a deep layered belief system and strong cultural and social relations. And although there are signs of passing time on them, they are still a living example of the bond that exists between that what was and the present, and shows the emotional dependency between man and home, which is quickly disappearing in the modern world.

Despite the now-widespread crisis of ideology, the model that grew on the foundation of the fathers’ faith, respect for the past, for the legacy of generations, and for customs, has become a permanent part of the lives and memories of local residents. As opposed to the modern world, the main and integral distinctive feature of norms regulating social behavior in this region is religion, present in almost every home. Residents cultivate traditions, following a certain code of duty toward their small private homeland. Home, as a space for living in the folk tradition, has ideological value, and symbolism still influences the organization, preservation and experiencing of the space [13, p.247, 250].

Citing the words of Sebastian Bernat, it can be concluded that in the analysis of the phenomenon of the home, it is difficult to separate the intangible aspects “*from their material roots, intangible values of the landscape (including historical values, originality, uniqueness, symbolism) strongly affect the intellectual and emotional sphere*” [31, p.129]. The inseparable connection between the two is also contained in the Unesco Convention of 2003, which states that: “*(...) there is a far-reaching interdependence between material cultural heritage and intangible cultural heritage* [32], and: *If material culture upholds the identity of the nation, then certainly spiritual, intangible heritage creates, shapes, enriches and stimulates material expression*” [33].

The prospect of survival and continuity of the cultural memory of the homes and the customs and rituals connected to the home, as well as the survival of the wooden architecture itself in the villages of south-eastern Podlasie is becoming more and more precarious every year. This is mainly due to the demographic situation and the inevitably progressing phenomenon of the depopulation of rural areas in the eastern region. Field research shows that at the moment, the villages are inhabited by generations of people aged 60 – 90, most of whom are retired and no longer employed in agriculture⁵. This state was caused, among others, by the economic and social situation that took place in Poland after 1990, and more specifically mass emigration to cities, change of life model, self-realization of the young generation outside agriculture, the expansion of mass media, and thus the spread of mass culture [34], [13, p.248]. This situation is confirmed by Sokrat Janowicz, who writes: “*Belorussian life is characterized by a certain paradox: the city swallows the ethnic mass at a dizzying pace (...)*” [35, p.241].

Most of the children and grandchildren have left to neighboring cities, visiting grandparents mainly for holidays or family celebrations. An aging population and the desertion of the villages by young people have caused certain elements of folk culture, both material and spiritual, to change. In the architectural context, this is manifested by a growing number of abandoned houses, with the number increasing every year. An important problem is the low durability of wood as a building material. It is quickly destroyed, and older residents do not have funds to modernize their homes. On the other hand, in the village landscape, new buildings are increasingly found among traditional buildings, whose form, roof shape and building material are far from local standards developed over the years. New owners – usually not family-related to those originally living here, mostly come for vacation and seek to modernize their summer houses. Wooden windows are replaced by plastic ones, and facades are covered with siding, and it is increasingly common that beams are stripped of their decorative details [9, p.509].

The growing phenomenon of depopulation of the villages of the Polish-Belarusian borderland also affects the spiritual layer of the community. Among the inhabitants, the frequency of traditional household practices is diminishing or disappearing altogether. Often, it also happens that behavioral patterns, passed down in families for generations, are colored with contemporary elements brought to the countryside by the younger generations. The situations described are an inevitable echo of civilization advancement that has not been indifferent to the rural areas of eastern Poland.

5. Conclusions

Nowadays, globalization and its trends have priority over the building of community and a relationship with one's place of residence. This is why the issue of spiritual and material protection of the borderland heritage is today a priority in order to maintain the identity of these areas, and to be remembered and respected by future generations. The enormous cultural capital that the villages of south-eastern Podlasie have at their disposal is its most important attribute, which should be preserved at all costs.

⁵ Field research was conducted individually and with a group of students as part of the inventory practice organized by the Faculty of Architecture at the Białystok University of Technology from 2008-2019. Research included villages from Bielsk Podlaski, Czyże, Hajnówka, Narew communes and concerned rural wooden houses (architecture, construction, detail) and customs related to the residential space of local communities.

The villages of eastern Poland are areas where many wooden buildings have survived. The current forms of protection of wooden houses concern only buildings which have the status of monument. The owners of such buildings receive funds to keep them in proper condition. The procedure for applying for such funding is not easy, which discourages interested persons from taking actions aimed at changing the legal status of a residential building. In the areas of the Polish-Belarusian borderland, many houses are not listed in the register of monuments, but have significant cultural value. Protecting them against liquidation consists of including them, where possible, in local plans, or in case of the inability of maintaining the building, informing potential buyers about the possibility of buying or leasing the house, including the possibility of relocating the house to another area. Although the issue of the protection of wooden buildings is included in the activities of cultural institutions and the conservationists, so far mainly legally unregulated actions have been taken. In fact, their condition depends on the will and decisions of private owners who, due to lack of financial resources, do not always care about keeping the house in proper condition. For the most part, these houses are from the 1930s and 1940s and are distinguished by rich architectural detail [34].

The protection of the intangible elements of the heritage of the communities living in these areas is also extremely important. However, this requires a comprehensive and multi-directional studies approach. Ongoing debates around the country about the protection of cultural heritage emphasize that such activities should primarily be carried out by various entities, including conservators, local governments, universities, schools, and focused on cognitive, educational, revitalization and touristic projects. They also articulate active and practical engagement and inclusion of rural communities. These activities can serve as a way to activate the community and pay tribute to the values they represent, as well as serve as a way to build intergenerational bonds.

The activities of municipalities that are closest to local communities have the most impact on the aspect of protection *in situ*. Besides the relevant provisions in cultural policy, which is part of the regional or local development strategy, this is done by promoting local cultural tourism, which in the future may contribute to the economic dynamism of these areas. Common concern for heritage is identification, documentation, research and promotion, as well as transmission and formal and informal education. That is why, as part of initiatives supporting the promotion of the heritage of ethnic groups in Eastern Podlasie, grassroots projects run by local communities are also appearing more and more often. They aim to disseminate their knowledge and skills related to tradition (oral, music, building practices, handicrafts and culinary traditions), while leading to increasing awareness of the need to maintain them. In the case of Eastern Podlasie, as Małgorzata Durydiwka and Piotr Kociszewski note, the multiculturalism of this area and the possibility to interact with locals who continue to practice traditions can find a “*permanent place in the catalog of cultural heritage*” or be recreated [36, p. 6].

The postulate for the intergenerational vector of information coincides with the provisions of the Unesco Convention on the Protection of the World Cultural and Natural Heritage of 1976, in which article 27 addresses the issue of strengthening the attachment to cultural and natural heritage [37], as well as the latest Unesco Convention of 2003 on the protection of intangible heritage [32], which talks about securing and respecting all manifestations (customs, rituals, ideas, values, skills and related objects and artifacts) inherited from ancestors, as well as raising public awareness on this topic.

The idea of protecting cultural heritage, both architectural and spiritual, puts an emphasis on the active role of local communities in transferring their knowledge and skills. “*Culture, as*

Stanisław Ossowski wrote, *is (...) a certain group of psychological dispositions transmitted in the womb of a given community by social contact and interdependencies from the entire system of interpersonal relations*” [27, p.163]. It is “(...) communities, (...) indigenous peoples, groups and, in some cases, individual persons, according to the Unesco Convention, that play a significant role in the creation, protection, maintenance and reproduction of intangible cultural heritage (...) which are passed down from generation to generation, is constantly reproduced by communities and groups in relation to their surroundings, the impact of nature and their history, and provides them with a sense of identity and continuity (...)” [32]. Gathering memories from people still living in these communities is therefore the most important means of preserving their culture. However, it should not be understood only as a retrospective event or commemoration of local history, but above all, as activity directed towards the future [38, p.84, citing: 46].

This intergenerational transmission of information has an extremely important semantic core that can not be translatable over other content that can bring mutual benefit. On the one hand, it can play a leading role in maintaining a sense of identity and maintaining cultural continuity within the rural community. On the other hand, it can contribute to the consolidation, dissemination and connection of traditional (spiritual and material) culture – with universal culture, by respecting the past, present and future. This is probably the last moment to use and transfer the knowledge of the communities living here to the next generation, and a step towards preserving the traces of the past. Borderland homes, as places of value, will survive in as much as society will be able to reproduce them [39, p.432]. Heritage, as Gregory Ashworth wrote, “*is a decision to draw from the past or [and] pass on to the future*” [40, p.44].

Acknowledgement

The study has been implemented from the resources of the WZ/AiU/2/2020 public research funds financed by the Ministry of Science and Higher Education of Poland.

References

- [1] Giddens A., *Nowoczesność i tożsamość*. Warszawa 2007. 1-322. 978-83-01-14691-7.
- [2] Sadowski A., *Spoleczne problemy wschodniego pogranicza*. Dział Wydawnictw Filii Uniwersytetu w Białymstoku, Białystok 2001.
- [3] Sadowski A., *Spoleczne problemy miejscowości pn.-wsch. Polski w procesie transformacji*. Białystok 2001. 83-89031-11-6.
- [4] Barwiński M., *Podlasie jako pogranicze narodowościowo-wyznaniowe*. Łódź 2004. 83-7171-789-X.
- [5] Sadowski A., *Wschodnie pogranicze w perspektywie socjologicznej*. Wyd. Ekonomia i Środowisko, Białystok 1995. 83-85792-15-X.
- [6] Barwiński M., *Podlasie jako region pogranicza*, [in:] *Studia z Geografii Politycznej i Historycznej*, vol. 3 (2014), p. 281–306. Available: <http://sgph.geo.uni.lodz.pl/uploads/files/t3/11-Barwinski.pdf> [Access: 05.02.2020]
- [7] Hawryluk J., *Kraje ruskie, Bielsk, Mielnik, Drohiczyn. Rusini – Ukraińcy na Podlaszu – fakty i kontrowersje*. Podlaskie Wydawnictwo „Osnowy”, Bielsk Podlaski 2001. 83-914297-1-7.
- [8] Sadowski A., *Narody wielkie i małe*. Uniwersytet Religioznawstwa, Uniwersytet Jagielloński, Kraków 1991.
- [9] Sulima M., „Społeczno-kulturowy tygiel pogranicza etnicznego: tradycja i nowoczesność (na przykładzie wsi podlaskiej)”, [in:] *Habitaty: reaktywacja małych społeczności lokalnych/Habitats: Reactivation of small local societies*, edit. Z. Bać, Oficyna Wydawnicza Politechniki Wrocławskiej, Wrocław 2016. 506–514.

- [10] Pokropek M., Pokropek W., „Tradycyjne budownictwo drzewne w Polsce”, [in:] T.1: *Budownictwo ludowe. Chalupy i ich regionalne zróżnicowanie*. Neriton, Warszawa 1985.
- [11] Szewczyk J., *Piec i komin w tradycyjnym budownictwie ludowym Podlasia*. Oficyna Wydawnicza Politechniki Białostockiej, Białystok 2011.
- [12] Sielicki F., *Folklor białoruski*. Wrocław 1983.
- [13] Sulima M., *Dom pogranicza w kulturze wsi podlaskiej*. Oficyna Wydawnicza Politechniki Białostockiej, Białystok 2018, s. 1-277. 978-83-65596-56-7.
- [14] Pawluczuk W., „Prawosławie jako typ kultury. Prawosławie jako typ kultury”, [in:] *Materiały I edycji Wszechnicy Kultury Prawosławnej 1998/1999*, edit. Zienuk J., Białystok 1999, p. 41-48.
- [15] Bułgakow S. *Prawosławie. Zarys nauki kościoła prawosławnego*. Orthdruk, Formica, Białystok, Warszawa 1992.
- [16] Sulima M., „Gra symboli w detalu okna domu wiejskiego”, *Czasopismo Techniczne*, Architektura, R. 109, z. 15-t. 2 (2012), 2012, p. 576–581.
- [17] Kozera A. N., *Z badań nad folklorem muzycznym Podlasia. Portrety muzyków ludowych*. <http://chopin.man.bialystok.pl/umfc/wp-content/uploads/2016/04/03-01.pdf> [Access: 04.11.2019]
- [18] Tolstaja S. N., *Ojczyzna w ludowej tradycji słowiańskiej. Pojęcie ojczyzny we współczesnych językach europejskich*. Instytut Europy Środkowo-wschodniej, Lublin 1993. 1-318. 83-85854-08-8.
- [19] Eliade M., *Sacrum i profanum*. Wydawnictwo KR, Warszawa 1996. 83-86989-06-8.
- [20] Kolberg O., *Dziela wszystkie. Białoruś – Polesie*, t. 52, Polskie Towarzystwo Ludoznawcze Wrocław – Poznań 1968.
- [21] Bachelard G., *Wyobrażenia poetycka*. Państwowy Instytut Wydawniczy, Warszawa 1975.
- [22] Rembierz M., „Egzystencjalne i aksjologiczne doświadczenie domu rodzinnego”, [in:] *Kultura dnia codziennego i świętecznego w rodzinie*, edit. Dyczewski L., Wadowski D., Redakcja Wydawnicza Katolickiego Uniwersytetu Lubelskiego, Lublin 1998, p. 41-58.
- [23] Benedyktowicz D., Benedyktowicz Z., *Symbolika domu w tradycji ludowej (part I)*. Polska Sztuka Ludowa (3), 1990, 48-61.
- [24] Bartmiński J., *Ojczyzna w pieśniach i wierszach chłopskich*. Polska Sztuka Ludowa (3), 1990, 9-13.
- [25] Ossowski S., *O ojczyźnie i narodzie*. Warszawa 1984. 83-01-04021-1.
- [26] Buczyńska-Garewicz H., *Miejsca, strony, okolice. Przyczynek do fenomenologii przestrzeni*. Kraków 2006. 83-242-0608-6.
- [27] Ossowski S., *Z zagadnień psychologii społecznej. Dzieła, t. III*. PWN, Warszawa, 1967.
- [28] Bartmiński J., *Polskie rozumienie ojczyzny i jego warianty. Pojęcie ojczyzny we współczesnych językach europejskich*. edit. J. Bartmiński, Instytut Europy Środkowo-Wschodniej, Lublin 1993. 23-48. 83-85854-08-8.
- [29] Hałas E., „Intymne wartości domu”, [in:] *Kultura dnia codziennego i świętecznego w rodzinie*, edit. Dyczewski L., Wadowski D., Redakcja Wydawnicza Katolickiego Uniwersytetu Lubelskiego, Lublin 1998, p. 31-40. 83-228-0664-7.
- [30] Wieruszewska M., „Krajobraz kulturowy wsi w percepcji wizualnej”, [in:] *Lokalne dziedzictwo kulturowe w doświadczeniu mieszkańców wsi*, edit. Bukraba-Rylska I., Wieruszewska M., Burdyka K., IRWIR PAN, Warszawa 2017, p. 1-242. 978-83-7383-876-5.
- [31] Bernat S., „Niematerialne wartości krajobrazów kulturowych”, [in:] *Niematerialne dziedzictwo kulturowe: źródła, wartości, ochrona*, edit. Adamowski J., Wydawnictwo Uniwersytetu M. Curie-Skłodowskiej, Narodowy Instytut Dziedzictwa, Lublin-Warszawa, 2013, p. 1-367. 978-83-7784-426-7.

-
- [32] UNESCO Convention for the Safeguarding of the Intangible Cultural Heritage 2003. Available: http://www.unesco.pl/fileadmin/user_upload/pdf/Konwencja_o_ochronie_dz_niemater_2003.pdf [Access: 15.10.2019]
- [33] National Heritage Board of Poland, *UNESCO nonmaterial cultural heritage*. Available: https://www.nid.pl/pl/Dla_wlascicieli_i_zaradcow/opieka-nad-zabytkami/niematerialne-dziedzictwo-kulturowe-unesco/ [Access: 15.10.2018]
- [34] Sulima M., *Dom mieszkalny w zagrodzie pogranicza etnicznego jako zjawisko architektoniczno-kulturowe (na przykładzie wsi podlaskiej)*. PhD dissertation. Faculty of Architecture, Warsaw University of Technology, Warszawa 2013.
- [35] Janowicz S., *Ojczyśćość. Białoruskie ślady i znaki*. WK Borussia Olsztyn 2001. 1-256. 83-915690-0-4.
- [36] Durydiwka M, Kociszewski P, „Wielokulturowość Podlasia i możliwości jej wykorzystania w turystyce”. Available: http://www.turystykakulturowa.org/pdf/2013_06_01.pdf [Access: 05.01.2020]
- [37] UNESCO Convention Concerning the Protection of the World Cultural and Natural Heritage. Available: http://www.unesco.pl/fileadmin/user_upload/pdf/Konwencja_o_ochronie_swiatowego_dziedzictwa.pdf [Access: 15 Oct 2019]
- [38] Waszczyńska K., „Przekaz międzypokoleniowy i jego znaczenie w kontekście konwencji UNESCO w sprawie niematerialnego dziedzictwa kulturowego. Refleksje etnologa”, [in:] *Niematerialne dziedzictwo kulturowe: identyfikacja, dokumentacja, ochrona, interpretacja. Pojęcia, poglądy, Materiały z Ogólnopolskiej Konferencji Naukowej Węgorzewo 2011*, Warszawa – Węgorzewo 2013.
- [39] Halbwachs M., *Spoleczne ramy pamięci*. Wydawnictwo Naukowe PWN, Warszawa 2008. 1-438. 978-83-01-15511-7.
- [40] Ashworth G., *Planowanie dziedzictwa*. Międzynarodowe Centrum Kultury, Kraków 2015. 1-314. 978-83-63463-34-2.
- [41] Pawluczuk W., *Światopogląd jednostki w warunkach rozpadu społeczności tradycyjnej*. Warszawa 1972.
- [42] Łokotko A., *Belorusskoe narodnoe zodčestvo: seredina XIX–XX w.*. Navuka i Technika, Mińsk 1991.
- [43] Becker. H., *Rozwój myśli społecznej od wiedzy ludowej do socjologii*. Warszawa 1964.
- [44] Tatarkiewicz T., W., *Wspomnienia*. Państwowy Instytut Wydawniczy, Warszawa 1979.
- [45] Znaniecki F., *Social Relations and Social Roles*. San Francisco 1965.
- [46] Hałas E., „Przeszłość i przyszła terażniejszość: refleksyjna pamięć kulturowa”, [in:] *Kultura jako pamięć. Postradycyjne znaczenie przeszłości*, 10 Jul 2011, Warsaw.

